Molecular, Cellular and Mechanical basis of Epithelial Morphogenesis during *Tribolium* Embryogenesis

DISSERTATION

ZUR ERLANGUNG DES AKADEMISCHEN GRADES

Doctor of Philosophy (Ph. D.)

vorgelegt
der Fakultät Mathematik und Naturwissenschaften
der Technischen Universität Dresden

von

JAIN, AKANKSHA
GEBOREN 04.05.1989 in Delhi, India
BETREUER
DR. PAVEL TOMANCAK

DATE OF DEFENSE
25-04-2018

Die Dissertation wurde in der Zeit von 09/2013 bis 09/2017 im Max Planck Institute for Molecular Cell Biology and Genetics angefertigt

ABSTRACT

Embryonic development entails a series of morphogenetic events which require a precise coordination of molecular mechanisms coupled with cellular dynamics. Phyla such as arthropods show morphological and gene expression similarities during middle embryogenesis (at the phylotypic germband stage), yet early embryogenesis adopts diverse developmental strategies. In an effort towards understanding patterns of conservation and divergence during development, investigations are required beyond the traditional model systems. Therefore, in the past three decades, several insect species representing various insect orders have been established as experimental model systems for comparative developmental studies. Among these, the red flour beetle *Tribolium castaneum* has emerged as the best studied holometabolous insect model after the fruit fly *Drosophila melanogaster*. Unlike *Drosophila*, *Tribolium* is a short-germ insect that retains many ancestral characters common to most insects. The early embryogenesis of *Tribolium* shows dynamic epithelial rearrangements with an epibolic expansion of the extraembryonic tissue serosa over the embryo, the folding of the embryo in between the serosa and the second extra embryonic tissue amnion and the folding of the amnion underneath the embryo. These extensive tissues are evolutionarily conserved epithelia that undergo different tissue movements and are present in varying proportions in different insects, providing exceptional material to compare and contrast morphogenesis during early embryogenesis. However, most of the previous work on insects including *Tribolium* have largely focused on the conservation and divergence of gene expression patterns and on gene regulatory interactions. Consequently, very little studies on dynamic cell behaviour have been done and we lack detailed information about the cellular and tissue dynamics during these early morphogenetic events.

During my PhD, I first established a live imaging and data analysis pipeline

for studying *Tribolium* embryogenesis in 4-D. I combined live confocal and lightsheet imaging of transgenic or transiently labelled embryos with mechanical or genetic perturbations using laser ablations and gene knockdowns. Using this pipeline quantifications of cell dynamics and tissue behaviours can be done to compare different regions of the embryo as the development proceeds.

In the second and third part of my thesis, I describe the actomyosin dynamics and associated cell behaviours during the stages of serosa epibolic expansion, amniotic fold formation and serosa window closure. I cloned and characterised the cellular dynamics of the *Tribolium* spaghetti squash gene (Tc-squash) - the non-muscle Myosin II regulatory light chain, which is the main molecular force generator in epithelial cells. Interestingly, the analysis of Tc-squash dynamics indicates a conserved role of Myosin II in controlling similar cell behaviours across short germ and long germ embryos.

In the last part of the thesis, I report the dynamics of an actomyosin cable that emerges at the interface of the serosa and amnion. This cable increases in tension during development, concomitant with serosa tissue expansion and increased tensions in the serosa. It behaves as a modified purse string as it's circumference shrinks due to a decrease in the number of cable forming cells over time. This shrinkage is an individual contractile property of the cells forming the cable. This indicates that a supracellular and contractile actomyosin cable might be functional during serosa window closure in insects with distinct serosa and amnion tissues. Further, the tension in the cable might depend on the relative proportion of the serosa, amnion and embryonic regions.

Using these integrated approaches, I have correlated global cellular dynamics during early embryogenesis with actomyosin behaviours, and then performed a high-resolution analysis and perturbations of selected events. The established imaging, image processing and perturbation tools can serve as an important basis for future investigations into the tissue mechanics underlying *Tribolium* embryogenesis and can also be adapted for comparisons of morphogenesis in other insect embryos. More broadly, correlating the existing genetic, mechanical and biochemical understanding of developmental processes from *Drosophila* with species such as *Tribolium*, could help identify deeply conserved design principles that lead to different morphologies through differences in underlying regulation.

Dedication

This thesis is dedicated to my grandfather, *Vijay K. Jain*, who wanted to have a doctor in the family. And to my grandmother, *Rama Jain*, who had a big heart.

ACKNOWLEDGEMENTS

This thesis would not have been possible without the contributions of many incredible people whom I have been fortunate enough to have known over the years.

I want to begin my acknowledgements by thanking Pavel, my PhD supervisor. The past 4 years have been an amazing and enriching journey. I have learnt many things from you and I wish to follow your example in many spheres of my life, of which especially your attitude tops the list. You are the first boss I know who doesn't believe in making their minion's life miserable. If you ever read this, keep rocking! I next want to thank my second supervisor Tassos. You convinced me regarding this project and I ended up in Dresden without having any intentions to. True to your promise you have guided me in all aspects of my PhD and more importantly, thank you for always being concerned about me enjoying the research life as well. I wonder if anyone else competes with you in long distance mentoring or if anyone else was lucky enough to learn cloning over skype! People on several occasions asked me how hellish is it to deal with two supervisors on two different continents. Contrary to that, I maintain that this was a very unique experience and I have enjoyed managing your (mostly) complementary guidances more than I could have imagined.

I also want to thank Stephan Grill and Jan Huisken for their valuable inputs during my TAC meetings and otherwise in various discussions. My research wouldn't have begun without the kind help of Kristen Panfilio and Siegfried Roth, Thorsten, Matt and other members of the Panfilio and Roth labs. Thank you for teaching me everything Beetle in my one month in Cologne and for helping me with the starting steps, for continuing to be interested in my research, exchanging ideas and collaborating.

I next want to thank the Tomancak lab. As we always say, "Tt's survival

of the weirdest here!". I couldn't have been more at home in any other place. The 333N has maintained a special environment. The members past and present have all possessed uncanny knacks for outrageous humour, jokes and absolutely cruel randomness. To add to it, the regular doses of care and warmth have made my day many times over. You all were my first friends in Dresden and I missed home a little less because of all the things we did together, from having lunch together to the various parties, mushroomings and coffees. Christopher, thanks for turning me into a nerd and geek, I owe you all the computational knowledge that I have picked up. Mette for being the kindest person I know, being a friend and helping often without asking. Wen, for being the mischief maker, the co-crazy sufferer, buddy and the source of countless Yu, Wen, Why and She jokes. I know I don,Äôt need to spell it out. Dim Pap, Michi, Pavel M, Helena, Tobias, Mimi and Dr. Gutschwein, all the members who have moved on, Pete, Alex, Asli, Ivana, the parasites Miquel and Anni, the kids and all the other extensions, it was great working with you in a wonderful scientific environment and amongst friends. Stefan, for being the beetle buddy and suffering through the setting up of Tribolium and for being equally boggled as me on several occasions.

I next want to thank the amazing C-Bee-Gee. The MPI is probably has the most unique amalgamation of science and fun and in the rich environment it offers. Not only the research is exceptional, the facilities, the activities and the staff have influenced my journey in several ways. I have remained amazed with the facility services in the Institute, No one can be prompter in helping and no one can care more than what I experienced here. I want to thank the LMF, especially Jan, Davide, Sebastian and Britta who each helped me with the imaging in various phases and cared when things broke down. I want to the thank the most amazing scientific collaboration I have experienced in my career, Sir Dr. Robert Haase and more recently Argo, the fly kitchen and all the other services for making work smooth. I also want to thank the international office and the PhD office for making the expat life and the student life easier, of course Katja for the extra smiles with coffee.

A big part of my PhD experience is the three years I served as a StudRep. I absolutely loved and still crave for the problem solving, the meetings and being a part of a group that bridges the students and the administration. The group was fantastic with some of the most fun, chilled, concerned and capable people who volunteer to make a difference and contribute personal time for having things in the program run smoothly. I want to thank my fellow students for electing me!

I cannot imagine this professional journey without thinking of the friends

I have made in Dresden. Gopi (+1) and Jaydeep thanks for all the cooking, bollywood and jokes, Passant and Catia for being my first good, non-Indian friends :P. The friends who became a family away from home in Dresden and who slowly helped in making Dresden my second home, Avin, Mansi, Pradnya, Srija, Samata, Nandu, Prbs, Ani, Udi, Rahul, Neha, Susmita, Tohid, Guru, Vamshi and Loki (The Athens tudwe) and I am sure I am still missing 20 more :(You guys are awesum! Since I am thanking friends here, of course, a big thank you goes to my TIFR friends, who cared despite each one of us having moved on in life and being located in different parts of the globe. For keeping in touch although I might have erred. For friendship and for science, Rohini, Dhaniya, Vandy, Bobo, hunti, Stitha, Pankaj, Sameer, Sudi, and Ritu.

I wouldn't have been where I am and I wouldn't have been who I am without my family. To my parents and brother who dream for me and who are my backbone, my achievements are all for you and because of you. My aunts and uncles, the family which makes me feel loved all these miles away, the kiddos, and my friends back in India, thanks for making me feel special. My most emotional acknowledgment is reserved for my grandparents. I would always regret that they wouldn't see me becoming a doctor. Without them several of my dreams wouldn't have been imaginable.

AUTHOR'S DECLARATION

Erklärung entsprechend §5.5 der Promotionsordnung

Hiermit versichere ich, dass ich die vorliegende Arbeit ohne unzulässige Hilfe Dritter und ohne Benutzung anderer als der angegebenen Hilfsmittel angefertigt habe; die aus fremden Quellen direkt oder indirekt übernommenen Gedanken sind als solche kenntlich gemacht. Die Arbeit wurde bisher weder im Inland noch im Ausland in gleicher oder ähnlicher Form einer anderen Prüfungsbehörde vorgelegt.

Die Dissertation wurde im Zeitraum vom 24-9-13 bis 27-9-17 verfasst und von Dr. Pavel Tomancak at the Max Planck Institute of Molecular Cell Biology and Genetics, Dresden betreut.

Meine Person betreffend erkläre ich hiermit, dass keine früheren erfolglosen Promotionsverfahren stattgefunden haben.

Ich erkenne die Promotionsordnung der Fakultät für Mathematik und Naturwissen- schaften, Technische Universität Dresden an.

SIGNED: ..... DATE: .....

AUTHOR'S DECLARATION

Erklärung entsprechend §5.5 der Promotionsordnung

I herewith declare that I have produced this paper without the prohibited assistance of third parties and without making use of aids other than those specified; notions taken over directly or indirectly from other sources have been identified as such. This paper has not previously been presented in identical or similar form to any other German or foreign examination board. The thesis work was conducted from 24.09.2013 to 27.09.2017 under the supervision of Dr. Pavel Tomancak at the Max Planck Institute of Molecular Cell Biology and Genetics, Dresden.

I declare that I have not undertaken any previous unsuccessful doctorate proceedings. I declare that I recognize the doctorate regulations of the Fakultät für Mathematik und Naturwissenschaften of the Technische Universität Dresden.

SIGNED: ..... DATE: .....

"Well, in our country," said Alice, still panting a little,
"you'd generally get to somewhere else if you run very fast for a long time, as we've been doing.".
"A slow sort of country!" said the Queen.
"Now, here, you see, it takes all the running you can do, to keep in the same place.
If you want to get somewhere else, you must run at least twice as fast as that!"

– Lewis Caroll's Through the Looking Glass

TABLE OF CONTENTS

List of Tables

List of Figures

CHAPTER 1

INTRODUCTION

The marvellous orchestration of precise developmental events during embryogenesis has remained fascinating for centuries. To add to that, the remarkable diversity in early embryogenesis and in adults of different organisms increases the fascination of development. Through decades of research, what emerged is a picture of general principles that guide morphogenesis during development. Very similar to the art of 'Origami' where a combination of paper folds can create diverse outputs, the formation of diverse morphologies during embryogenesis can be attributed to 'embryonic origami'. However, in case of living systems, the paper folds are replaced by tissue folding, extensions, cell divisions, cell shape changes and other morphogenetic events. Several invertebrate, vertebrate and plant species have been established as model systems to study tissue morphogenesis. Extensive studies have examined conservation and novel interactions of gene regulatory networks in these systems. These studies were then complemented with descriptions of cell behaviour to link gene expression with tissue morphology. The focus has then shifted to under-

standing tissue morphogenesis in terms of biomechanics, that is, proteins that function in force production in cells and the response of tissues to such forces. Current studies are bridging scales to understand how the gene expression information is translated into mechanical outputs of changing cell shapes by the activity of generic effector proteins.

The next and most recent dimension in deciphering the generation of biological form, is to combine the knowledge from various levels and organisms and start understanding the evolution of morphogenetic mechanisms. Although most of the previous work in this direction focused on the traditional model systems such as *Drosophila melanogaster*, *Xenopus laevis*, zebrafish and mouse, interest in the field of evo-devo has led to establishment of several new species as model organisms. The comparison of new species is offering insights into changes in gene expression patterns, functions and of regulatory mechanisms in creating diversity. Finally, the establishment of live imaging tools and microscopy has finally made comparison of morphogenetic cell behaviours across species and associated protein functions, possible.

With an interest in evolution of morphogenesis, during my PhD, I have striven to elucidate the mechanisms of morphogenesis that eventually change the 3-Dimensional organization and shape of embryos between species. Morphological diversity is largely attributed to changes in expression of functionally conserved proteins [Carroll, 2008]. The expression patterns of regulatory genes and gene functions show both conserved as well as divergent behaviours between insect embryos. However, whether and how changes in expression patterns of regulatory genes modulate the activity of proteins that are involved in morphogenesis and change the subsequent cellular dynamics is not clear.

I have focused on the early embryogenesis of the red flour beetle *Tribolium castaneum*, which is a well-established insect system for understanding gene functions during embryonic development and have compared tissue morphogenesis between the fly and the beetle to provide an evolutionary perspective. My approach combines studying protein behaviour (actomyosin dynamics) in the context of changing cellular morphologies (cell shape changes) and

correlating it with regulatory gene functions. I have used state of the art 4D microscopy, live imaging and biophysics to understand the tissue mechanics during *Tribolium* development. Together these approaches aim at giving a holistic picture of the various mechanisms of morphogenesis which play a role in beetle embryogenesis and in future this information can then be expanded to other insect model systems for a comprehensive evolutionary development comparison.

1.1 Evo-Devo of insects

The last twenty years have witnessed the rapid growth of a new approach to understanding the evolution of organismal form. The main focus of this field of Evolutionary Developmental Biology, or 'Evo-Devo', has been the comparison of developmental genetic mechanisms at different taxonomic levels ranging from intra-species microevolutionary comparisons to large-scale macroevolutionary comparisons across phyla [Arthur, 2002]. From the very beginning, arthropods represented the most fertile ground to understand how developmental mechanisms evolve to generate new body plans [Akam, 2000]

Arthropods exhibit a dramatic diversity in their lifestyles and associated morphologies and developmental strategies, offering rich raw material for Evo-Devo comparisons. Insects are the most speciose group of arthropods (and animals) with a catalogued number of 925,000 species (estimated number of 5 million or more) accounting for more than 80% of all known animal species (Grimaldi/Engel, Book: Evolution of the Insects). Recent phylogenomic studies have suggested that insects (and hexapods) comprise a monophyletic group that originated about 480 million years ago from a common crustacean ancestor [Misof et al., 2014]. In fact, several independent analyses have identified some cave-dwelling crustaceans, the remipedes, as the closest extant relatives of insects.

Insect Evo-Devo is strongly supported by the availability of an extensive bibliography on the embryogenesis of all insect orders spanning more than

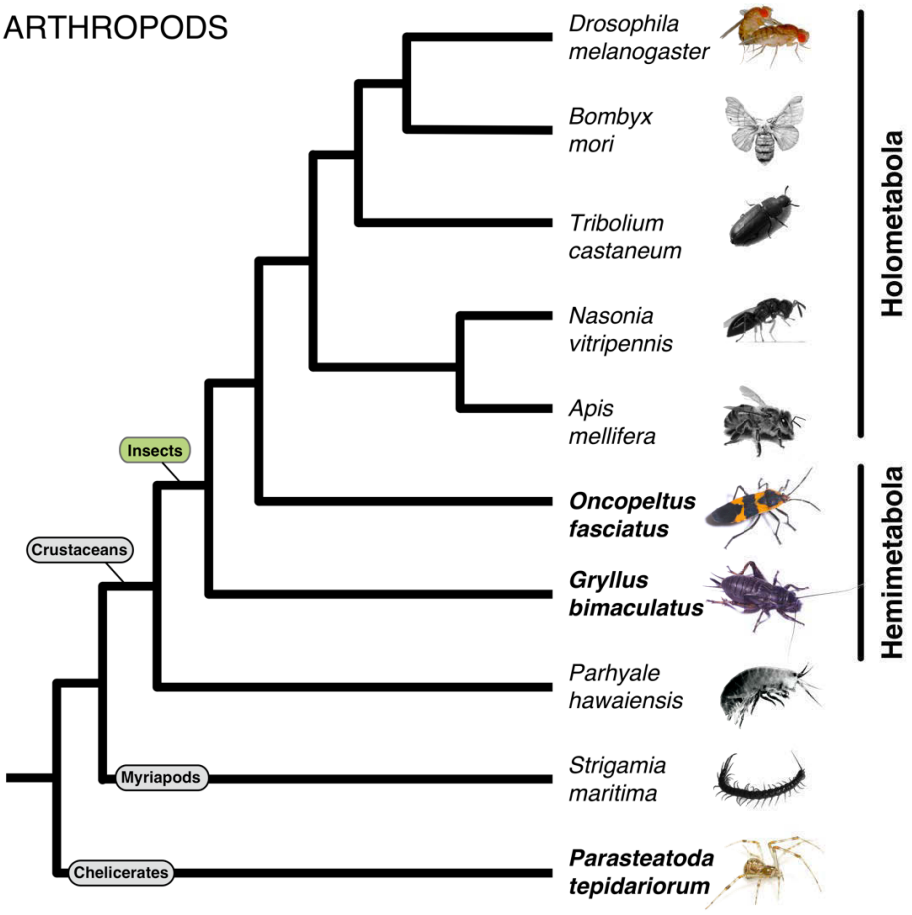

Figure 1.1: Phylogeny of arthropods Arthropod species belonging to different orders which have been established as experimental model systems are shown.

150 years (Book: Developmental Systems: Insect edited by Counce & Waddington), together with the history of technological innovations and fundamental discoveries using the fly model system *Drosophila melanogaster* [Bilder and Irvine, 2017]. The Evo-Devo field was marked by the introduction of powerful and versatile technologies that are applicable to a wide range of species and that have narrowed the technological gap between *Drosophila* and several emerging arthropod and insect experimental organisms [Gilles and Averof, 2014]. These advances enabled to study the function of widely conserved genes

in diverse arthropods, to study biological processes that are not present or accessible in *Drosophila* and to conduct unbiased genome-wide screens to identify novel gene functions in emerging model systems.

The emerging non-insect arthropod models, which have attracted relatively more attention and are supported by a growing number of experimental tools and resources include the spider *Parasteatoda tepidariorum*, the centipede *Strigamia maritima*, and the crustacean *Parhyale hawaiensis*. The most promising emerging insect models that are representative of the various insect orders are the cricket *Gryllus bimaculatus* (order Orthoptera), the milkweed bug *Oncopeltus fasciatus* (order Hemiptera), the wasp *Nasonia vitripennis* (order Hymenoptera), the honeybee *Apis mellifera* (order Hymenoptera), the cockroach *Periplaneta Americana* (order Blattodea), and the beetle *Tribolium castaneum* (order Coleoptera) [Schmidt-Ott and Kwan, 2016a]. All these species have been put forward as favourable developmental genetic systems to study the expression and function of developmental patterning genes. Importantly, some of these emerging models like *Parhyale, Gryllus* and *Tribolium* are not only genetically but also optically tractable, thus enabling to also study in live embryos the molecular and cellular dynamics responsible for tissue and organ morphogenesis. My PhD work concentrated on early embryogenesis of the the red flour beetle *Tribolium castaneum* (Fig 1.3, A), which is arguably the next best studied insect and arthropod model system after *Drosophila* melanogaster.

1.2 *Tribolium castaneum*

Compared to *Drosophila*, *Tribolium* is a more basally branching holometabolous insect belonging to the most diverse insect order, the Coleoptera (about 350,000 described species). Starting with the seminal work by the geneticist Alexander Sokoloff in the 1960s, *Tribolium* has become an increasingly popular and powerful system for studies of agricultural pest control and developmental genetics [Sokoloff, 1966]. It is easy to maintain in laboratory cultures on a

wheat flour diet and has a short life cycle of 24 days at 32°C (Fig 1.2) [Gregor, 2009] . *Tribolium* is amenable to both forward and reverse genetic approaches [Beeman et al., 1989; Posnien et al., 2009; Sulston and Anderson, 1996], its genome is sequenced and resources for genome-wide research are available [Brown and Denell, 1996; Brown et al., 1993; Richards et al., 2008; Trauner et al., 2008]. Several methodologies and protocols established in *Drosophila* have been also applied in *Tribolium*, enabling the rigorous comparison of molecular and cellular mechanisms operating during development of the two species. Gene expression can be studied in fixed specimens by immunohistochemistry and *in situ* hybridisation [Schinko et al., 2009]. Gene functions can be knocked-down with very high efficiency in embryos, larvae and pupae including on a genome-wide scale with systemic RNA interference (RNAi) (iBeetle screen) [Posnien et al., 2009; Schmitt-Engel et al., 2015]. A number of transposon based systems have been tested successfully in *Tribolium* allowing the development of diverse transgenic approaches, like heat-inducible and binary UAS/Gal4 mis-expression systems and a large collection of enhancer trap lines providing valuable cell and tissue markers is available [Lorenzen et al., 2003; Pavlopoulos, 2004; Schinko et al., 2012, 2010]. Also, CRISPR/Cas9-based knock-out and knock-in approaches allow the efficient targeted modification of the *Tribolium* genome [Gilles et al., 2015]. Fluorescent live imaging has been made possible thanks to an increasing number of stable transgenic lines and transient method for fluorescent labelling of various cellular compartments [Benton et al., 2013; Hilbrant et al., 2016; Sarrazin et al., 2012; van Drongelen and Vazquez-Faci, 2017].

Importantly, *Tribolium* retains several characters that make it a better representative of insect development. Unlike the long-germ *Drosophila* embryo, the *Tribolium* embryo exemplifies the short-germ type that is considered the ancestral state of insect embryogenesis [Anderson, 1972; Counce, 1961; Davis and Patel, 2002; Lynch et al., 2011; Schmidt-Ott and Kwan, 2016b; Stern, 2004]. In *Tribolium*, after fertilization of the egg, several rounds of nuclei division occur followed by nuclear migration to the surface of the egg forming

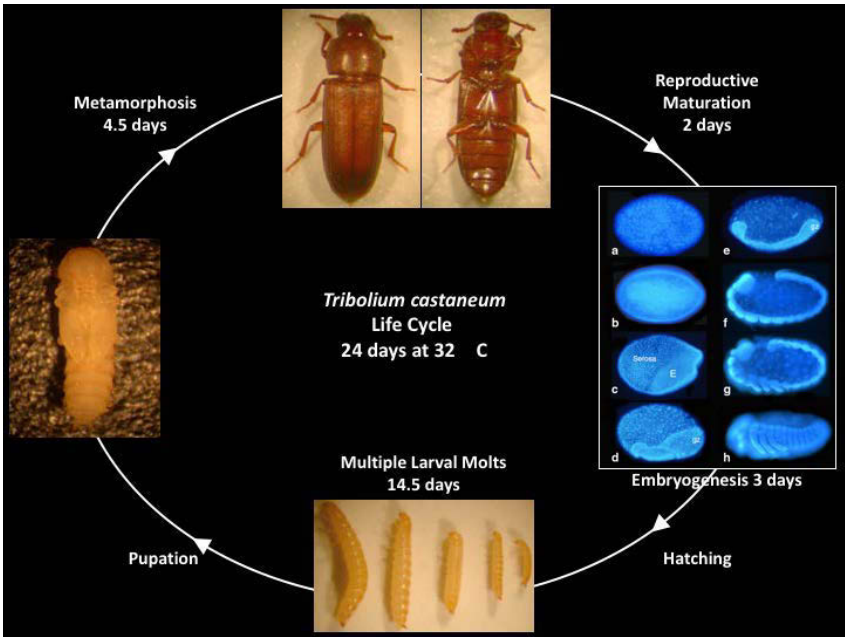

Figure 1.2: Life cycle of *Tribolium castaneum*. Life cycle of the red flour beetle *Tribolium castaneum* at 32C is shown. The adults take about two days for reproductive maturation and lay eggs. Embryogenesis lasts for 3 days followed by hatching of the larvae. The larvae undergo 5 molts lasting 14.5 days followed by metamorphosis in the pupae for another 4.5 days. The adults then undergo eclosion from the pupae.

a uniform blastoderm. This is followed by cellularisation and cell divisions forming a differentiated blastoderm. The embryo specifies only the anterior head and thoracic segments at the blastoderm stage, while the posterior abdominal segments are added sequentially from a posterior 'segment-addition zone' during later embryogenesis. Additionally, only a part of the blastoderm epithelium forms the embryo proper and the rest of the blastoderm gives rise to two extraembryonic tissues- the amnion and the serosa (Fig 1.3). The early embryonic development of *Tribolium castaneum* has been previously described in detail with light and electron microscopy [Benton et al., 2013; Handel et al., 2000]. It can be divided into a number of landmark events for convenient staging and comparison across embryos, as listed below (Fig 1.3):

- **Syncytial cleavage stage**: The *Tribolium* egg is surrounded by a trans-

parent vitelline membrane and an opaque chorion. Fertilization of the egg is followed by a rapid sequence of synchronous nuclear divisions which are not accompanied by cytokinesis. The nuclei then move outwards and populate the egg cortex forming the syncytial blastoderm, where nuclei are contained within a common cytoplasm.

- **Formation of uniform blastoderm**: After 12 rounds of synchronous nuclear divisions are complete, the cortical nuclei become enclosed by membranes during the interphase of the 13^{th} cycle giving rise to a cuboidal epithelial monolayer known as the uniform blastoderm.

- **Blastoderm Differentiation**: The uniform blastoderm divides into an anterior cap of extraembryonic primordium forming the serosa tissue. The posterior two-thirds of the blastoderm gives rise to the embryonic primordium and a second extra-embryonic membrane, the amnion. Unlike the serosa cells that do not divide and become polyploid, the embryonic cells undergo a 13^{th} round of asynchronous cell divisions. Moreover, the serosa cells start becoming squamous (shorten along their apical-basal axis) as they start their epibolic expansion over the egg surface, while the embryonic cells become columnar (lengthen along their apical-basal axis) followed by the embryonic condensation ventrally.

- **Primitive pit and posterior amniotic fold formation**: During the onset of blastoderm differentiation, the posterior pole becomes slightly flattened and detaches from the vitelline membrane forming the primitive pit. Later on, starting from this region the embryonic primordium folds on itself forming the posterior amniotic fold.

- **Formation of the serosa window**: In tight association with the proceeding serosa epiboly and embryo condensation, the posterior amniotic fold expands laterally (horseshoe amniotic fold) and then anteriorly (oval amniotic fold). The oval amniotic fold creates an open space at the ventral side on the embryo known as serosa window.

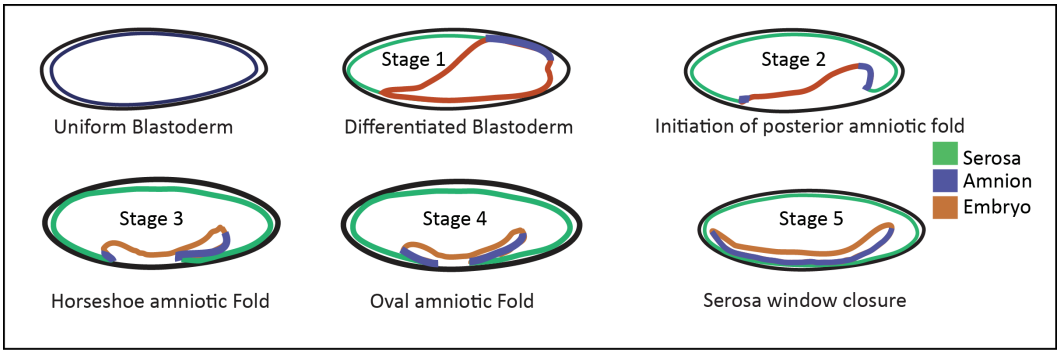

Figure 1.3: Early embryogenesis of *Tribolium castaneum*. A) Schematics illustrate the stages in early *Tribolium castaneum* embryogenesis. The three different tissues, serosa, amnion and embryo are indicated

- **Gastrulation (Mesoderm invagination)**: In parallel with amniotic fold progression, the future mesodermal cells internalise along the ventral midline of the condensing embryo with a posterior to anterior progression.

- **Serosa window closure**: The serosa window contracts and closes completely, thereby separating the thin outer serosa envelope from the inner amnion that covers the germband (gastrulating embryo) ventrally. The internalized germband extends in the anterior posterior direction as the remaining segments are formed sequentially.

In my imaging studies, I have covered all the processes taking place from blastoderm cellularisation up to serosa window closure, spanning about 6 hours of development at 32°C from 9 to 15 hours after egg lay (AEL). For ease of reference, I will be referring to these stages of *Tribolium* embryogenesis in the results sections of the thesis (summarized in the schematic of Fig 1.3).

1.3 Fluorescence live imaging and lightsheet microscopy

Fluorescence live imaging to study developmental dynamics has become a routine approach, since it offers powerful approaches to perform quantitative studies on the structure and function of cells in intact embryos [Pantazis and Supatto, 2014]. Depending on the spatial and temporal requirements and the signal-to-noise ratio needed, morphogenetic processes can be imaged in vivo with a broad range of fluorescence microscopy modalities, ranging from widefield and laser scanning microscopy (confocal, spinning disc or two-photon) to the various super-resolution optical techniques [Combs, 2010; Ettinger and Wittmann, 2014; Schermelleh et al., 2010; Stelzer et al., 1991; Thorn, 2016].

Optical sectioning in fluorescence microscopy increases the spatial resolution. It allows for imaging of a single region of a live sample, analogous to physical sections of a fixed tissue [Conchello and Lichtman, 2005]. Optical sectioning can be achieved by collecting fluorescence from a small region of a sample that is completely illuminated (in case of confocal point scanning systems) or by illuminating a small region of the sample and collecting the data (in case of lightsheet microscopy).

Confocal microscopy (CLSM), utilising the point scanning or spinning disc method, is probably the most popular method for studying molecular and cellular dynamics during development. In CLSM, optical sectioning is achieved by using a pin hole placed in the detection path, which rejects out of focus light and its size controls the thickness of the optical section acquired [Conchello and Lichtman, 2005; Stelzer et al., 1991]. This results in higher spatial resolution compared to epifluorescence and widefield systems. Additionally, various experimental implementations of CSLM are available such as fluorescence resonance energy transfer (FRET), fluorescence correlation spectroscopy (FCS), fluorescence recovery after photobleaching (FRAP) and photoablations [Medina and Schwille, 2002; White and Stelzer, 1999]. Further, the possibility to acquire multiple channels and image several samples together in confocal

systems increase their applications.

In recent years, it has become possible to study embryonic development of non-model arthropod species using CLSM live imaging [Benton et al., 2013; Sarrazin et al., 2012]. This relies on generation of transgenic lines with labelled nuclei, membranes and other cytoskeletal or subcellular proteins, using transposon mediated transgenesis or more recently, CRISPR/Cas mediated knock in [Gilles and Averof, 2014; Gilles et al., 2015]. Alternatively, transient labelling by injection of mRNA which codes for fluorescent proteins or use of fluorescent dyes circumvents the need for transgenics [Benton et al., 2013]. A description of cell and tissue dynamics during early embryogenesis of *Tribolium* was provided using a point scanning confocal system in transiently labelled embryos [Benton et al., 2013]. Multiple embryos were imaged together at single cell resolution in wildtype as well as gene knockdown conditions, to provide a qualitative description of early embryogenesis. As the next step in studying cellular dynamics and proteins involved, I have expanded the implementations of fluorescence microscopy to study *Tribolium* embryogenesis. I have used the FRAP assay to estimate protein dynamics during development and photo ablations to measure tensions in a tissue. Therefore, the superior lateral resolutions, the possibility to image several samples together and the various photo-manipulations in confocal systems make them suitable for describing molecular and cellular dynamics in *Tribolium*. A comparison of fluorescence microscopy methods that I used for studying *Tribolium* embryogenesis is provided in table 1.1 [Huisken and Stainier, 2009].

However, in confocal microscopes the entire sample is illuminated by lasers while imaging. This often results in high phototoxicity and photobleaching of signal which limits the use of confocal microscopy to shorter time scales, usually up to a few hours [Icha et al., 2017; Laissue et al., 2017]. Additionally, there is limited light penetration due to scattering and non-transparent tissues and acquisition rates are also slower in point scanning. The speed limitation is overcome in spinning disc confocal microscopes while two photon systems allow for increased resolution in deeper tissue layers and lesser phototoxicity

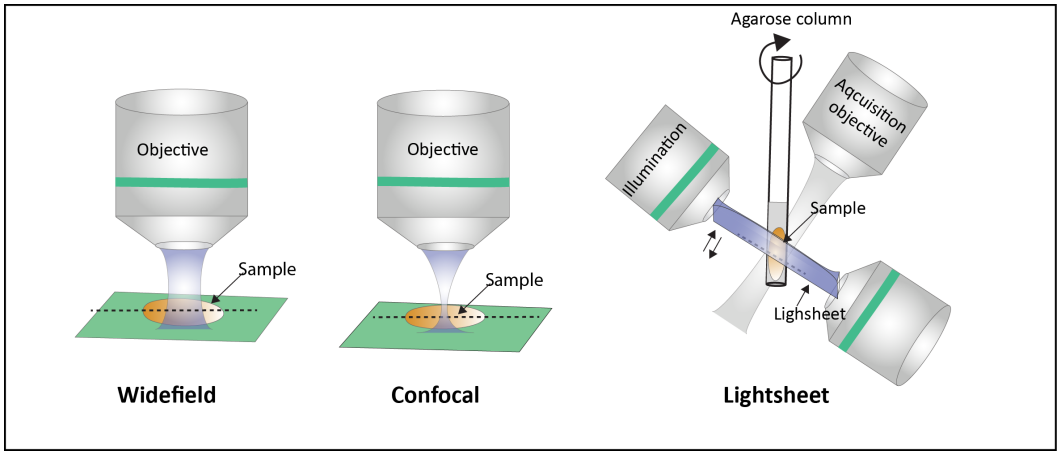

Figure 1.4: Fluorescence microscopy. (A) Illustrations of widefield microscopy, confocal microscopy and lightsheet microscopy principles. The illumination and acquisition objective are the same in case of widefield and confocal microscopy. The sample is illuminated by a cone of light. A thin lightsheet is created by the illumination objectives which are arranged perpendicular to the acquisition objective in Selective plane illumination microscopy. The sample is suspended in an agarose column and immersed in a buffer.

as only a small region is exposed [Helmchen and Denk, 2005]. This in turn can also be detrimental at longer time scales as it produces heat. Thus, the applications of CLSM based microscopes is limited for studying embryogenesis *in toto* (complete and total), at high resolutions as well as over several hours to days [Huisken and Stainier, 2009].

The introduction of lightsheet microscopy is another milestone in live imaging analysis of developmental processes [Huisken et al., 2004]. In contrast to widefield and confocal systems, in the various versions of lightsheet microscopy, only a small volume of the sample is illuminated using a lightsheet that moves back and forth across the sample [Huisken et al., 2004; Keller et al., 2008]. The principles of widefield, confocal and lightsheet microscopy are illustrated in Fig 1.4. In the selective plane illumination (SPIM) version of lightsheet microscopy, the lightsheet is produced by a pair of illumination objectives which are situated perpendicular to the imaging objective. This allows for optical sectioning by only exciting fluorophores in a relatively thin region of

Properties	**Epifluorescence**	**Confocal (Zeiss 710, LSM 880)**	**Zeiss LZ1 SPIM**
Illumination	Uniform, illumination, entire sample	Point focus and acquisition, entire sample	Dual side illumination, small volume of sample
X-Y res	poor	Best	Intermediate
Z res	poor	Intermediate	Isotropic x-y-z (Multiview)
Photo damage	High	High	Very low
Speed	-	Slow	Fast
Sample number	Multiple samples can be scanned	Multiposition possible	Low, 1-2 embryos
Multiview	No	No	Yes
Photo Manipulations	No	Yes	No
Z depth (Depth of field)	-	80-90 μm	150 μm
Scattering	High	Low	Low
Usage	Quick screening of sample	Photoactivation, Laser ablation, short timelapses, Higher res. images	Long timelapses of development, full 3D reconstruction of entire embryos possible

Table 1.1: Comparison of Zeiss point scanning Confocal and SPIM systems

the sample. It also reduces phototoxicity as only a thin region of the sample is illuminated. The lightsheet is placed at the focus of the detection objective. The thickness of the lightsheet determines the thickness of the optical section. Fluorescence from the entire illuminated volume is collected by a camera which allows for very fast imaging. Such arrangement is unlike the traditional fluorescence microscopes in which a single objective serves the purpose of illumination as well as acquisition [Huisken et al., 2004; Pitrone et al., 2013].

Lightsheet imaging allows for long-term imaging of sample up to a few

days due to reduced phototoxicity [Chhetri et al., 2015; Keller and Stelzer, 2008; Tomer et al., 2011]. Additionally, it is possible to acquire images from multiple angles (usually referred to as views), by rotating the sample which is suspended in the center of the imaging chamber. The aligning of multiple views through image registration and subsequent fusion of z stacks collected from different angles, allows for complete 3-D reconstruction of embryos. The post processing, combined with advanced data analysis, now allows for visualisation of complete embryogenesis, segmentation and analysis of all the cells in the embryo lineage reconstructions of all cells and nuclei and other such system level measurements [Amat et al., 2015, 2014; Khairy and Keller, 2011; Stegmaier et al., 2016]. With increased generation of complete descriptions for different organisms, it would become possible to describe development at any stage in its entirety and also study provide detailed analysis of gene knockdown conditions.

Lightsheet microscopy has been adapted to image the entire embryonic development of *Tribolium* [Hilbrant et al., 2016; Strobl and Stelzer, 2014]. The low phototoxicity and special sample embedding ensured normal embryo development which could hatch and develop into fertile adults. This imaging technique, however, did not utilise the multiview fusion modality for 3D reconstruction of *Tribolium*. Also, only the available transgenic line (EFA::nGFP, [Sarrazin et al., 2012]) was imaged to describe embryogenesis. It is however, possible to image dual channels with nuclei and membrane labels through transient labelling. Therefore, for a complete and quantitative analysis of tissue morphogenesis in the entire embryo, a lightsheet imaging pipeline incorporating transient labelling, multiview data acquisition, fusion and data analysis needs to be established. This can be achieved by adapting the various available methods for SPIM data analysis for *Tribolium* embryogenesis as well as building new image analysis tools for specific questions. This could allow for measurements of various morphogenetic mechanisms over the course of *Tribolium* development, such as, apical constrictions, change in tissue density and cell areas, cell divisions and lineages and calculating optical movements

of the embryonic tissues.

1.4 Morphogenesis

The first observable event during embryogenesis is the division of a single fertilised cell into several cells that coordinate and eventually give rise to shapes. C.H Waddington in his book Principles of embryology, 1956 wrote that "three main processes are seen during embryogenesis. First is the histological differentiation, which is the gradual change in the nature of a mass of living matter such as cells. Second is the arising of differences between various parts of an embryo. This spatial differentiation is also termed as regionalization or segregation. The third is the moulding of a mass of tissue into a coherent structure, which has a unitary character of its own, usually recognized by giving it a name as an anatomical organ". He then goes on to define this moulding as morphogenesis or the “forming of a mass of cells into a new shape is known as morphogenesis. The morphogenesis of an organ is accompanied by tissue differentiation and often by the appearance of distinct spatial subunits (regionalization)" [Book: Principles of embryology, C.H. Waddington, 1956].

Several morphogenetic processes are seen during embryogenesis. The initial mass of cells assembles into tissues, which are remodelled to generate various shapes and form organs. In most insects, a monolayerd epithelium is formed at the blastoderm stage. This layer undergoes various foldings to form the three germ layers through the process of gastrulation [Pilot and Lecuit, 2005]. During my PhD, I have focused on morphogenetic mechanisms that remodel the epithelial tissues formed at the blastoderm stage during early embryonic development of *Tribolium*.

Epithelial tissue

The epithelium is one of the four major tissues in animals and is also the most abundant, lining the cavities and surfaces of blood vessels and organs

throughout the body. Epithelial cells can be squamous, cuboidal or columnar based on their shape and can be arranged in a single layer (simple epithelium) or multiple layers (stratified epithelium) [Fristrom, 1988]. The epithelial cells are connected to each other via cell-cell junctions. These allow formation of membrane like epithelium tissues and are also required for force transmission across an epithelium. The epithelial cells are polarised cells and exhibit two types of spatial coordinate system- apico-basal polarity and planar polarity [Guillot and Lecuit, 2013; Lecuit and Le Goff, 2007].

The epithelium serves as a strong barrier to the external environment. This requires epithelia to have high resistance to environmental stresses. Epithelial tissues can respond to an external stress in various ways. If a stress, such as a pull by the adjoining tissue, is applied for a short while, epithelial cells can stretch. This involves a change in the aspect ratio of cells depending on the direction of the stress. However, the cellular junctions and neighbours are maintained. This ability to stretch depends on the intercellular adhesion and also on the active contribution by the contractile cell cortex. If the stress is applied for longer time scales, epithelial cells exhibit fluidic behaviour. This requires neighbour exchange by cells through junction remodelling and cell intercalations [Guillot and Lecuit, 2013].

Epithelia can exhibit diverse sheet like behaviours, such as folding, stretching and tissue separations. During embryogenesis in syncytial insects like *Tribolium* and *Drosophila*, initially a single layer of epithelium surrounds the yolk and it later rearranges to form the germ layers. In *Drosophila* epithelium folding happens during gastrulation and cephalic furrow formation, epithelium stretching is seen during the formation of the dorsal amnioserosa and epithelial tissue separations are seen at parasegment boundaries [Guillot and Lecuit, 2013; Lecuit and Le Goff, 2007]. In *Tribolium* epithelium stretching happens in the serosa and epithelium folds are seen at the posterior pole and in the ventral furrow, however, the molecular mechanisms of these behaviours are unknown.

Molecular force generators

Actin is a family of globular proteins that can polymerise to form microfilaments. These filaments are part of the cellular cytoskeleton and can also function in force generation in muscle sarcomeres and in the cortex of non-muscle cells [Lecuit and Lenne, 2007]. The actin filaments can behave in a contractile manner upon the activity of the molecular motor myosin. The Myosin family of motor proteins binds to actin filaments [Hartman and Spudich, 2012]. Some if its members like the non-muscle Myosin II can also form filaments, that pull onto actin and together the contractile actomyosin apparatus is the major force generator in epithelial cells. The cellular organisation of actin cortex, Myosin filaments and junction proteins is illustrated in Fig 1.5. Actin forms different types of networks- isotropic, branched or bundled networks depending on the cross linkers and associated proteins [Bieling et al., 2016; Munjal and Lecuit, 2014]. These networks are pulled by the Myosin filaments to generate contractility at the cortex.

The cells are attached to neighbour cells via cell-cell junctions such as the adherens junctions and to the extra cellular matrix via integrins. The subcellular forces generated in single cells by actomyosin contractility is transmitted in a tissue from cell to cell through junctions [Lecuit and Le Goff, 2007; Lecuit and Lenne, 2007; Munjal and Lecuit, 2014].

The activity of myosin, and the actomyosin mediated contractility in cells, is regulated through a conserved signalling pathway which involves the small GTPase RhoA. Rho1 activates the Rho associated kinase, ROK, which activates Myosin by phosphorylating the Myosin regulatory light chain (MRLC) and inhibiting the Myosin phosphatase. This is a highly conserved signalling pathway that is under the regulation of membrane proteins which also set up polarity in epithelial tissues [Harris, 2017; Munjal and Lecuit, 2014]

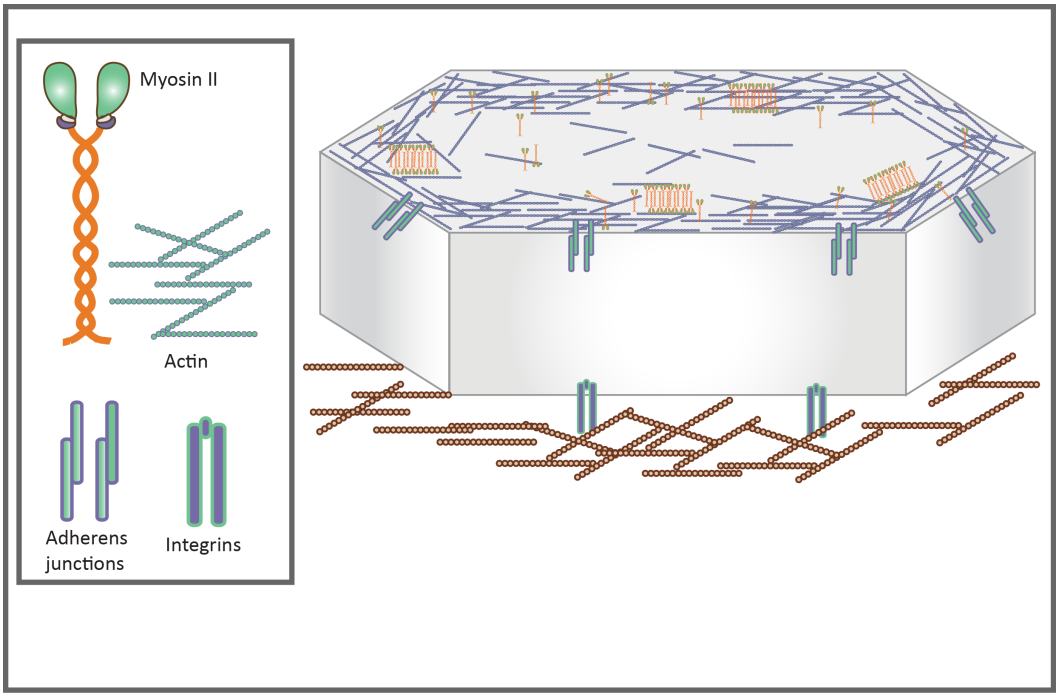

Figure 1.5: Molecular force generating machinery in cells. Illustration shows the cellular localisation of the contractility machinery. The actin networks are organised at the cell cortex and Myosin II forms filaments that bind to the actin networks. The cells attach to the extracellular matrix via integrins and adherens junctions function in cell-cell contacts.

Epithelial Polarity

The epithelial cells are able to self-organise into sheets with the apical areas of all cells facing one side due to setting up of the apico-basal polarity [Flores-Benitez and Knust, 2016; Tepass, 2012]. Orthogonal to the apico-basal polarity, the planar polarity is defined [Zallen, 2007]. Both of these systems lead to asymmetries in the tissue which is required for structuring and global shaping and are highly conserved across cell types in animals [Hale and Strutt, 2015; Johnston and Sanson, 2011]. The cell polarity pathways regulate the activity of actomyosin and therefore, play an important role in epithelial morphogenesis [Umetsu and Kuranaga, 2017].

Apico-basal polarity

Four different domains can be identified in epithelial cells- apical, junctional, lateral and basal. These domains are defined by specific and asymmetric localisation of various molecules [Johnston and Sanson, 2011]. The apical domain in many epithelial cells is identified by the localisation of crumbs protein. The internal FERM binding domain of crumbs brings moesin and BH-spectrin to the apical membrane. Its C-terminal PDZ-binding motif binds to Stardust, PatJ, PAR-6 and atypical protein kinase C (aPKC), together forming the apical complex. This complex probably also includes active Cdc42. The apical complex excludes Bazooka (Baz)/PAR-3 from the apical surface. This limits the extent of the intercellular junctions to the apical side of the lateral domain [Flores-Benitez and Knust, 2016; Johnston and Sanson, 2011; Tepass, 2012].

Intercellular junctions that form between cells are the tight junctions in mammals and the adherens junctions in *Drosophila*. The position of Baz/PAR-3 determines the extent of intercellular junctions as it associates directly with Echinoid and Armadillo in *Drosophila*, Nectin1 & 3 and JAM1-3 in mammals [Tepass, 2012]. These are the components of the cell adhesion complexes that form the junctional domain at the boundary between apical and lateral domains. PAR-1 phosphorylates Bazooka/PAR-3 and limits the extent of the adherens junctions in the lateral domain. Scribble, Dlg (Discs-large) and Lgl (Lethal(2)giant larvae) inhibit the activity of the apical complex, partly through the binding of Lgl to aPKC. Vice versa, aPKC phosphorylates Lgl and excludes it from the apical domain [Tepass, 2012].

An alteration in the ratio of the apical: lateral: basal domain is seen in all morphogenetic movements in different epithelium sheets. A decrease in the lateral domains along with a concomitant increase in apical and basal domains leads to increased surface area in the epithelium and decrease in its thickness [Johnston and Sanson, 2011]. A reciprocal change decreases the area and increases its thickness. E.g. of epithelial thinning is epiboly in vertebrates and the anterior follicle cells when cells become squamous in *Drosophila*. Epithelial

thickening is seen in vertebrate placodes and plates such as otic placode and neural plate, and follicle cells in *Drosophila* that are in contact with the oocyte and become columnar. Amnioserosa formation in *Drosophila* involves cuboidal to squamous transition of the dorsal epithelium in the embryo [Johnston and Sanson, 2011].

Planar cell polarity

Planar cell polarity (PCP) is the molecular mechanism that creates asymmetries in the plane of epithelial tissues, orthogonal to the axis of apico-basal polarity. It translates global patterning information in the embryos to regulate morphogenetic cell behaviours. PCP is mediated by a core set of proteins that localize to the lateral and medial cell-cell interfaces [Gray et al., 2011]. It is an evolutionary conserved mechanism that has been extensively studied in insects and vertebrates and converges to the Wnt pathway and Frizzled signalling [Gray et al., 2011; Hale and Strutt, 2015; Sokol, 2015; Wallingford, 2012].

In addition to its role in fate specification in the embryos, the Wnt signalling acts as a morphogen gradient and modulates the PCP pathway, as a signalling leading to coordinated polarization of neighbouring cells in the plane of the tissue [Sokol, 2015] and the signalling is transmitted locally from one cell to the next. The Wnt signalling mediated by the Frizzled receptor regulates downstream effectors such as the Rho pathway mediated Myosin contractility in various morphogenetic process. In *Xenopus* embryos the Wnt/PCP signalling mediates cortico-cytoplasmic rotation of certain cortical components, to the future dorsal side, playing an important role in dorso-ventral specification [Sokol, 2015].

PCP plays a role in dynamic cell populations undergoing morphogenesis. Body axis elongation in vertebrates and invertebrates occurs by oriented cell divisions, cell motility, cell-shape changes, or cell rearrangements and PCP has been shown to play a role in specifying these polarized behaviours of cells. The intercalation of cells by neighbour exchange is a key process that functions in

mesoderm extension in *Xenopus*. The elongation and closure of the neural tube also requires some PCP components [Wallingford, 2012; Wang and Nathans, 2007].

Cellular models of morphogenesis

The polarity pathways regulate conserved signalling which in turn regulates actomyosin contractility at the sub-cellular level [Harris, 2017]. The activity of the actomyosin molecular force generators, results in changes in the shape of cells. These cellular level forces are transmitted across a tissue through cell-cell junctions and result in changes in tissue architecture [Guillot and Lecuit, 2013]. The main cell shape and size changes which modify tissue architecture are illustrated in Fig 1.6. Based on the major cellular events which function in diverse epithelia, tissue morphogenetic mechanisms can be grouped into the following categories:

- Cell shape change: Apical constrictions and cell intercalations
- Cell position change: Cell intercalations and collective cell migration
- Cell number: Patterned cell proliferation and cell death
- Cell size: Epithelial thickening or thinning

In *Tribolium*, previous studies have described that apical constrictions are seen in the ventral furrow [Handel et al., 2004]. Cell intercalations were described in the embryo [Benton et al., 2013]. It was postulated that a supra-cellular actomyosin cable leads to the serosa window closure in the embryos [Benton et al., 2013; Handel et al., 2000]. However, the molecular mechanism of these morphogenetic behaviours, the signalling and polarity pathways and the role of actomyosin contractility has not been studied. Therefore, investigations of morphogenetic mechanisms during *Tribolium* embryogenesis requires an understanding of the cell dynamics which play a role in these processes and the identification of the molecules involved in the cell and tissue behaviours.

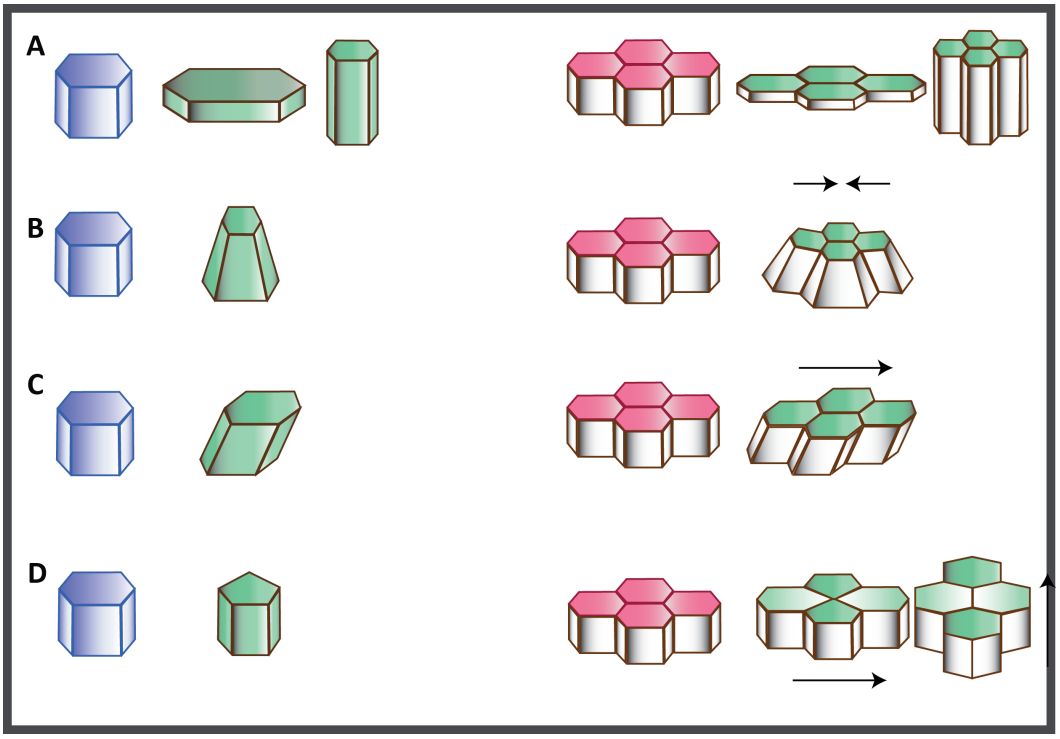

Figure 1.6: Cell shape changes that lead to tissue morpogenesis. A) Epithelial cells can be cuboid. columnar or squamous. This can lead to flattening of tissue or condensation without cell divisions. **B)** Cell shorten their apical side to undergo apical constrictions which an bend a tissue. **C)** Shear in cells can lead to differential movement of the apical side vs the basal side of a tissue. **D)** Cells change shape and remodel junctions to exchange neighbours in a tissue. Such transitions are also called as t1 transitions.

Apical constrictions: transition to wedge shaped cells

Apical constriction is the primary mechanism by which epithelial sheets bend or create invaginations [Sawyer et al., 2010]. They have been implicated in generating a variety of epithelial topologies, such as folds, pits or tubes. A decrease in the apical side of a tissue along with a concomitant increase in its basal area can create curvature in epithelial sheets. These distinct changes in apical vs. the basal domains can form the characteristic wedge or bottle shaped cells and bend an epithelial sheet to create an invagination [Sawyer et al., 2010]. For example, gastrulation in *Drosophila*, Zebrafish etc., cephalic

furrow in *Drosophila* and neural tubes hinge formation. Apical constrictions also function in extrusion of cells from an epithelium, such as in epithelia-mesenchyme transition or in case of apoptotic cells, delamination, wound contraction and healing [Martin and Goldstein, 2014; Sweeton et al., 1991].

In *Xenopus*, the core PCP protein Vangl2 exhibits an apical localization at the blastopore lip in the embryo, and regulates apical constrictions of bottle shaped cells and ectopic constriction of ectoderm cells triggered by the actin-binding protein Shroom3 [Ossipova et al., 2015, 2014]. The different cell types that undergo apical constrictions can assemble contractile actomyosin structures in distinct regions of the cell: the apico-lateral junctional domain and the apico-medial cortex network [Sawyer et al., 2010]. The inner ear placode invagination in chick, involves two phases, Phase I with basal expansion of cells and Phase II with apical constrictions. The Phase II requires Myosin II contractility, which is mediated at cell junctions [Sai et al., 2014].

Apical constrictions can occur via a purse string mechanism, in which a circumferential junctional domain of actomyosin fibres undergoes contraction, such as during chick neurulation [Copp and Greene, 2009]. Whereas, In *Drosophila* mesoderm invagination, apical constriction occurs via a pulsed ratchet like mechanism [Martin et al., 2009]. The cells undergo constriction followed by a paused state in which the constricted area is maintained akin to a ratchet. In these cells, actomyosin networks are found on the apico-medial domain of cells. These generate tension on the apical surface and can result in cortical flows that are visible as Myosin foci coalescing in the center of the cell apex [Martin, 2010; Martin et al., 2009]. This apico-medial pool of Myosin foci has been shown to enrich in pulses correlating with decrease in cell's apical domain. It spans across the cortex connecting junctions from opposite sides and powers apical constrictions by pulling the apical adherens junction towards the center [Martin et al., 2009; Roh-Johnson et al., 2012].

The patterning molecules and membrane signalling can specify spatial domains in the tissue which undergoes apical constrictions. The transcription factors *twist* and *snail* are involved in regulating apical constrictions in gastru-

lating cells in *Drosophila* [Mason et al., 2013]. *snail* initiates contractile pulses while *twist* maintains cell shape during the ratchet like pulsed constrictions. *twist* up regulates *snail* expression and also activates the expression of fog and T48. T48 activates the guanine nucleotide exchange factor, RhoGEF2 apically and consequently the Rho1 signalling. ROK (Rho Kinase) and Myosin II are seen at the medio-apical domains of cells, absent from junctions and ROK is required for constriction of actin cables into foci probably by Myosin II [Mason et al., 2013]. Fog is a secreted ligand that induces apical constrictions via its receptor mist, that signals through a G alpha protein- RhoGEF2 and Rho kinase (ROK) to activate Myosin II [Dawes-Hoang et al., 2005]. The fog signalling is mediated through concertina, a Heterotrimeric G alpha protein (HGP). Another HGP, ric-8 stabilizes cortical actin and suppresses cell blebbing in apical constriction in the ventral furrow of *Drosophila*, probably playing a key role in withstanding hydrostatic pressure generated in cells during tissue folding [Kanesaki et al., 2013]. T48 is a transmembrane protein that functions in parallel and recruits junction G proteins and RhoGEF2 to the apical domains of the cells [Martin et al., 2009].

In vertebrate neural tube formation, Shroom (an F actin binding protein that localises to the apical tips of adherens cell junctions) mediates the specific targeting of actin and Myosin to the junctional domains [Hildebrand and Soriano, 1999; McGreevy et al., 2015; Mohan et al., 2012]. However, in *Drosophila*, its single Shroom codes for two different isoforms, the long form (dShrmA) that localises to the adherens junctions and stimulates apical constriction and a short form, dShrmB, which localises to the apical cortex to assemble a more medial/apical contractile network [Bolinger et al., 2010]. This could play a role in pulsed contractions of the medial apical actomyosin cortex that drives apical constrictions in mesoderm invagination and shrinking of amnioserosa during dorsal closure. Therefore, specific subcellular targeting of Myosin could play a central role in the mechanism of apical constrictions adopted by different cell types.

Cell rearrangements: Cell intercalations

Cell intercalations occur when cells exchange their neighbours in a tissue. This underlies convergent extensions, which lead to tissue extension in one axis without cell divisions [Walck-Shannon and Hardin, 2014]. Cell intercalations require coordination in migration and adhesion of cells, which in turn often requires polarization of cells. Cell intercalations are called as mediolateral, if they occur in the same plane of the tissue, such as in gastrulation and germband extension in flies. They can also be radial, as seen during frog and fish epiboly, that leads to tissue thinning when cells exchange neighbours throughout the thickness of a multi-layered tissue [Walck-Shannon and Hardin, 2014].

Pioneering experiments in vertebrates showed that convergent extensions occur by polarized protrusions in the mediolateral plane of the gastrula mesenchymal cells and is PCP dependent. These make stable attachments with neighbours leading to interdigitation and crawling of cells [Keller, 2002; Keller et al., 2000]. More recently, it was shown that PCP organizes actomyosin contractility during intercalations of vertebrate gastrula mesenchyme cells by a septin mediated compartmentalization of the actomyosin contractile machinery [Shindo and Wallingford, 2014].

The cells which undergo intercalations, exhibit Myosin and junction component polarity before the neighbour exchange [Bertet et al., 2004]. This indicates that Myosin mediated shrinkage of the vertical boundaries may lead to the dorso-ventral movement of cells. During germband intercalations in *Drosophila*, cells remain interconnected via adherens junctions. The contractile actomyosin filaments are enriched at the anterior-posterior boundaries [Irvine and Wieschaus, 1994; Zallen and Wieschaus, 2004]. The planar polarized distribution of contractile actomyosin structures can not only change cell shapes, Myosin II can destabilize intercellular adhesion and PAR- 3 can promote adherens junction stability and localization [Rozbicki et al., 2015].

In *Drosophila* germband extension, convergent extension employs junctional shrinkage mechanism [Zallen, 2007]. Junctional shrinkage is also im-

portant for intercalations in neural tube formation. Cell intercalations can also be directed by the anterior-posterior patterning systems, distinct from the core PCP pathway. In *Drosophila*, striped expression of pair rule genes is required for axis elongation, rosette formation and the polarized distribution of cytoskeletal and junctional proteins [Irvine and Wieschaus, 1994]. Additionally, the pair rule genes regulate the striped expression of *toll* genes providing a positional code which regulates the planar polarity of Myosin and cell intercalations [Paré et al., 2014].

Rosette formations in *Drosophila* germband cells provides an efficient mechanism of cell intercalations [Zallen and Zallen, 2004]. The cells form rows and converge to a point by junction shrinkage and then extend in perpendicular direction by forming new junctions. Besides germband extension, intercalations by rosette formation are also seen in several tube extensions such as the tracheal tubes in *Drosophila*, chick neural tube, renal tubules in mice and *Xenopus laevis* and the cochlea of the mammalian inner ear [Wang and Nathans, 2007].

Actomyosin cables: or tissue-tissue interactions

Supracellular actomyosin cables are formed by polarised actin and Myosin assemblies in a tissue [Röper, 2014]. Unlike intracellular actomyosin cables that are important for cytokinesis, supracellular cables are formed at the apical junctional domains and seemingly stretch across several cells. They function in various processes such as wound healing, delamination, tissue separation, at compartment boundaries and dorsal closure. Actin and Myosin form actomyosin cables by aligning their filaments in a bundle [Munjal and Lecuit, 2014; Röper, 2014]. These bundles can have sarcomere like repeated organization with bipolar Myosin filaments that can generate contractility by sliding the antiparallel actin filaments. In certain instances, actin cables can form with no repeated organization or filament polarity.

The cables are formed when cells of dissimilar types are sensed across the boundary, for e.g., the localized assembly of a cable occurs due to differential

expression of a hemophilic receptor, Echinoid in tissues [Chang et al., 2011]. Within a cell, circumferential actin cables in the junctional domain undergo a purse string like contractility to create apical constrictions, for e.g., at the hinge points during neural tube closure [Abreu-Blanco et al., 2013; Bement et al., 1993]. Due to differential gene expression, cells form homotypic as well as heterotypic contacts and Myosin starts accumulating at the heterotypic contacts. The Table 1.2 provides a detailed summary of cellular process in which actomyosin cables are reported, the upstream signals which have been identified and the molecular anisotropies on either side of the cable that are important for its formation [Röper, 2014].

Identification and analysis of cables from invertebrates and vertebrates have categorized them into three main types of actomyosin cables:

1. **Circumferential cables**, seen in wound healing, dorsal closure and salivary gland invagination [Bement et al., 1993]

2. **Static cables** that maintain compartment identity and prevent tissue mixing [Aliee et al., 2012; Dahmann et al., 2011; Umetsu and Dahmann, 2015]

3. **Short cables** that aid in morphogenesis [Zallen and Wieschaus, 2004].

Circumferential cables function in wound closure. They assemble in cells facing a wound and generate centripetal tension that leads to closure of the gap. Dorsal closure in *Drosophila* is very similar to wound closure and the embryonic epidermis moves in to cover a region previously occupied by extra embryonic amnioserosa cells [Kiehart et al., 2000]. An actomyosin cable forms at the boundary of the epidermis and amnioserosa cells and has a leading edge, which behaves in a “purse string" manner [Franke et al., 2005]. The absence of Echinoid from the leading edge and anisotropic localisation of PCP factors such as Frizzled or Flamingo leads to the accumulation of Myosin at the edge [Kaltschmidt et al., 2002]. In addition, a circumferential actomyosin cable leads to salivary gland invagination in *Drosophila* [Röper, 2012]. In this case,

the cells on the inside boundary, which will form a tube, assemble the cable. The apical polarity complex protein Crumbs is differentially expressed in these cells such that it is reduced at the boundary membrane, which assembles the actomyosin cable. Crumbs recruits the negative regulator of Myosin, aPKC and in the region that lacks Crumbs, ROK phosphorylates and activates Myosin. In addition, Crumbs distribution is also anisotropic in the leading edge during dorsal closure, indicating towards a common mechanism of cable assembly [Röper, 2012].

The second type of cables is seen at compartment boundaries [Dahmann et al., 2011]. These cables are static and prevent the mixing of cells from two different compartments or tissue types. These include the cables present between parasegments in *Drosophila* germband and in the D-V and A-P boundaries in larval wing disc, at the boundary between ectoderm-mesoderm, axial mesoderm-presomitic mesoderm and between the midbrain-hindbrain in the neuroderm in vertebrate brains [Monier et al., 2009, 2011]. In *Drosophila* embryos, the actomyosin cables provide a taut boundary that prevents mixing when cell divisions happen. The *Drosophila* static cables at the parasegment boundaries and the wing are formed by rows of cell on both sides of the cable [Umetsu and Dahmann, 2015]. In the wing discs, Notch signalling mediated depletion of Par3 at the boundary directs cable assembly [Major and Irvine, 2006].

The short actomyosin cables that aid in morphogenesis are dynamic and transient. These cables direct cell rearrangements in epithelial sheets during morphogenesis, such as in germband extension in *Drosophila* [Fernandez-Gonzalez et al., 2009; Zallen, 2007; Zallen and Wieschaus, 2004; Zallen and Zallen, 2004]. The actomyosin cables are formed perpendicular to the axis of extension, over the vertical boundaries of 3-6 cells. The cells are pulled by the cables and forms rosettes, which resolve in the perpendicular direction, leading to cell intercalations. Formation of these short cables requires ROK dependent Par3 depletion from vertical edges, thereby leading to actomyosin enrichment [Simoes and Tepass, 2016]. Similar dynamic Myosin cables are also seen during

Tissue/process	Upstream signal	Molecular asymmetry/ anisotropy
Wound healing (Dm)	H2o2/loss of contact	bazooka, Cadherin?, Crumbs?, echinoid?
Dorsal closure (Dm)	Dpp, JnK, Wg, Notch	Echinoid, Flamingo, Frizzled, Canoe, Dlg, Crumbs?
Parasagment boundaries (Dm)	Notch, Wg	unknown
Wing disc DV boundary (Dm)	Wg, Hh	unknown
Rhombomere / ventricle formation (chick)	unknown	unknown
Germband extension (chick)	pair rule gene expression/ A-P patterning	Rok, Baz, Cadherin, Arm
Neural plate extension/ folding (chick)	PCP: ?	Celsr1/Flamingo, DAAM, RoCK1

Table 1.2: Signalling and molecules involved in actomyosin cable formation

tracheal pit invagination in flies. These cables also form rosettes in vertebrate kidney tubule formation, convergent extensions during neural tube closure in the chick [Wallingford, 2012]. Previous studies in *Tribolium* have hypothesised that a circumferential actomyosin cable might play a role in serosa window closure [Benton et al., 2013; Handel et al., 2000]. The actomyosin dynamics and the associated cellular and mechanical dynamics have remained unexplored. Additionally, the information on epithelial polarity and the upstream signals which might lead to the formation of the cable have also not been studied.

1.5 Thesis objective

Aims of the project

The aim of this project was to study the tissue mechanics which play a

role in serosa expansion and serosa window closure during embryogenesis of *Tribolium*. To study these processes, the project was divided into the following objectives:

Aim I

Set up a live imaging pipeline to provide quantitative description of cell dynamics in developing *Tribolium* embryos using nuclear, membrane and cytoskeletal fluorescent markers

In order to study the tissue mechanics at play during early *Tribolium* embryogenesis a detailed characterisation and quantification of tissue morphogenesis is needed. It is imperative to track nuclei in 3D, and measure a number of cell attributes such as change in cell shapes, apical surface area, cell volume, strain and contacts with neighboring cells over the course of development. For this we needed to standardise a SPIM imaging and analysis pipeline that could generate high resolution developmental movies.

In the first results chapter I have described the image acquisition and analysis workflow in detail. The pipeline includes the following steps: labelling the embryos through mRNA injection, acquisition and processing of 4D SPIM timelapses, visualisation and quantification of 3D data using 2D maps. Using these steps it is possible to create 4D timelapse movies of wildtype and knockdown embryos that are labelled with single or dual colour using nuclear, membrane and cytoskeleton markers. Additionally, it is possible to make quantitative measurements from these movies of tissue dynamics such as cell density and cell area change across the embryo.

Aim II

Study the tissue mechanics during serosa expansion and serosa window closure

Actin and Myosin are the main components of the contractile cytoskeleton machinery in cells. Previous observations in *Tribolium* combined with several

studies in other model systems have suggested a major role for actomyosin networks in mediating cell shape changes, cell rearrangements and global tissue rearrangements during embryogenesis.

In order to study their contribution towards tissue mechanics in the beetle, the first step was to clone and characterise the non-muscle Myosin II and describe its dynamics. The results for this are described in the second chapter. With establishment of imaging and labelling tools for studying actomyosin mediated cell dynamics, it becomes possible to investigate specific morphogenesis events. In the third results chapter, I have focused on the process of serosa expansion and serosa window closure. My results indicate that a contractile actomyosin cable forms between the serosa and the amnion and functions during serosa window closure. I have characterised the cable formation, it's dynamics and the tension change in the cable and the serosa tissue during development. The serosa tissue changes in its mechanical properties during expansion and the tensions in the cable increase overtime, as it becomes harder to pull the serosa around the embryo. These results pave ways for future studies on actomyosin cable formation and dynamics, the mechanisms leading to formation of continuous serosa epithelium and conserved actomyosin dynamics across insects.

CHAPTER 2

4D LIGHTSHEET IMAGING AND ANALYSIS PIPELINE OF *Tribolium* EMBRYOS

Introduction

Fluorescent live imaging has been very recently adapted for *Tribolium* embryogenesis [Benton et al., 2013; Hilbrant et al., 2016; Strobl and Stelzer, 2014]. It is possible to create transgenic lines for the beetle using piggyBac or Minos-based transposons and a few transgenic lines which label nuclei (EFA-nGFP [Sarrazin et al., 2012], Hist::eGFP, Peter Kitzmann unpublished) and Actin (LA::eGFP)[van Drongelen and Vazquez-Faci, 2017] have been created. Additionally, a new method established transient fluorescent labelling approaches for imaging the embryos circumventing the necessity of establishing transgenic lines for live imaging of cytoskeleton and other proteins[Benton et al., 2013]. Using this approach, eggs were injected with mRNA encoding the nuclear and membrane fluorescent markers Histone::mCherry and GAP43::eYFP, respectively, and were then imaged using timelapse confocal

microscopy [Benton et al., 2013]. However, the low temporal resolution (5 minutes), photo-bleaching, and the restricted imaging field and depth achieved with conventional confocal microscopes provided limited access to single cell behaviours and allowed primarily the tracking of tissue-level dynamics. In order to study the various morphogenetic events in the *Tribolium* embryo at a higher spatial and temporal resolution, I decided to image early embryogenesis using the **S**elective **P**lane **I**llumination **M**icroscopy **(SPIM)** implementation of lightsheet fluorescence microscopy. Lightsheet microscopy allows the imaging and computational reconstructions of developing embryos in their entirety by imaging them from multiple views, with minimal photo-bleaching and photo-damaging, at high spatiotemporal resolution, and over long periods of time [Huisken and Stainier, 2009; Huisken et al., 2004; Keller et al., 2008; Pitrone et al., 2013; Wolff et al., 2017]. In all my SPIM imaging experiments, I used the Zeiss lightsheet 1 (LZ1) instrument to collect multi-view and image datasets of *Tribolium* early embryonic development.

In this chapter, I have compiled my methodologies in a coherent pipeline for SPIM image acquisition, image processing and data analysis that can provide quantitative measurements for the entire embryo. First, I established a protocol for robust labelling and imaging of *Tribolium* embryos with the Zeiss lightsheet 1 (LZ1), a commercially available instrument from Zeiss. Alternatively, the pipeline is also applicable for datasets that are acquired with custom made LSFM microscopes or from open access platforms like OpenSPIM [Pitrone et al., 2013]. Second, I use map projections of the data as a tool to manage large scale 3D datasets into convenient 2D images. Lastly, I present a few examples of quantifications of cell and tissue dynamics which can be made using the map projections: 1) nuclear flow fields that could serve as a proxy to understand the forces exerted in the blastodermal epithelium as previously shown in *Drosophila* [He et al., 2014], 2) cell shape, cell apical area changes and measuring cell anistropy contributing to the epiboly of the serosa tissue and condensation of the embryonic primordium an be measured to quantify epithelial development [Guirao et al., 2015]. Using these methods it becomes

possible to compare wildtype with genetically perturbed embryos, such as after embryonic RNAi knock-down of the *Tribolium zerknüllt 1* (Tc-zen1), *Tc-zen* gene.

2.1 Standardisation of an injection protocol for sample mounting and imaging with the Zeiss LZ1 SPIM

The most commonly used *Tribolium* transgenic line for live imaging has been the EFA-nGFP [Koelzer et al., 2015; Sarrazin et al., 2012; Strobl and Stelzer, 2014] that labels the nuclei during interphase but not during mitosis. However, for my imaging needs I had to label nuclei throughout the cell cycle, as well as the membranes, Actin or Myosin II either in single or double labelling experiments. Therefore, I decided to adopt the injection protocol from Benton et al. [2013], since it is a much faster and flexible approach than establishing transgenic lines, and it provides uniform and bright single or double labelling to image early embryogenesis.

In previous experiments, *Tribolium* eggs were injected while covered in halocarbon oil to prevent desiccation and they were imaged under a confocal microscope with oil dipping objectives. However, imaging with the LZ1 SPIM is done in water with water dipping objectives and the embryos are typically mounted in low melting agarose extruded from glass capillaries [Schmied et al., 2016]. The original injection protocol raised several problems, since I couldn't remove the halocarbon oil entirely post-injection and removal of the embryo from the injection slide invariably resulted in eggs bursting or not developing further. To address these problems, I established an alternative method that results in minimum disturbance to the injected eggs shown in Fig 2.1. I first make an agar bed onto glass slides by pouring about 750 μl of 1% agarose (in PBS or water) onto the slide (Fig 2.1 A, C). Once the agar dries the embryos are aligned with a thin soft brush onto the solidified agarose

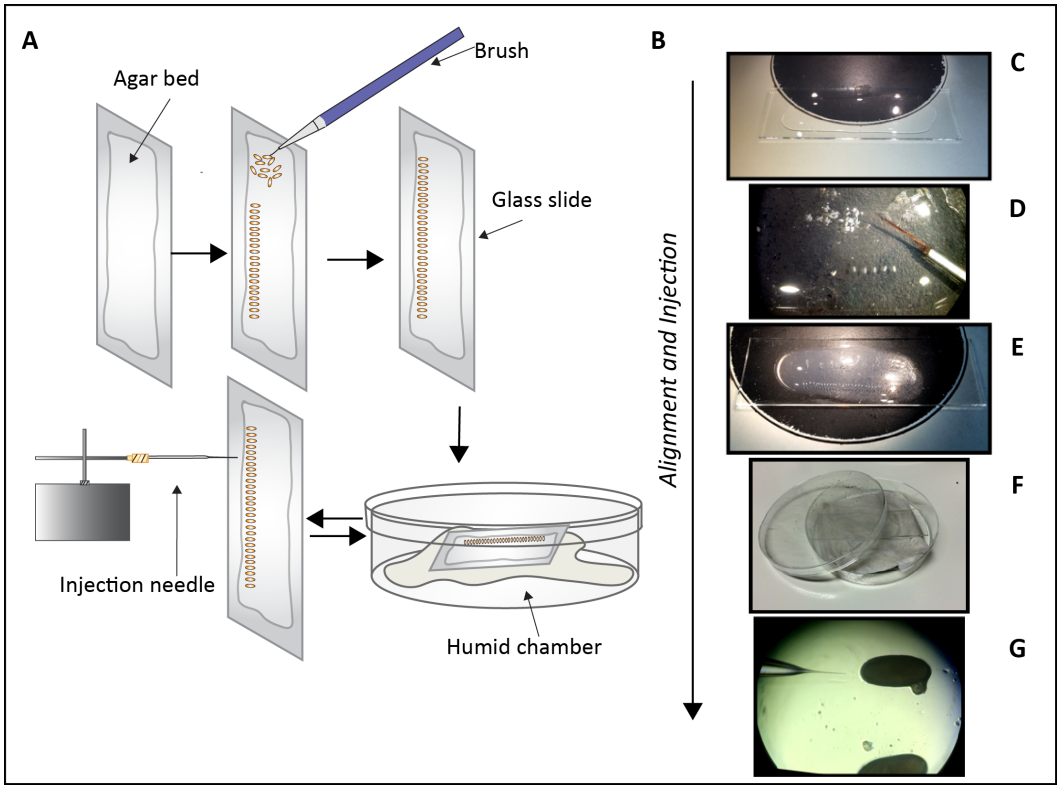

Figure 2.1: Injection method for labelling embryos. (A) Illustrations outline the injection method that is used for injecting mRNA and dsRNA to the embryos. **B)** Pictures showing the alignment and injection of *Tribolium* embryos. **C)** An agar bed is made on a glass slide with about 750μl of 1% agarose solution. **D, E)** The embryos are lined onto agar bed with a soft brush. **F)** They are incubated in humid chambers before and after injection. **G)** Image of the injection needle and an embryo through the stereoscope.

with their anterior poles facing the edge of the slide (Fig 2.1 D). Within 1-2 minutes of drying, the eggs stick to the agarose bed. The slides with the aligned eggs are then transferred in high humidity chambers made by putting wet tissues in plastic Petri plates till they are injected (Fig 2.1 F). Embryos are transferred immediately into the humid chambers after injections and aged for 2-3 hours at 32°C to allow for a strong and homogeneous labelling. The eggs detach easily from the agarose by adding a few drops of PBS or water. Embryos exhibiting the most uniform and strong fluorescence under an epifluorescence stereoscope are then mounted individually into capillaries. The embryos are

first transferred into an agarose: fluorescent microsphere mixture (1% agar in PBS or water + 1:1000 beads) as previously described [Preibisch et al., 2010; Schmied and Tomancak, 2016] and are then sucked into capillaries. After agarose solidification, the capillaries are mounted onto the LZ1 microscope for imaging. This technique allows for survival of about 50% of the injected and imaged embryos.

2.2 Double labelling of *Tribolium* embryos

To test combinations of the histone (nuclear), GAP43 (membrane), LifeAct (actin) and Tc-sqh (myosin II) labels, they were fused with different green and red fluorescent proteins and cloned in appropriate vectors for in vitro transcription (PCS2+ or pT7 plasmid vectors). I then tested and established the best combinations based on the following parameters: brightest signal, minimum photobleaching, spectral separation of the tested pair and ease of screening of the injected embryos under an epifluorescent stereoscope. Table 2.1 summarises the different available mRNA options for labelling. These mRNAs offered several possibilities for uniform dual colour labelling of different molecules, nuclei and cells. An example of double nuclear (Hist::mCherry) and Actin (LifeAct::eGFP) labelled embryo is shown in Fig 2.2. It was imaged with the LZI SPIM from different views such as dorsally (Fig 2.2 A) and ventrally (Fig 2.2 B) and the image stacks were projected as a maximum intensity projections.

2.3 Image processing with Fiji

Embryos were imaged overnight for about 16 hours at 25°C or 32°C starting from the uniform blastoderm stage (≈9Hrs AEL). The image processing using Fiji was adapted from the *Drosophila* protocols 2012; 2014. Each dataset ranged in size from 1-2 Tb depending on the number of channels (single or double) and other imaging parameters. The data were saved in the Zeiss czi

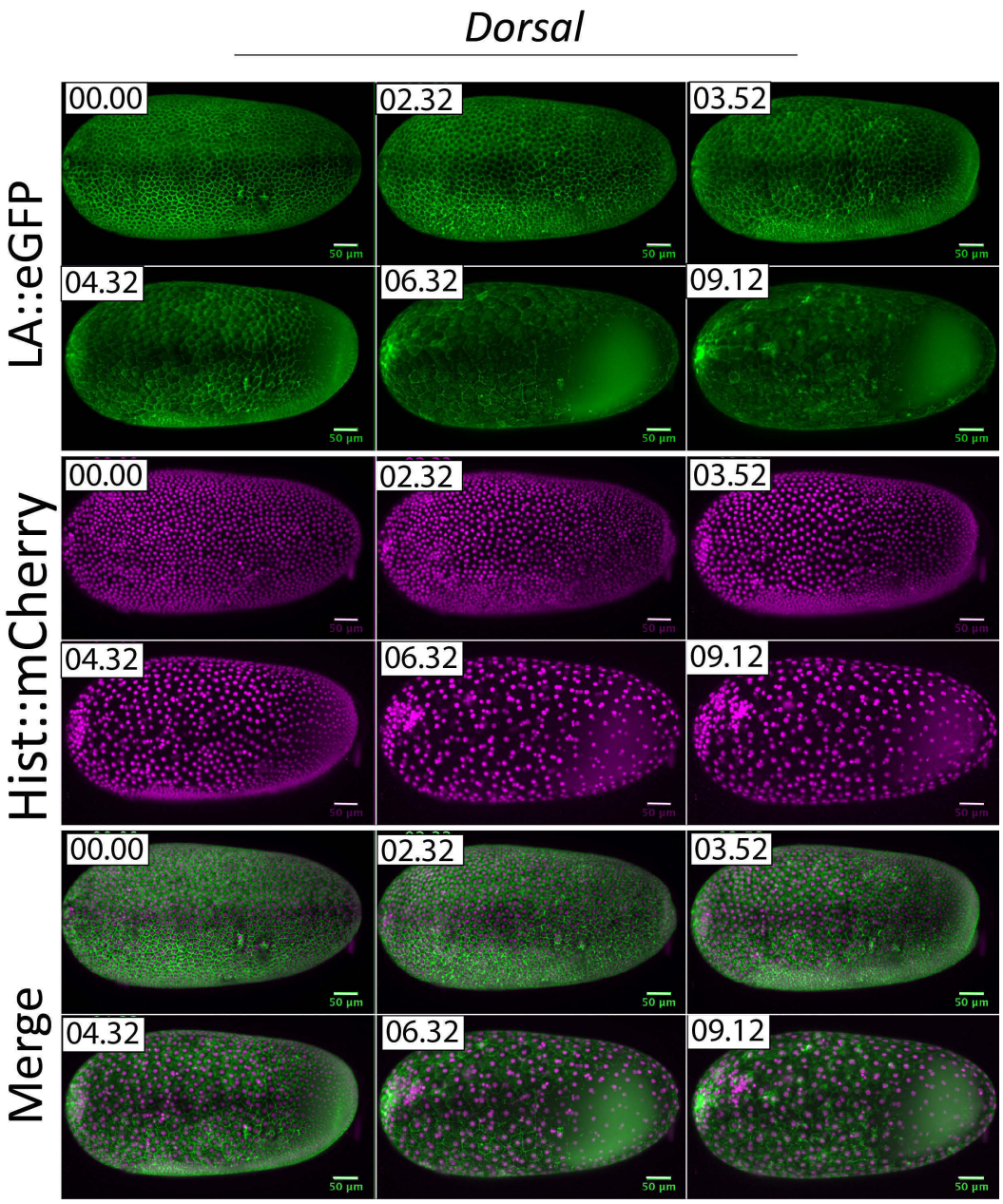

Figure 2.2: Dorsal view of double labelled embryos injected with mRNA and imaged with SPIM. Maximum intensity projections of a single (dorsal) view from a timelapse movie acquired using SPIM. The embryo was injected with mRNA to label Actin with lifeAct::eGFP and nuclei with Histone::mCherry. Times are given relative to the uniform blastoderm stage which is taken as T-0. Time 0 corresponds to ≈9 hours (± 30 minutes) after egg lay, and to ≈0.5 hour (± 20 minutes) after the 12th round of divisions. Scale bar is 50 μm.

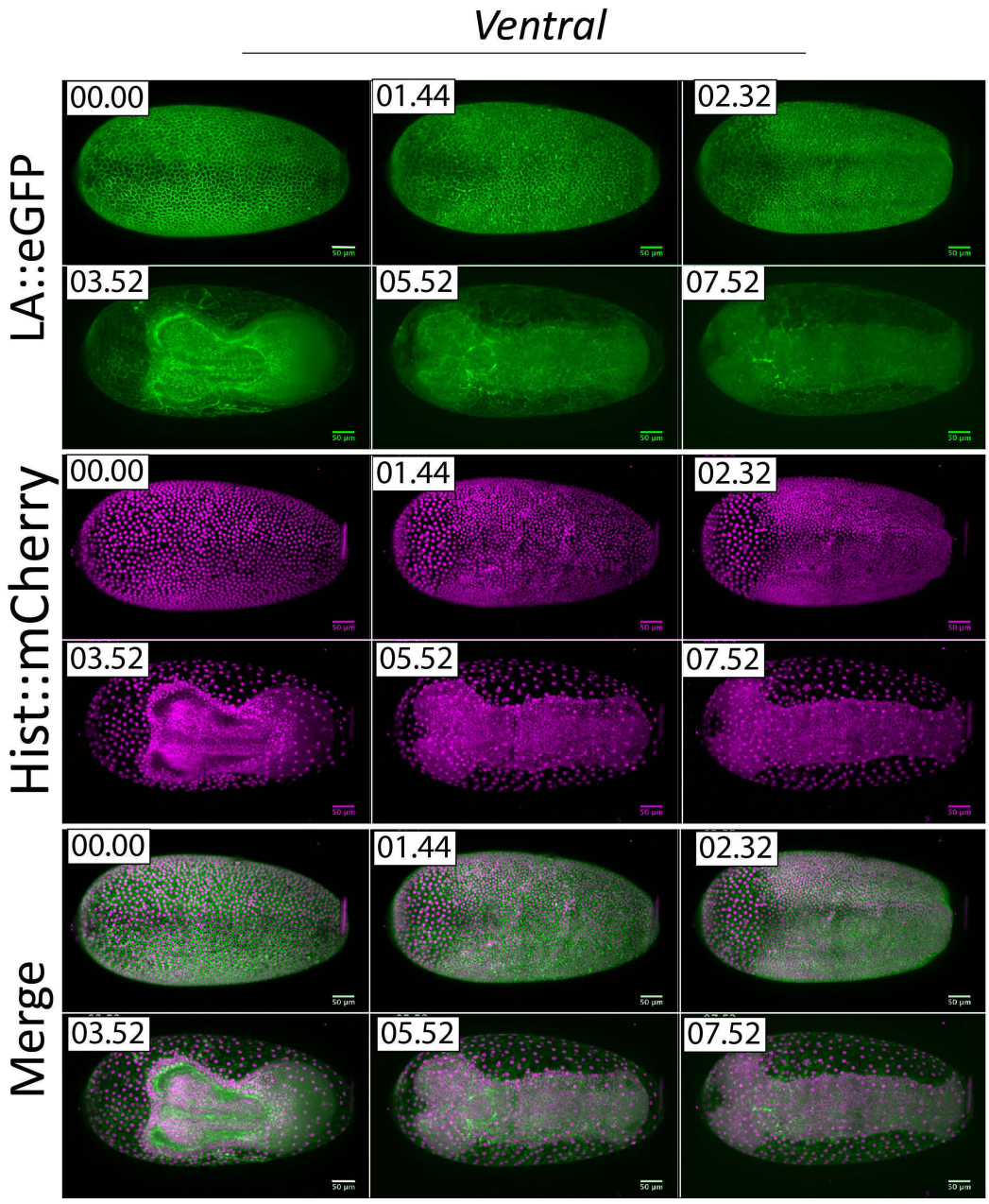

Figure 2.3: Ventral view of double labelled embryos imaged with SPIM. Maximum intensity projections of a single (ventral) view in a timelapse movie acquired using SPIM. The embryo was injected with mRNA to label Actin with lifeAct::eGFP (LA::eGFP) and nuclei with Histone::mCherry (Hist::mCherry).Times are given relative to the uniform blastoderm stage which is taken as T-0. Time 0 corresponds to ≈9 hours (± 30 minutes) after egg lay, and to ≈0.5 hour (± 20 minutes) after the 12th round of divisions. Scale bar is 50 μm.

Label	Green (488)	Yellow (515)	Red (561,594)
Membrane		GAP43::YFP	GAP43::mKate2
Nuclei	Hist::eGFP		Hist::RFPruby Hist::mCherry
Actin	LifeAct:EGFP Syn21LA::eGFP		LifeAct::mKate2 LifeAct::mCherry
Myosin	TcSqsh:eGFP Syn21TcSqsh:eGFP		TcSqsh::RFPruby

Table 2.1: Fusion constructs for fluorescence imaging with mRNA injections.

file format with each file containing the data for the acquired channels, in each angle and each time-point. I then processed the movies to combine the different views using the Multiview reconstruction plugin in Fiji [Preibisch et al., 2014, 2010]. The various steps in this plugin involved: defining an xml file for the dataset, resaving the dataset into the hdf5 file format, segmentation of the beads in each angle, bead-based registration of the different views in each time-point, temporal registration across timepoints, cropping of the registered volume by defining a bounding box, and fusion of the registered input angles into a single output volume in each time-point using either a content-based algorithm or a multi-view deconvolution step [Preibisch et al., 2010; Schmied et al., 2014].

Overview of LSFM image processing pipeline

1. **Image file preprocessing**:

   During a multiview LSFM timelapse recording, each acquired timepoint is composed of multiple z-stacks corresponding to the different views and channels. The first task involves opening the raw data and resaving often in a new file format (like .tif, hdf5 or other formats offering lossless compression for smaller file size). This step is often accompanied by file renaming to encode the metadata information in the file name (i.e. which time point, view, or channel the file contains).

2. **Dataset Definition**

   (Plugins>Multiview Reconstruction>Define MultiView Dataset):

   The Multiview Reconstruction Fiji plugin enables users to define the multiview LSFM dataset and create an XML file that is used to access the image data and perform all subsequent processing steps.The XML file that is created retains all the information regarding the complete dataset.

3. **Detect Interest Points for Registration**

   (Plugins>Multiview Reconstruction> Detect Interest Points for Registration):

   The next step is to find interest points in the images that will be used for registration, like fluorescent beads, nuclei or membrane markers. I used fluorescent beads embedded in the mounting medium together with the embryo as markers to align the different views to each other (Estapor microspheres, X beads for green channel only, Y for red channel). The beads in each view are identified (segmented) based on their size and intensity. The sigma value for my datasets varied between 0.899 to 1.035 and the threshold usually between 0.0024 - 0.0050.

4. **Multiview registration**

   (Plugins>Multiview Reconstruction> Register Dataset based on Interest Points):

   Segmented beads are then matched between the different views in each time point, and the views are aligned (registered) resulting in a transformation model for each view that is able to arrange the views optimally in 3D space with respect to each other (spatial registration)(Fig 2.4, A). Registration is then extended between time points for correcting drift in the sample that often occurs over time, (timelapse registration).

5. **Multiview fusion**

(Plugins>Multiview Reconstruction> Fuse/Deconvolve Dataset):

Once the entire dataset is aligned, the individual views can be fused together (using the transformation parameters from step 4) into a single output 3D image per time point and channel with a more isotropic resolution (Fig 2.4, B, C). Voxel intensities in the fused image can be calculated by just averaging between input views, by content-based algorithms, or by multiview deconvolution for a best signal-to-noise ratio (this is by far the most computationally demanding step in the pipeline) [Preibisch et al., 2014, 2010]. Deconvolution requires the knowledge of point spread functions (PSFs), which can be extracted from the segmented fluorescent beads. Alternatively, one can proceed directly after registration to data visualization and tracking without fusion.

Finally, the different views are fused to give a complete 3D image of the entire embryo. Fig 2.4, shows the 5 individual views that were acquired in one timepoint and then fused to cover the entire volume. The fused embryo can be rendered in any desired view (e.g. lateral, ventral, dorsal or the anterior and posterior polar views).

Previous work in the lab has established a processing pipeline for *Drosophila* embryogenesis data with this plugin. However, due to the large size of the data it can take almost a week to processing one dataset on a workstation. Therefore, Schmied et al. [2016] also established an automated workflow for parallel processing of large datasets on a computer cluster using the snakemake workflow system. I optimised the parameters for multiview processing using Fiji and then adapted the snakemake workflow scripts for *Tribolium* SPIM datasets. In practical terms, I processed three timepoints across the dataset on a local workstation to estimate the various parameters to be applied to all timepoints. I then used these parameters and processed the entire dataset on the cluster. This reduced the total time required for processing each dataset to about 2 days.

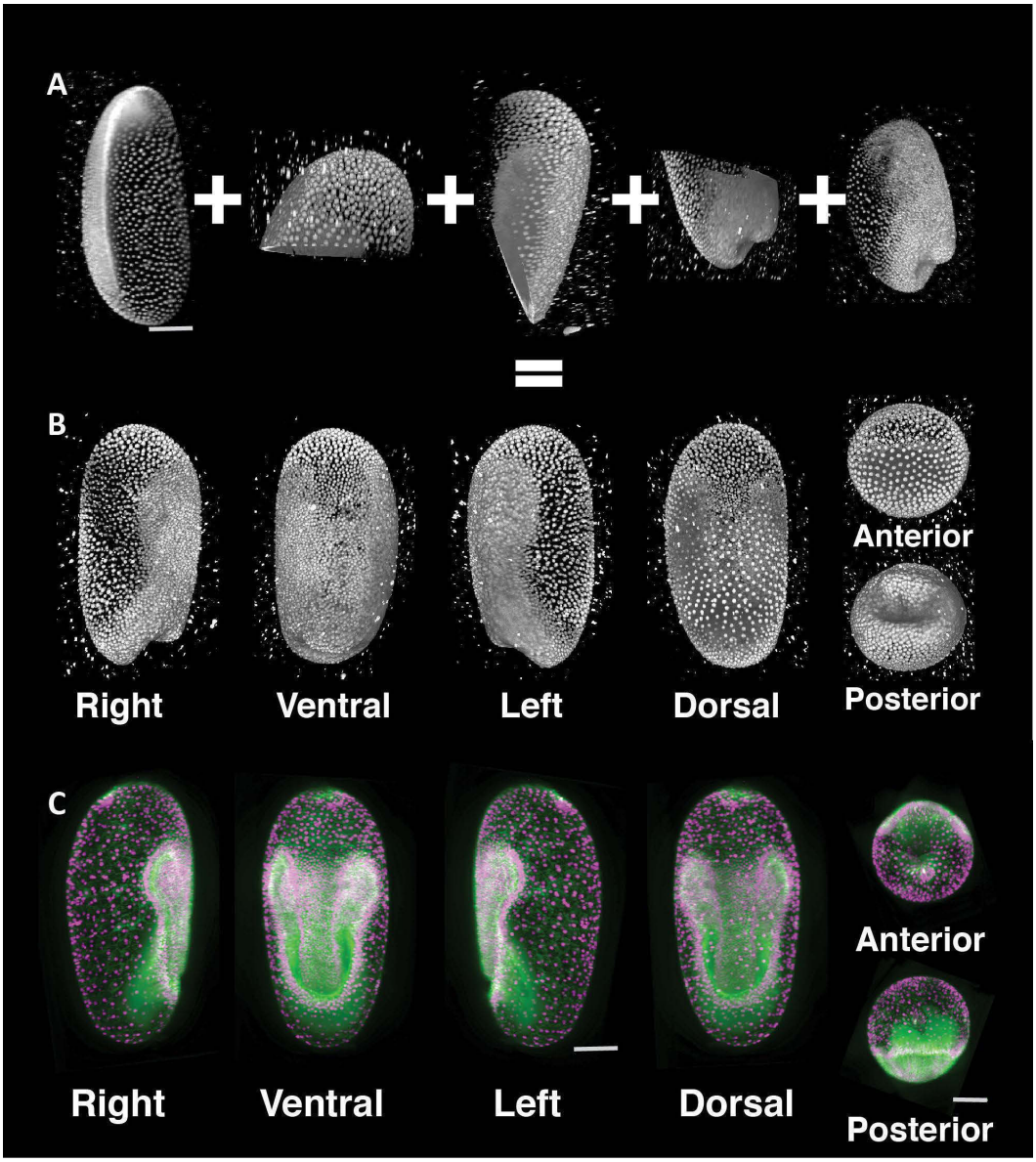

Figure 2.4: Multiview reconstruction and image processing with Fiji SPIM imaging was done on transgenic *Tribolium* embryos that uniformly expresses H2A::GFP **(A)** driven under αTubulin promoter (kindly provided to us by Peter Kitzmann, Bucher lab) and transiently labelled embryos that were injected with mRNA to label Actin with lifeAct::eGFP and nuclei with Histone::mCherry **(C)**. **(A)** Shows the five different views that were simultaneously imaged.**(B)** Fused output after registration, fusion and 3D rendering from the same. **(C)** Fused output after image registration and fusion from a transiently labelled embryo.

2.4 Long term timelapse imaging of *Tribolium* embryogenesis with SPIM

Once I optimized the conditions for injecting and labelling embryos with Zeiss SPIM setup, I tested a number of image acquisition parameters with the LZ1. The *Tribolium* embryos are about 500 μm long and 300 μm wide. They fit well in the field of view obtained with a 20X detection objective and with an optical zoom of 0.6-0.7X

The LZ1 microscope offers the possibility for embryo translation (move in x, y, z) and rotation during imaging. The best spatial resolution is achieved with higher number of acquired angles to maximise the overlap in different regions of the sample and the best temporal resolutions require the smaller number of acquired angles to make the acquisition faster. In order to achieve a time interval between 30 seconds to 2-minute between successive timepoints, I first tested the image quality obtained with different number of overlapping views to achieve the best trade-off between spatial and temporal resolution. I imaged a double labelled embryo from 4 views, spaced at (0°, 45°, 135° and 180° angles) (Fig 2.5, A). This results in a partial overlap of 3, 4 or 5 views in different regions of the embryo . I then assessed the quality of the fused volumes (Fig 2.5 B, B').

The views were registered, fused and deconvolved using the Fiji plugins, as described in the previous section. I observed that the best image quality is seen in regions which are sampled from 4, 3 and then 2 neighbouring views(indicated by numbers in Fig 2.5, B) while the image quality deteriorates in regions imaged from a single view and at the edges of two imaging frames (Fig 2.5, B').

The development of the embryo is fastest at higher temperatures and it slows down considerable at lower temperatures [Gregor, 2009; HOWE, 1967]. Additionally, the exposure time of the camera, the size of the optical slices and the rest time between successive acquisitions also lead to increased or decreased time resolutions. Therefore, I also tried different combinations of

these parameters , as listed in table 2.2 to increase the temporal resolution.

Temperatures	32° C	27°C	25°C	22°C
Camera exposure time	30ms	50ms		
Views	3	4	5	
Z step	1.5μm	2μm		
Rest time	60 S	20-30 s	No rest	

Table 2.2: Imaging conditions tested with Zeiss LZ1

I observed that imaging the embryo from 3 angles spaced at 120° and with about 90 optical slices acquired every 2μm in each angle, is sufficient to cover the entire embryo (Fig 2.5 C). These conditions provide the fastest temporal sampling of 60-90 sec at the expense of image quality, due to the small overlap between acquired angles (Fig 2.5 B, C); the signal deteriorates with depth and at the edges of the acquired z-stacks and cannot be improved computationally after multi-view fusion. The image quality improves with 4 angles acquired every 90° or 5 angles acquired every 72° each (Fig 2.5 B, B'). Imaging 5 angles provides sufficient overlap such that every region of the embryo is imaged from at least 2 neighbouring views (Fig 2.5 C). It also provides the best trade-off between temporal resolution (between 1-2 minutes) and spatial resolution. I decided to image the embryos with 5 overlapping views at 25° or 32°C in most of my experiments, with 2μm optical slicing, 30msec camera exposure time and 30-60s rest time between successive acquisitions. These conditions provided optimum spatial and temporal resolution for downstream data analysis steps.

After these optimization experiments, injected or transgenic *Tribolium* embryos were routinely imaged with a temporal resolution ranging between 1.5 to 2 min. Such a high temporal sampling of *Tribolium* early embryogenesis has not been reported previously with either confocal or lightsheet imaging. The raw and fused data could be visualized with the BigDataViewer plugin in Fiji [Pietzsch et al., 2015] sliced in any desired orientation or they could be rendered using the Fiji 3D Viewer or simple maximum projections. The

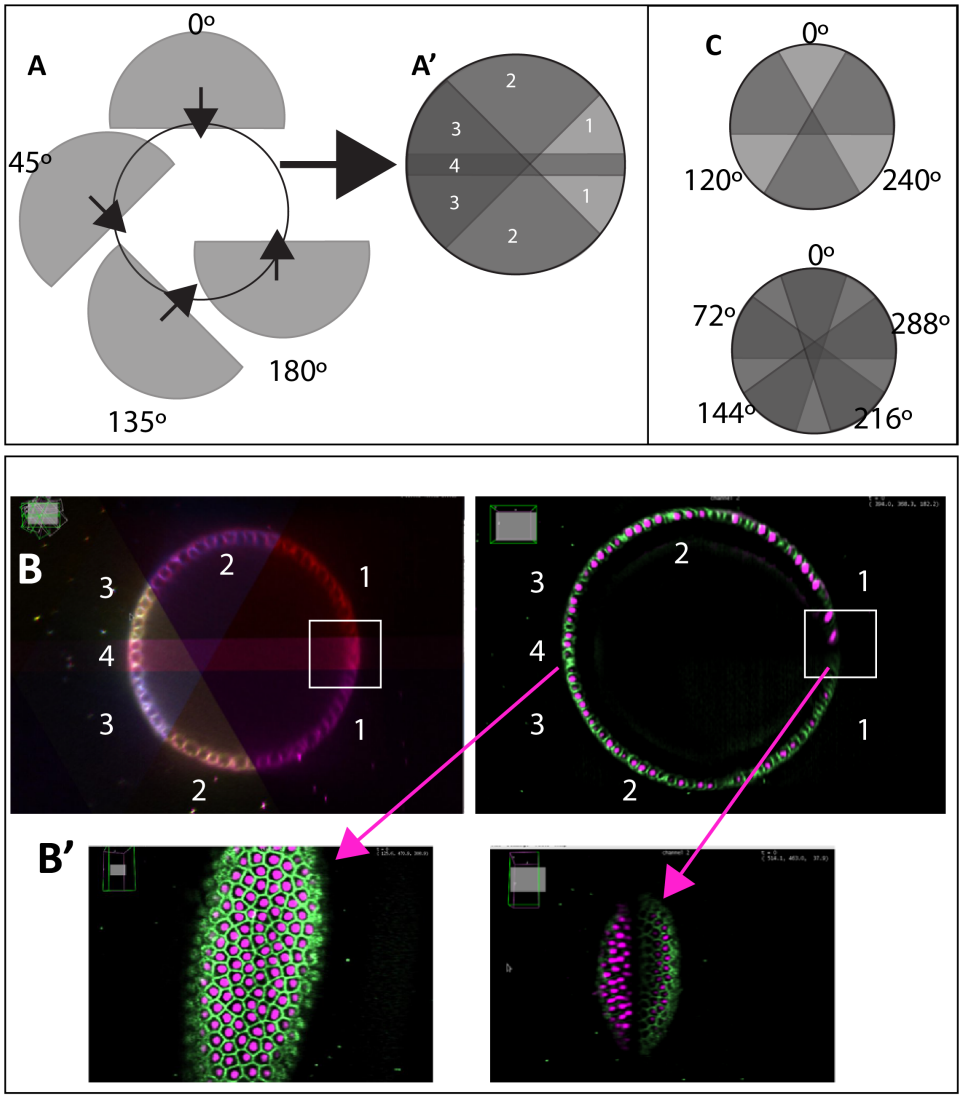

Figure 2.5: Standardisation of Multiview acquisition parameters. A) Schematic showing the acquisition angles in a Multiview imaged embryo. The embryo was imaged from 0°,45°,135° and 180° as shown. **A'** Following image registration, different regions of the embryo show non-uniform overlap as indicated by the numbers. **B)** Cross section of a multiview registered, fused and deconvolved dataset. Numbers correspond to the number of overlapping regions. The box indicates comparable regions between registered angles and the fused output. **B')** Surface projection from a 4 angle overlap region and a 2 angle overlap region. **C)** Illustrates imaging with 3 overlapping views and 5 overlapping views collected every 120° or 72 ° respectively. Darker regions indicate higher overlap.

defined imaging parameters resulted in single cell and nuclear resolution in the volumetric rendering and cross sections (Fig 2.6 I and II) (Fig 2.6 III). This high spatial resolution was observed both in the superficial enveloping serosa layer, as well as with the inner tissues like the involuting amnion, the condensing ectoderm and the internalizing mesoderm. Overall, this imaging strategy provided the opportunity to observe the nuclear and cellular behaviours simultaneously in different regions of the embryo and compare their dynamics.

2.5 2D cartographic projections of 3D data as a method to visualise and analyse SPIM data

One of the most prominent issues with SPIM imaging is the multi-dimensionality and very large size of each acquired dataset that complicate downstream visualization and analysis. A typical dataset consisted of several hundred timepoints acquired every 1.5-2 min over 10-16 hours of development, with each timepoint containing several 3-4 GB z-stacks corresponding to the different angles and channels. Currently, commercial software for image analysis (e.g. Imaris, Amira etc.) are not able to handle this type of datasets. The few segmentation and quantification pipelines that have been established and that can deal with the raw or fused SPIM datasets, also require very serious investment in time and effort [Amat et al., 2015, 2014; Stegmaier et al., 2016; Wolff et al., 2017]. An alternative method that has come up is to projected the 3D datasets as 2D cartographic maps [Heemskerk and Streichan, 2015; Schmid et al., 2013]. This method allows for easy handling and visualising of large size datasets. Therefore, I decided to use tissue cartography as a method to reduce the dimensionality and size of my datasets, in order to accelerate the extraction of biologically meaningful information.

Tissue cartography entails the projection of regular or irregular 3D curved

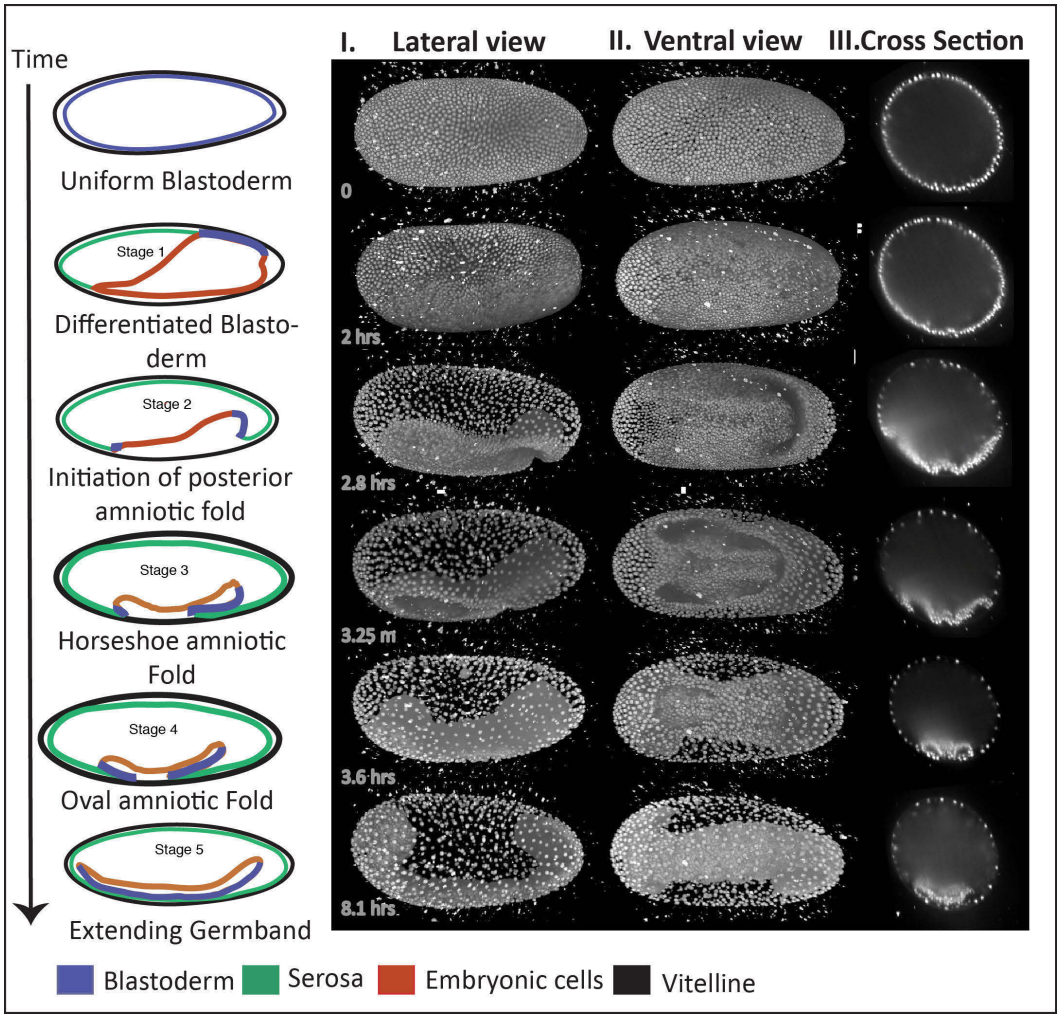

Figure 2.6: Timelapse imaging of *Tribolium* embryos using SPIM Fused and 3D rendered SPIM images of a transgenic *Tribolium* embryo that uniformly expresses H2A::GFP driven under Tubulin promoter (kindly provided to us by Peter Kitzmann, Bucher lab). The schematic on the left shows the different stages of embryogenesis. I. Lateral view of the fused data II. Ventral view and III. Cross section showing different layers in the embryo. Times are given relative to the uniform blastoderm stage which is shown as T-0. Time 0 corresponds to ≈9 hours (±30 minutes) after egg lay, and to ≈0.5 hour (±20 minutes) after the 12th round of divisions

data onto a 2D surface in a manner analogous to making maps of Earth that show geographic data on a flat grid of longitude and latitude. Tissue cartography was established recently as a method to exploit the spherical

or ellipsoidal shape of imaged samples such as zebrafish and *Drosophila* [Schmid et al., 2013] (Fig2.7). Such layered samples can be transformed into a surface of interest (SOI) by computing a radial maximum intensity projection. After this step, the visualization and analysis of the desired process becomes straightforward as the multi-dimensional SPIM datasets are transformed into manageable 2D, unwrapped projections. For my *Tribolium* SPIM datasets, I used a comprehensive and open access method for tissue cartography called as **ImSAnE (Image Surface Analysis Environment)** that deals with a key issue in cartography: it allows corrections for the distortions that are inherent to the mapping of curved surfaces onto a plane, thereby allowing the measurement of geometric quantities like size, shape, direction and velocity [Heemskerk and Streichan, 2015]. ImSAnE is an open-source MATLAB toolbox that can be used to identify SOIs in the embryo, map SOIs onto several layers at specified distance based on their z depth in the embryo, and stores the geometric metadata for corrected measurements (Fig 2.7). The ImSANE workflow for creating 2D maps for *Tribolium* data includes the following steps:

1. Recognise the SOIs in the embryo using the open-source software for image segmentation Ilastik (Fig 2.8) [Sommer et al., 2011].

2. Export a point cloud representing the SOI to MATLAB and visualise it in 3D (Fig 2.9 A).

3. Fit a sphere or cylinder to the point cloud (Fig 2.9 B).

4. Construct a bounding box around the sample based on the fitted sphere or cylinder.

5. Project the data onto various maps including a cylindrical projection (Fig 2.9 C), an area-preserving map and polar maps.

6. In collaboration with Robert Haase (Scientific Image Analysis facility in the MPI-CBG), Sebastian Streichan (KITP, UCSB) and Vladimir Ulman

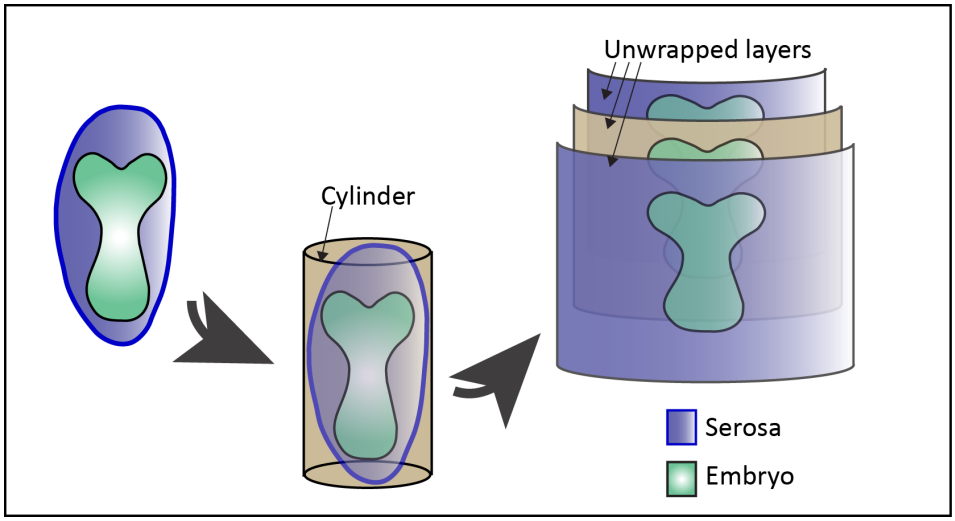

Figure 2.7: Principle of 2D maps projected using ImSANE Schematic shows the principle of cartographic projections. A cylinder is fitted to the embryo and the surface is unrolled into layers with specified thickness.

(Tomancak lab), I developed tools to quantify a number of nuclear and cellular parameters on reconstructed maps.

Using this workflow, I generated 2D projections for SPIM imaged normal or genetically perturbed embryos labelled with the a different combinations of fluorescent reporters as listed in the table 2.1: EFA::nGFP, Hist::eGFP, GAP43::YFP and Hist::mCherry , LA::eGFP and Hist::mCherry, LA::eGFP and nGFP, TcSqsh::eGFP, LA::eGFP with *Tc-zen1* Knockdown, LA::eGFP and Hist::mCherry with *Tc-zen1* Knockdown, LA::eGFP and Hist::mCherry with *Tc-caudal* Knockdown.

An example 2D+t map projections of an embryo expressing H2A::GFP is shown in Fig 2.10. This embryo was imaged for 13 hours at 22°C from the uniform blastoderm stage to serosa window closure and early germband extension. It was imaged from 3 views spaced at 90° apart and was registered and fused using multiview reconstruction plugin in Fiji, as described before. In these maps, I aimed to measure the total number of serosa and embryonic nuclei over time and reconstruct their trajectories, to measure the relative contribution

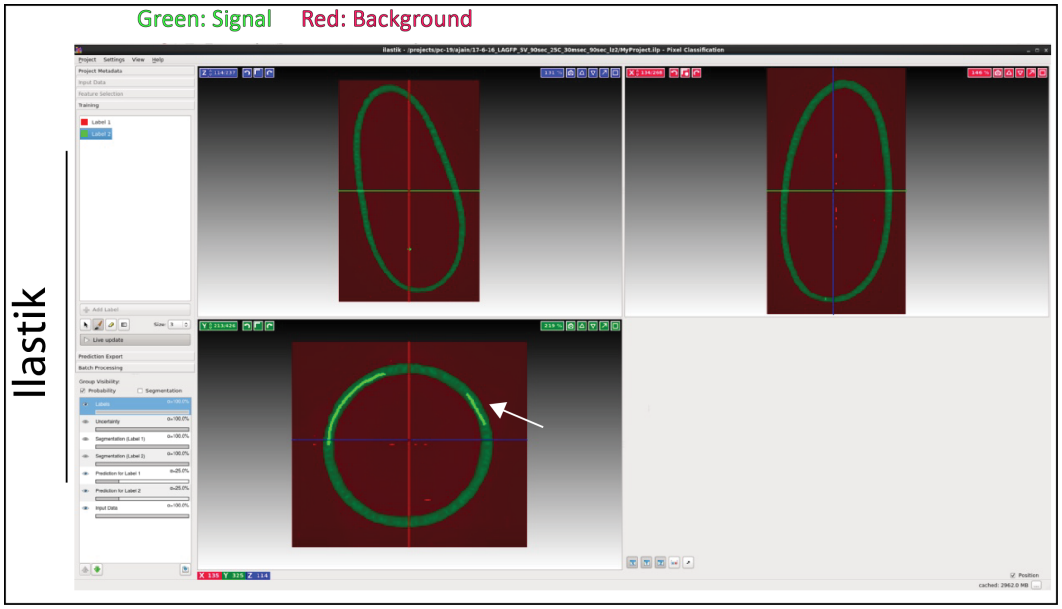

Figure 2.8: Segmentaion using Ilastik for generating 2D maps using ImSANE Ilastik is used to recognise the surface of the embryos. In green is the predicted region with the fluorescent signal and red is the background. Arrow points to the region where green lines were painted onto the embryo surface.

of the two tissues to the outer surface and compare their velocities to understand the rate of serosa expansion. The analysis of membrane-labeled embryos could also reveal the cell shape changes and their anisotropies during embryo development. These measurements will be performed in wildtype and RNAi knockdown backgrounds for a systematic comparison of their morphogenetic repertoires.

Quantification of cellular and nuclear dynamics from map projections of 4D SPIM data

To make these measurements accurately from 2D maps, it is absolutely necessary to correct the distortions arising from tissue projection. The transformed 2D maps are especially distorted at the anterior and posterior poles of the embryos as seen by the unnaturally large nuclei in these regions. To achieve

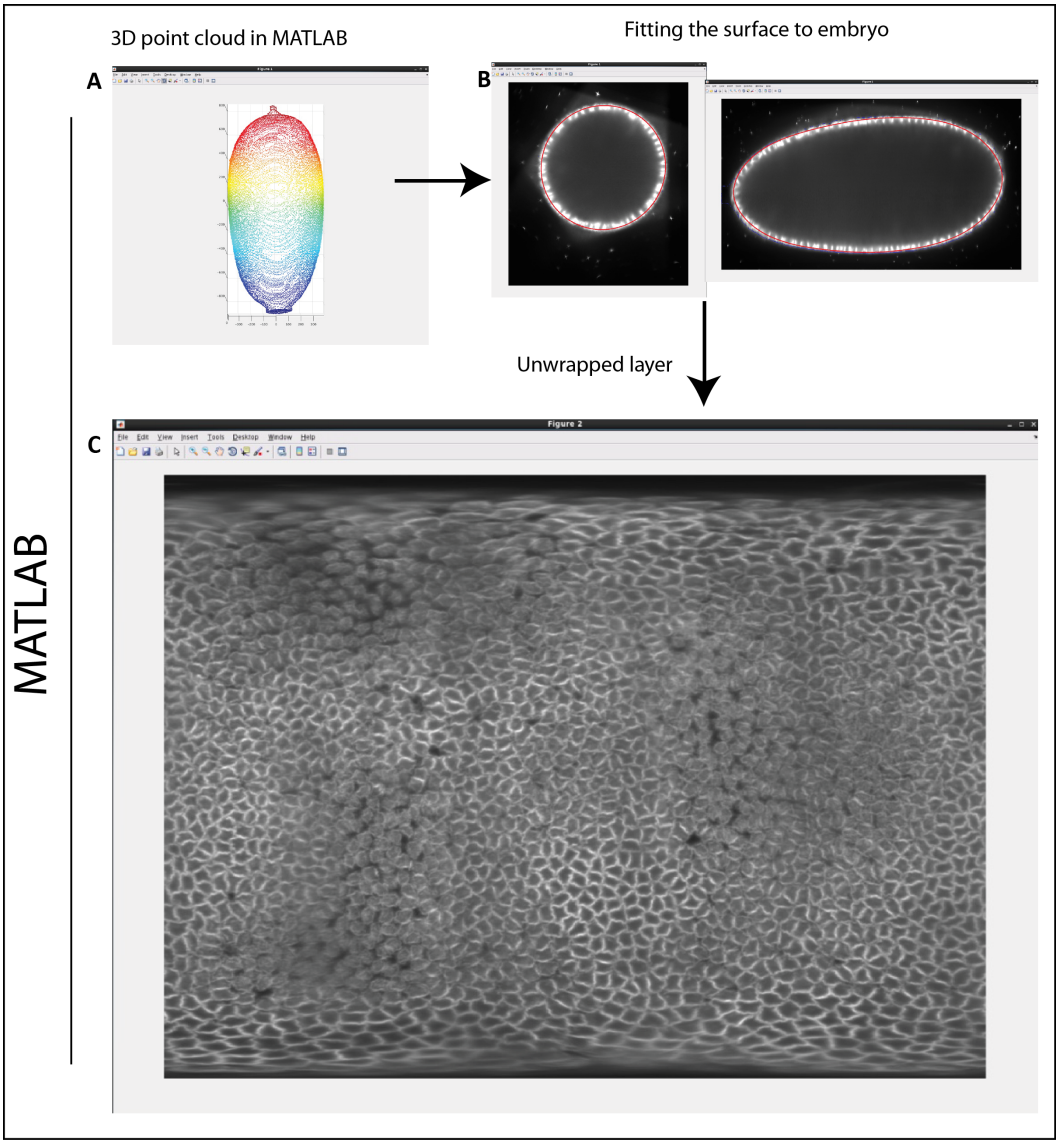

Figure 2.9: MATLAB steps for data projection using ImSANE The 3D point cloud which represents the surface of the embryo is visualised in MATLAB. The fitting of the surface is shown in red in a cross section and lateral section. The unfolded 3D embryo is unwrapped into a cylindrical projection as shown.

this, the nuclei or membranes are segmented using Ilastik [Sommer et al., 2011] to generate binary images (present 1, not present 0). These images are analysed by Fiji plugins generated by Robert Haase (MPI-CBG Image Analysis

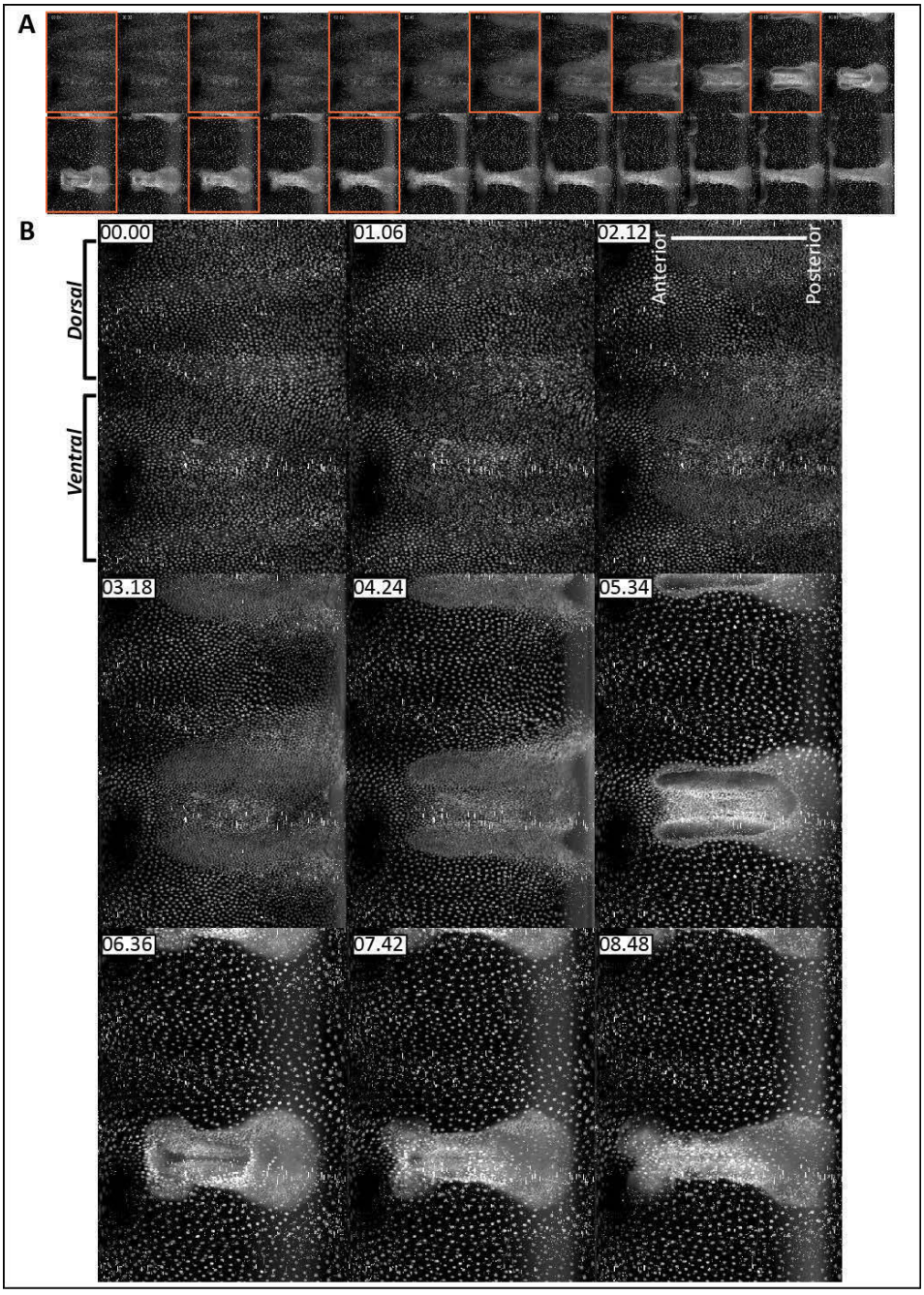

Figure 2.10: 2D cartographic maps of nuclei labelled embryos

Figure 2.10: 2D cartographic maps of nuclei labelled embryos. A) Time-series of 2D map projections from a fused SPIM movie of a transgenic *Tribolium* embryo that uniformly expresses H2A::GFP driven under Tubulin promoter (Kindly provided to us by Peter Kitzmann, Bucher lab). The movie covers about 13 hrs of development at 22°C. **B)**) Selected images highlighted in orange in A), are shown as an inset. Times are given relative to the uniform blastoderm stage which is shown as T-0. Time 0 corresponds to ≈9 hours (±30 minutes) after egg lay, and to ≈0.5 hour (±20 minutes) after the 12th round of divisions.

facility). These plugins quantify various parameters such as number of nuclei, density of nuclei, apical area of cells, number of cells in a given area and the average distance between the n number of closest neighbours. In a second step, these Fiji measurements are corrected based on the correct 3D pixel information from ImSANE (Vladimir Ulman, Tomancak lab).

Here I provide two examples of data analysis possible from map projections

1. **Particle Image velocimetry (PIV)**

   PIV analysis is a digital image correlation method that is routinely used in studying fluid flows [Westerweel, 1999]. It quantifies the displacement of fluorescent pixels between successive images. The area in the image which is correlated between two successive images is predefined, based on the size of the object being tracked [Thielicke, 2010; Thielicke and Stamhuis, 2014]. Its applications in studying biological tissues and cellular movements have also been explored. Using PIV on global movements such as nuclei, tissue flow and actomyosin dynamics etc., velocity estimations can be made [Bengough et al., 2009; Mayer et al., 2010; Naganathan et al., 2014]. This information is useful in measuring the relative movements of different regions of a tissue, in measuring fluid like behaviour of cells and proteins and in comparing tissue morphogenesis between wildtype and gene knockdown condition.

   I used the PIVlab app in MATLAB to measure the velocities of the nuclei as the serosa tissue expands and moves [Thielicke, 2010; Thielicke and Stamhuis, 2014] Fig 2.11. The quantifications were made from the beginning of the serosa expansion till germband extension on the

2D cartographic map projection shown in Fig 2.10. The nuclei were labelled with H2A::GFP and the frame rate was 90 sec acquired at 22°C. The images in Fig 2.11 A-F, show the velocities in different regions of the tissue as a heat map. The images are color coded as shown in the colour map at the bottom of each image, with blue being lowest and yellow being highest. The length and direction of the arrows refers to the magnitude and the direction of movement. The nuclei in the dorsal region of the embryo show the fastest movements as the serosa expansion begins (Fig 2.11, C). I averaged the total velocity of nuclei in two regions of the embryo on the dorsal side to calculate global tissue movements in these regions (boxes shown Fig 2.11, C, G). The average velocities showed that both the anterior and posterior regions of the dorsal serosa expand and increase in velocity over time (Fig 2.11, G). However, the posterior region moves much faster if compared to the anterior, around the time when the serosa flows over the posterior pole to generate the posterior amniotic fold. This behaviour is unprecedented and could provide important insights into the mechanics of the serosa tissue and the change in its properties during development. However, additional and more rigorous analysis is needed to calculate the flow velocities at different temperatures and under perturbed conditions.

2. **Tissue density analysis**

The Fiji plugins which I developed with Robert Haase (MPI-CBG Image Analysis facility) and Vladimir Ulman (Tomancak lab), would allow quantifying a number of parameters such as cell and nucleus area, number of cells and nuclei in a given area, relative change in density of cells and nuclei in different regions of the embryo during development. An example is shown in Fig 2.12 with the input polar map cartographic projection (Fig 2.12, A) and the segmented image (Fig 2.12, B). The polar maps are area conserving maps and do not corrections for measuring cell area. The output images are colour coded by cell neighbourhood

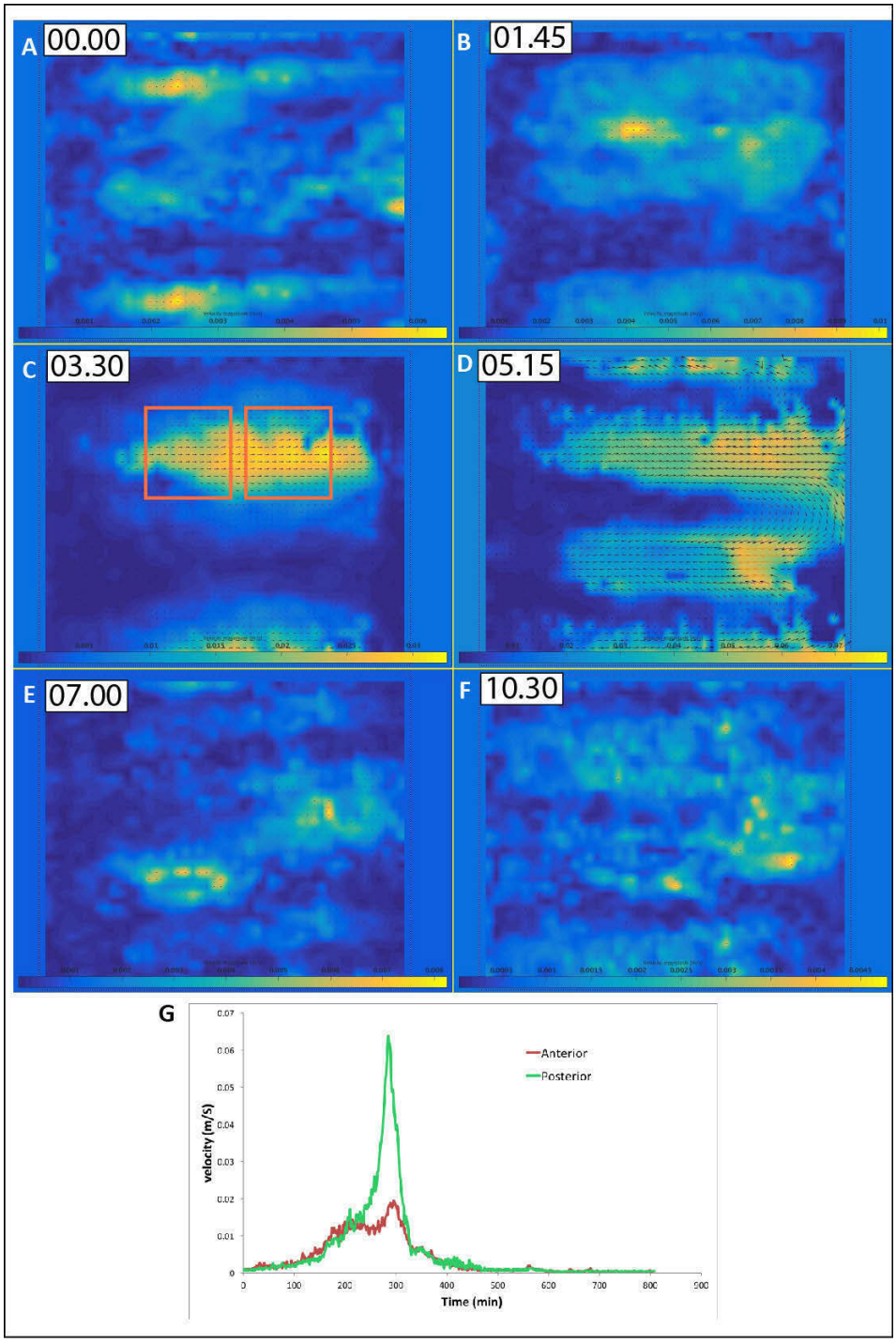

Figure 2.11: Particle Image Velocimetery analysis (PIV) on 2D maps.

Figure 2.11: Particle Image Velocimetery analysis (PIV) on 2D maps. A-F) Nuclei velocities measured using PIV analysis on 2D map projections. The arrows indicated the direction and magnitude of movement. **G)**) Velocity of nuclei movement was averaged for two regions, indicated with boxes in **C**. Red is for anterior and green is for posterior.

(number of neighbours in a 30 μm radius and the distance between 7 closest neighbours) (Fig 2.12, C and D). As expected, the region that starts condensing in the center of the maps shows the highest density.

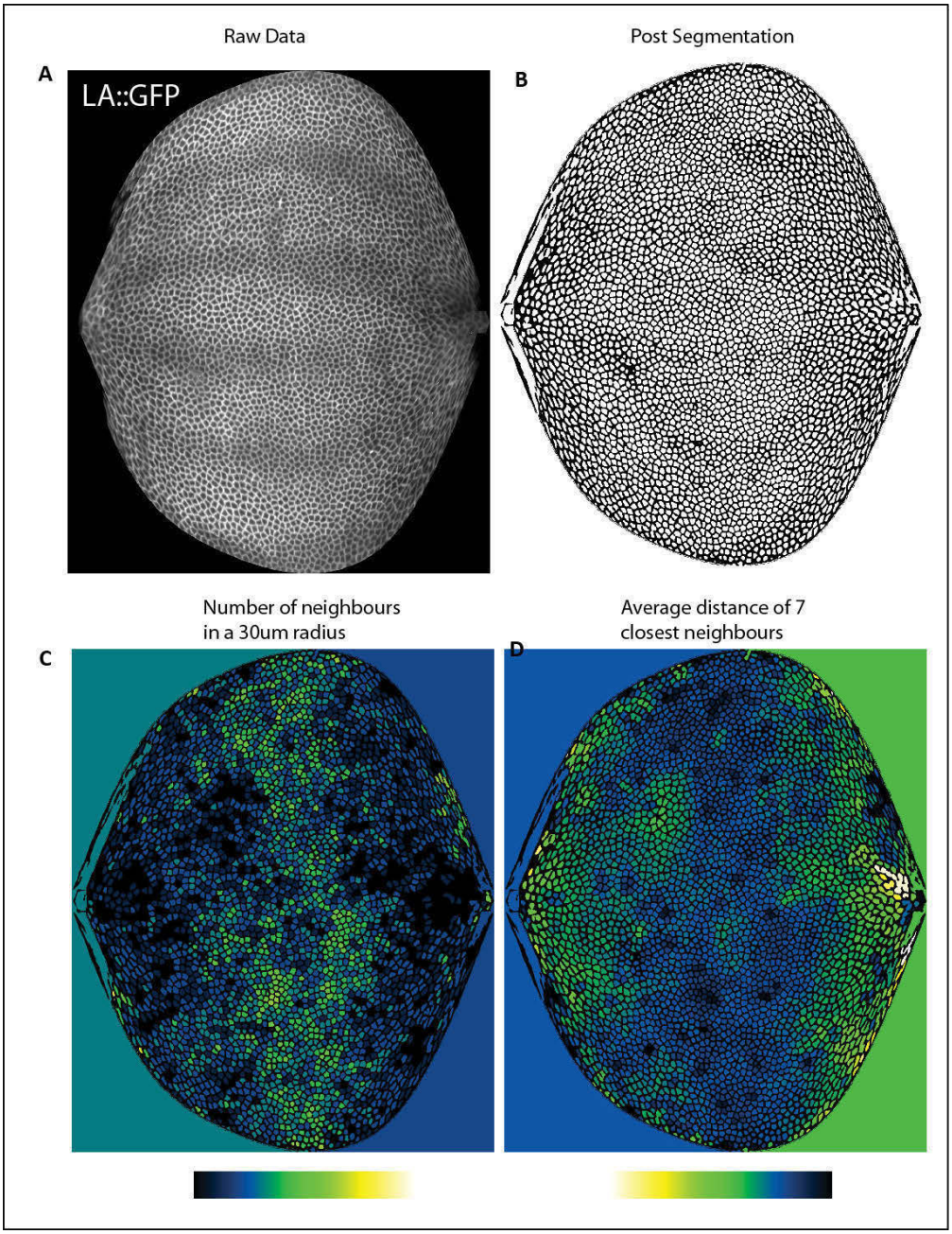

Figure 2.12: Segmentation and quantification of embryonic tissues

Figure 2.12: Segmentation and quantification of embryonic tissues A) 2D polar map projection from a fused SPIM movie of a transgenic *Tribolium* embryo that uniformly expresses LA::eGFP driven under Tubulin promoter (Kindly provided to us by Maurijn Van der Zee). The map is an area conserving projection of an example timepoint. The input raw data **(A)** and its segmented output **(B)** are shown. Segmentation of the membranes was done using the Ilastik software. **c)**The lower panel shows the output image which is color coded as in the LUT colour map. Blue is minimum number of neighbours in a radius of 30 μm and green is the maximum. textbfD)Similarly, the change in average distance between 7 closes neighbours is shown. Blue is minimum distance between 7 neighbour cells and green is the maximum.

2.6 Summary

I have established a pipeline for SPIM imaging of transgenic or transiently fluorescent *Tribolium* embryos with single or double labelled cells, nuclei and proteins. With this methodology, image datasets of early *Tribolium* embryogenesis were acquired at high spatial and temporal resolutions both under wildtype and knockdown conditions. Embryogenesis was reconstructed from multiple views obtained for hundreds of timepoints either on a local workstation or with parallel processing on the MPI-CBG computer cluster. To reduce the size and dimensionality of the reconstructed volumes and to aid visualization and analysis, each 4D dataset (3D+time) was transformed with tissues cartography into a 3D (2D+time) projections of development. Segmentation and quantification methods were developed for these maps which can provide quantification for the cellular and tissue dynamics on a global scale. All these computational steps were carried out with open-access software and were integrated in a singe pipeline that could be easily adapted for studying different developmental systems in future.

CHAPTER 3

CELLULAR DYNAMICS OF THE NON MUSCLE MYOSIN II REGULATORY LIGHT CHAIN - TC-SQUASH

Introduction

Myosin and Actin form contractile actomyosin filaments that generate forces required for tissue morphogenesis [Munjal and Lecuit, 2014]. Studies across various organisms have shown that Actin and the non-muscle Myosin II (referred to as Myosin henceforth) complexes show polarised subcellular localisations. These localisations determine when and where actomyosin mediated contractility will be exerted in developing embryos. A schematic illustration of different developmental stages in which Myosin plays an important role during tissue morphogenesis in *Drosophila* embryos is shown in Fig 3.1. Actomyosin complexes form contractile rings that function in basal cell closure during cellularisation (Fig 3.1, A) [Royou et al., 2004; Xue and Sokac, 2016], they are

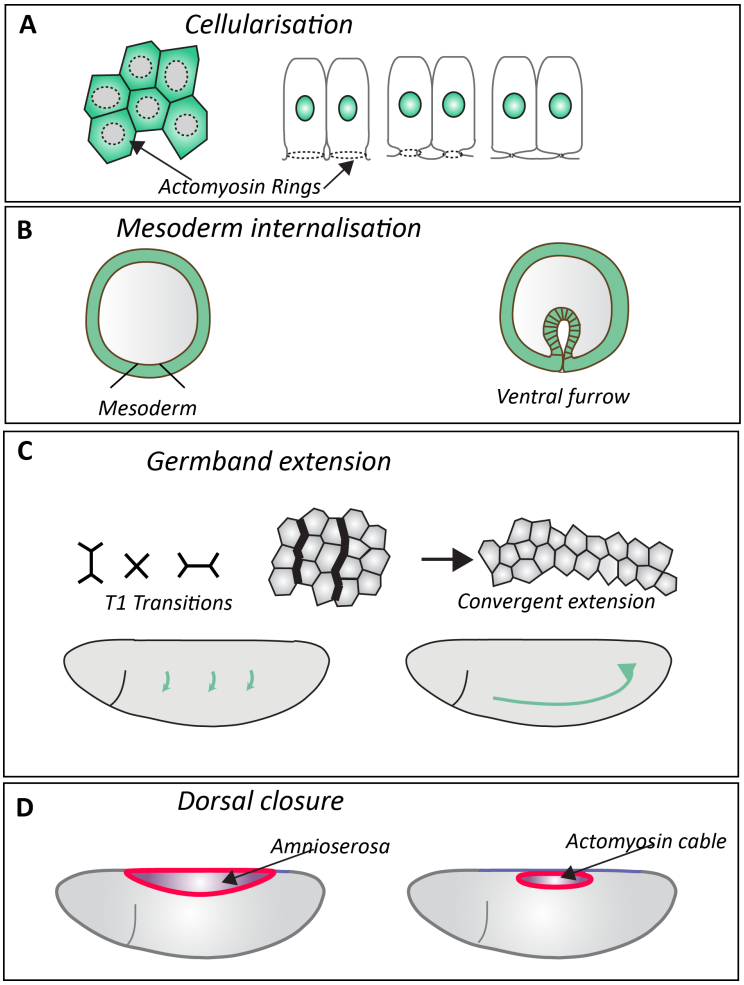

Figure 3.1: Illustration of various Myosin functions during *Drosophila* embryogenesis. Myosin shows various cellular localisations during *Drosophila* embryo development. **A)** Myosin localises to the furrow canals in between cells and forms rings at the basal sides of cells. **B)** Myosin becomes apical in the mesoderm cells. **C)** Myosin forms short cables that lead to T1 transitions during germband elongation. **D)** Myosin forms an actomyosin cable during dorsal closure

responsible for apical cell constriction during ventral furrow formation (Fig 3.1, B) [Martin et al., 2009], they show planar polarised localisation during the cell intercalation movements observed in germband extension, (Fig 3.1, C) [Zallen and Wieschaus, 2004] and they form a supracellular cable during dorsal closure (Fig 3.1, D) [Franke et al., 2005].

The non-muscle Myosin II belongs to the Myosin family of molecular motors which bind to the Actin cytoskeleton and move along Actin filaments via ATP hydrolyses in their head binding domain [Hartman and Spudich, 2012]. The various Myosin motors share conserved head domains but are highly variable in their tail domains, which are specific to each family member. The non-muscle Myosin II is the major motor generating cortical tensions in epithelial cells. It is a hexamer composed of two heavy chains (zipper in *Drosophila*) which have the ATP hydrolysis domain and bind to actin, two essential light chains (ELC) and two regulatory light chains (RLC or Spaghetti Squash) (schematic Fig 1.5). The N terminal end of the motor forms a globular head domain and the C terminal end forms a coiled coil tail region required for making homodimers. The homodimers can further form bipolar filaments which are processive complexes that bind to Actin filaments and can pull on them [Munjal and Lecuit, 2014].

Myosin motor activity is controlled by phosphorylation and dephosphorylation of the Myosin regulatory light chains [Kasza et al., 2014], which results in reversible conformational changes in the head and tail domain. Phosphorylation of the RLCs is effected by various signaling pathways modulating the activity of protein kinases like ROCK (Rho-associated coiled coil kinase) and citron kinase (both activated by the Rho signalling pathway), MRCK (myotonic dystrophy kinase-related Cdc42-binding kinase, activated by Cdc42) and MLCK (myosin light chain kinase, activated by Ca++) [Matsumura, 2005; Sellers, 2000]. These are conserved pathways that act downstream of developmental patterning genes and tissue specific transcription factors. For example, segmentation genes like the pair-rule genes Even-skipped, Runt [Zallen and Wieschaus, 2004] and transmembrane receptors like Echinoid, Crumbs and Toll [Harris, 2017] have been shown to control Myosin localisation during development.

To study the Myosin functions in *Tribolium* development, I cloned the coding sequence of the predicted *Tribolium* Spaghetti Squash gene and fused it with eGFP and RFP^{ruby} in a plasmid vector for in vitro transcription and

mRNA injection into preblastoderm embryos. In this chapter, I have described the dynamic subcellular localisations that Tc-Squash exhibited in different tissues and at different embryogenesis stages. Many of the observed patterns of Tc-Squash localisation were reminiscent of those described during *Drosophila* embryogenesis allowing a systematic comparison between these representative of long and short germ insect development.

3.1 Tc-Squash dynamics during *Tribolium* embryogenesis

Myosin exhibits highly polarised cellular localisations during tissue morphogenesis. These can be distinct on a subcellular level, between tissues and also depend on the developmental stage. In order to study the dynamic localisations of Myosin over the course of *Tribolium* development, first, a documentation that provides an overview of its behaviour during embryogenesis was needed.

In order to describe this, I first acquired 4D timelapse movies of embryos, labelled with Tc-Squash::eGFP, using the Zeiss LZ1 SPIM. The different movies were acquired from 3 or 5 views, at 25°C or 32°C. The 3D data was projected as cartographic maps (as described in the previous chapter). An overview of the dynamic localisations of Myosin over the course of *Tribolium* development is described below.

Before cellularisation, Tc-Squash is dissipated to the energids (the nuclei surrounded by distinct cytoplasm which migrate to the surface of the embryo before cellularisation) and slowly becomes restricted to cell junctions (Fig 3.2, A). It then forms prominent ring like structures, one per cell, during cellularisation (Fig 3.2, B). As the blastoderm differentiates, the Myosin intensity decreases from the flattening serosa cells and increases in the embryonic primordium (Fig 3.2, C and D). An increase in Myosin intensity with a speckled distribution appeared in dividing cells in the embryonic primordium, presumably at the cytokinetic rings (Fig 3.2, C). As the serosa and the future

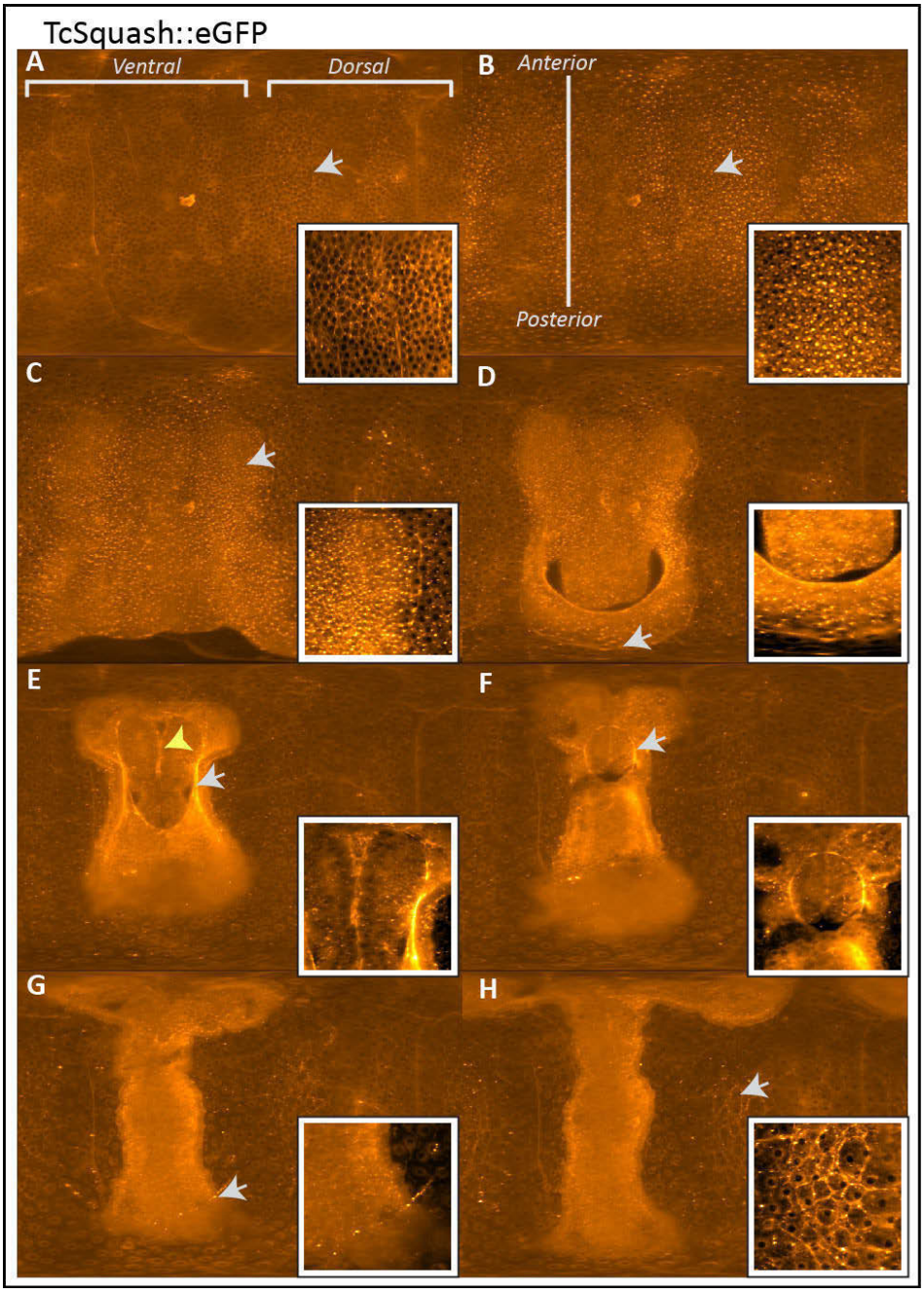

Figure 3.2: Tc-Squash dynamics during *Tribolium* embryogenesis

Figure 3.2: Tc-Squash dynamics during *Tribolium* embryogenesis Map projections of a 4D timelapse movie of *Tribolium* embryogenesis, labelled with Tc-Squash::eGFP acquired using the Zeiss LZ1 SPIM. Insets show zoomed in regions which are marked with arrows. Tc-Squash localises to cell junctions (arrow in **A**), as foci/dots in cells during cellularisation (arrow in **B**), during cytokinesis in cells in the embryonic region (arrow in **C**), Myosin forms a a supracellular cable between serosa and amnion(arrow in **D, E** and **F**), at the ventral furrow (arrowhead in **E**), in the yolk covering the segmentation zone (arrow in **G**) and in the yolk cells that undergo cleavage (arrow in **H**). Note that the Tc-Squash intensity increases progressively in cells in the embryonic region.

amnion become distinct, Myosin starts accumulating at the interface, eventually forming a supracellular cable like structure that spans across multiple cell boundaries (Fig 3.2, D, E and F). Myosin accumulation in the cable becomes progressively more prominent during formation of the serosa window. Myosin also shows apical enrichment in the *Tribolium* ventral furrow during mesoderm cells internalisation (Fig 3.2, E).). I also observed a crescent of Myosin enrichment in the yolk cell which covers the segmentation zone and this accumulation moves as the zone is uncovered by the yolk (Fig3.2, G). Finally, Myosin is also enriched in the yolk spheres that form during cleavage of the yolk mass concomitantly with the axial elongation of the embryo (Fig3.2, H).

3.2 Myosin drives basal cell closure during blastoderm cellularisation

The *Tribolium* syncytial blastoderm cellularises after 12 rounds of synchronous nuclear divisions. However, the membranes start invaginating between the nuclei after the 10th round of nuclear divisions. The invaginated membranes persist during the two subsequent nuclear divisions, and new invaginations occur between the daughter nuclei. *Drosophila*, Actin and Myosin form furrow canals at the invagination fronts and provide the contractile force necessary to pull down the membranes [Xue and Sokac, 2016].

I imaged Tc-Squash at high resolution to study its dynamics during cellu-

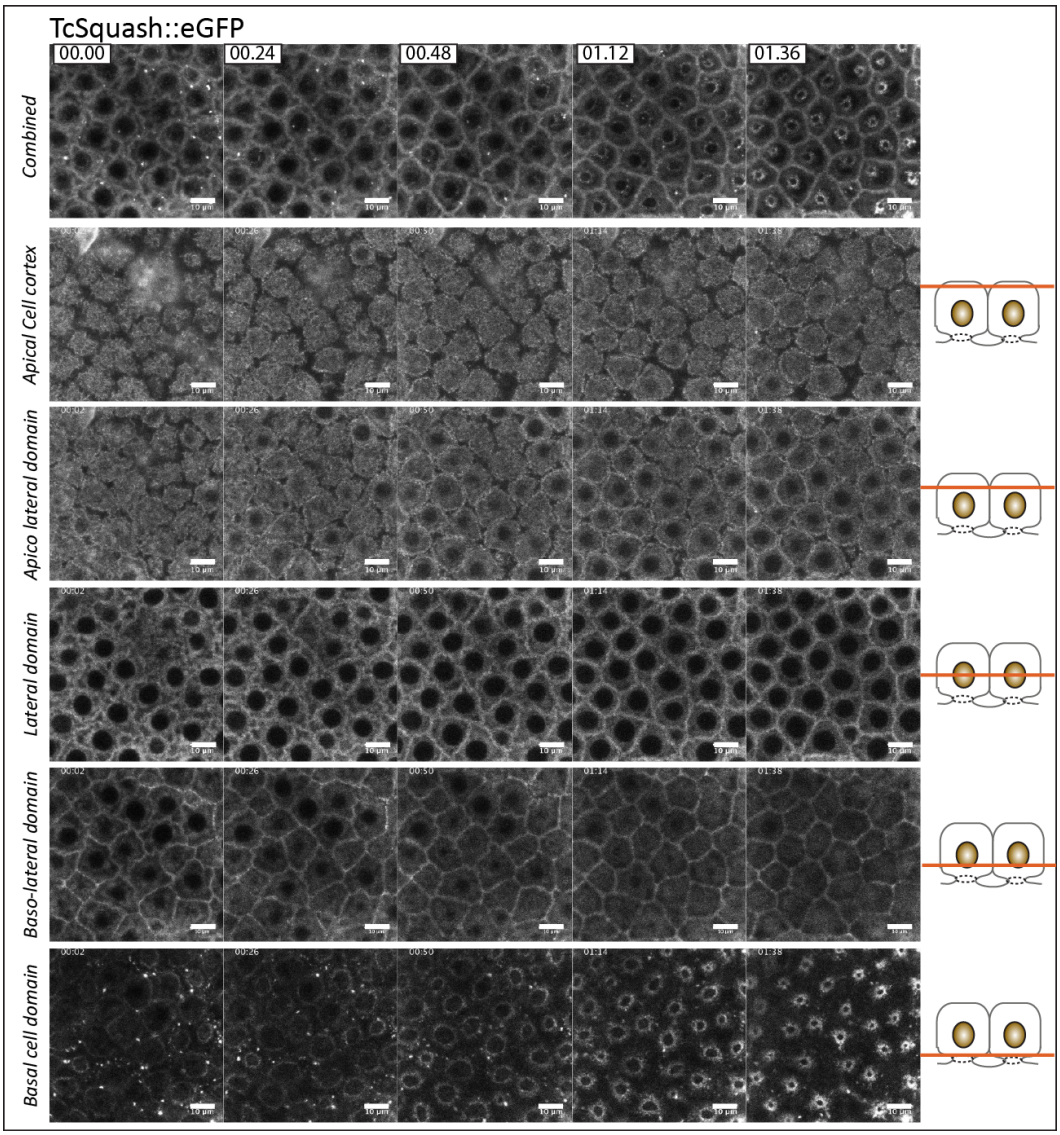

Figure 3.3: Tc-Squash shows distinct subcellular dynamics during cellularisation. Timelapse movie of Tc-Squash localisation during cellularisation in a transgenic line with GFP tagged Tc-Squash expressed uniformly under the tubulin promoter. The images are selected z slices from a z stack starting at the apical cortex region **B)**, apico-lateral **C)**, lateral **D)**, basolateral **E)** and basal cell regions **F)**. Row labelled as 'Combined' shows maximum projected images of single timepoints **A)**. Tc-Squash shows prominent intercellular rings at the basal cell region. The scale bar is 10um. Time is in minutes

larisation (Fig 3.3). I observed that Myosin is present throughout the forming cells from apical cortex to lateral sides and at the base. The Myosin at the apical cortex forms a dome shape and shows fluctuations, however, the apical domed cortex remains distinct between neighbouring cells (Fig 3.3, apical cell cortex). Myosin in the apico-lateral and the lateral domains of cells shows loose cell boundaries which constantly fluctuate in shape and increasingly become smoother. The increased tautness of the lateral domains corresponds to increased tension in the membranes as cellularisation proceeds probably reflective of adhesion junction formation between cells (Fig 3.3, apico lateral domain). The baso-lateral sides also show similar behaviour, with Myosin enrichment on the membranes. The most interesting and dynamic Myosin localisation was seen at the basal sides of the cell (Fig 3.3, basal cell domain). After the 12th synchronous division, Myosin forms intracellular rings, almost as big as the cell area in diameter at the basal side. These rings constrict concurrently with the closure of the basal cell side. When the cells close basally they give rise to an epithelial monolayer. Similar to most insects, *Tribolium* embryos form a cuboidal blastoderm epithelium. This is a marked difference to the well-studied *Drosophila* blastoderm that is composed of columnar cell upon cellularization. After completion of cellularisation, Myosin accumulates in a basal spot in each cell that may correspond to the ring canal that connects each cells to the underlying yolk-sac ([Handel et al., 2000]). A previous study on *Tribolium* cellularisation showed that the gap junction protein Innexin7a is needed to stabilize the forming basal membranes and enable basal cell closure, suggesting also the formation of junctions between the blastoderm cells and the underlying yolk plasma membrane [van der Zee et al., 2015]. This same study did not report any ring-like accumulation of Actin at the basal side during cellularisation ([van der Zee et al., 2015]). Therefore, it is still an open question, whether the constricting Myosin rings drive the formation of basal membranes in the *Tribolium* blastoderm by pulling on Actin filaments or some other cytoskeletal filaments, such as septins.

3.3 Myosin shows planar polarity in the embryonic tissue

The *Tribolium* blastoderm cellularises during interphase of the 13th cycle and blastoderm differentiation starts shortly afterwards. During differentiation, the cells in the embryonic primordium go through an asynchronous 13th round of divisions, they start changing their shape from cuboidal to columnar, and they condense towards the ventral side of the egg. At the tissue level, the embryonic epithelium undergoes a number of conspicuous rearrangements: the prospective mesoderm internalizes at the ventral side in a posterior to anterior direction, the prospective ectoderm condenses ventrally resealing the epithelium along the ventral midline and at the same time starts folding on itself forming a stereotyped sequence of amniotic folds. It has been shown that during embryonic condensation, ectodermal cells intercalate on a global scale along the dorsal-ventral axis decreasing the number of cells and junctions along this axis and increasing the number of cells and junctions along the anterior-posterior axis [Benton et al., 2016]. I could observe a polarised distribution of Tc-Squash in the lateral ectoderm during condensation. Myosin becomes enriched at the vertical cell contacts (oriented along the dorsal-ventral axis). This enrichment is either localised in individual cell contacts or spans multiple neighbouring vertical cell interfaces giving rise to short transient actomyosin cables. In the case of unicellular Myosin accumulation, the junctional remodeling mediating the rearrangement of 4 cell neighbors proceeds through an ordered pattern of disassembly and reassembly known as T1 transition [Rauzi et al., 2008]: the anisotropic distribution and contractility of the Myosin leads to the collapse of the vertical junction and the temporary fusion of the two old 3-way vertices into a single 4-way vertex that is resolved in perpendicular orientation into the two new 3-way vertices upon formation of the new horizontal junction (oriented along the anterior-posterior axis). This sequence of junctional remodeling has been previously described during germband extension in *Drosophila* [Bertet et al., 2004].

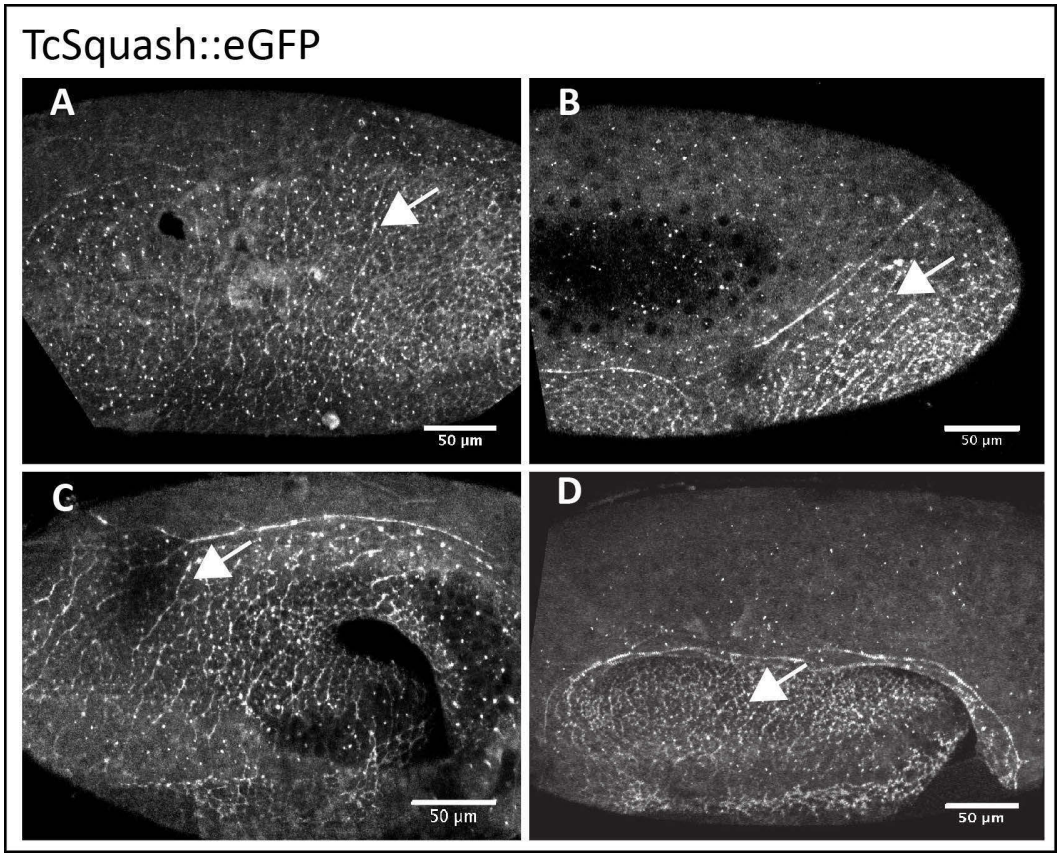

Figure 3.4: Tc-Squash is localised in a planar polarised manner in the *Tribolium* ectoderm. Images show Tc-Squash localisation in *Tribolium* embryos at successive developmental stages in a transgenic line with GFP tagged Tc-Squash expressed uniformly under the tubulin promoter. Arrows mark the Tc-Squash localisation in embryonic region. Lateral views of embryo at **A)**) Differentiated blastoderm, **B)**) and **C)**) primitive pit and posterior amniotic fold formation and **D)**) Serosa window formation stages. Tc-Squash shows polarisation in D-V axis of the embryo. Scale bar is 50 μm.

In addition to T1 transitions, in *Drosophila* multiple vertical junctions coalesce simultaneously during later elongation stages forming multicellular rosettes that are resolved into multiple new horizontal junctions [Blankenship et al., 2006; Walck-Shannon and Hardin, 2014]. Rosettes involves 5 or more cells that constrict their shared vertical interfaces in concert, meet at a single point creating high-order vertices, and then resolve in perpendicular orientation. Rosette formation is driven by a multicellular actomyosin cable

that is connecting all constricting cell boundaries. Although several short multicellular vertical Myosin cables were observed transiently in *Tribolium* , I could not confirm their involvement in rosette formation. Additional high resolution imaging and dual labelling with a membrane marker is needed to analyse the role of these cables in embryonic condensation.

3.4 Myosin accumulation and apical constriction of putative germ cells at the posterior pole

The first morphogenetic movement of the differentiated *Tribolium* blastoderm is detected at the posterior pole that gets displaced from the vitelline membrane. The posterior pole first becomes flat and then forms a pit, known as primitive pit, which is considered the posterior midgut rudiment [Handel et al., 2000]. It was previously suggested from electron microscopy analyses that primitive pit formation is effected by cells at the posterior pole reducing and flattening their apical sides [Handel et al., 2000]. I wanted to investigate the cell shape changes which lead to the formation of the posterior amniotic fold and study the Myosin dynamics in this process. This however, poses a technical issue if imaging is done using confocal microscopes.

The *Drosophila* and *Tribolium* embryos are relatively flat on the lateral sides, elongated in the anterior-posterior direction and highly curved at the two poles. This limits the possibility to image the poles since the embryos always lie on the flat side on slides and due to limited depth of field with 20X or 40X objectives, the cells at the pole are not visible. Therefore, the only alternative to image the cellular dynamics at the poles is to stick the embryos vertically on slides at their anterior or posterior poles. This however, again has limited depth of field which can be imaged and often causes perturbations to normal development. Fortunately, these issues are circumvented if the imaging is done using the multiview modality with SPIM. The multiple views not only

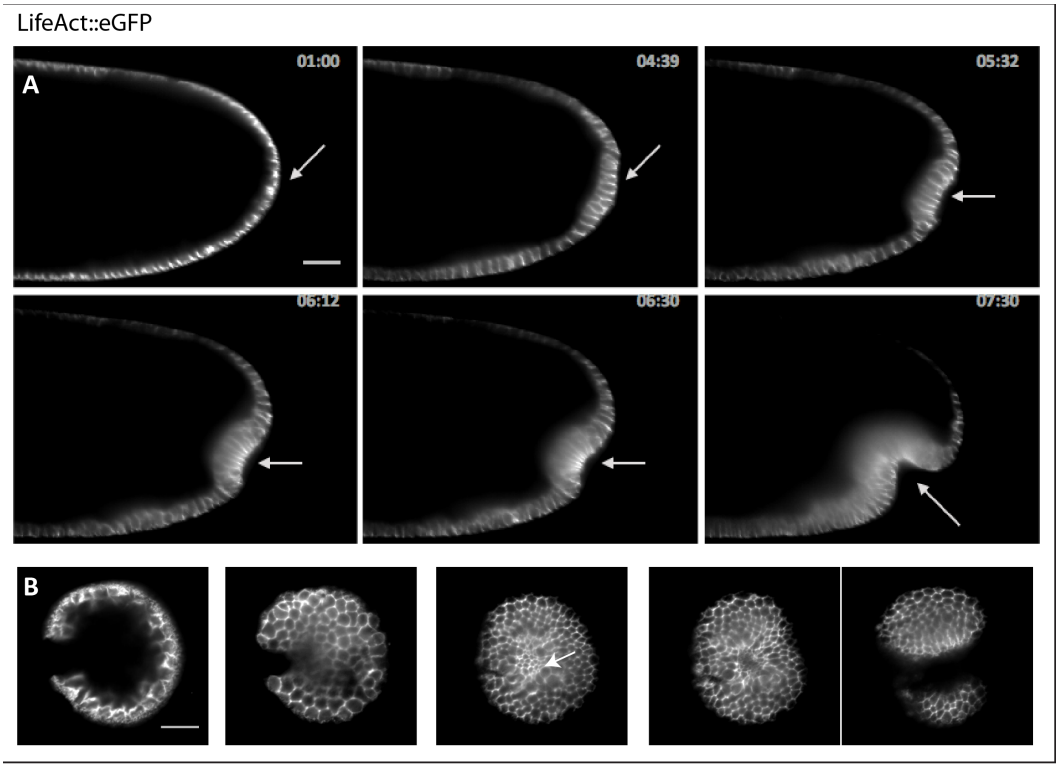

Figure 3.5: Apical constrictions at the posterior pole precede amniotic fold formation. Images from a timelapse movie of embryos labelled with LA::eGFP. The movie was acquired from 5 views at 1 minute time resolution and fused with multiview reconstruction plugin in Fiji. Selected images are shown using BigDataViewer. **A)** Lateral view shows LA::eGFP in cells. Arrow points to the posterior pole. **B)** Images show the posterior pole of embryos. Scale bar is 50 μm.

cover all the regions of the embryo, the increased depth of imaging with SPIM also aids in imaging the poles. With multiview registration and fusion of the different views (as described in the previous chapter), full and complete 3D reconstruction of embryos is possible. These datasets can be then opened with software like IMARIS or the BigDataViewer plugin in Fiji [Pietzsch et al., 2015], to visualise the cellular dynamics at the poles.

I investigated the formation of the primitive pit and the posterior amniotic fold by imaging the Actin and Myosin dynamics using the Zeiss LZ1 SPIM. I imaged embryos labelled with LA::eGFP or the Tc-Squash ::eGFP (Fig 3.5,

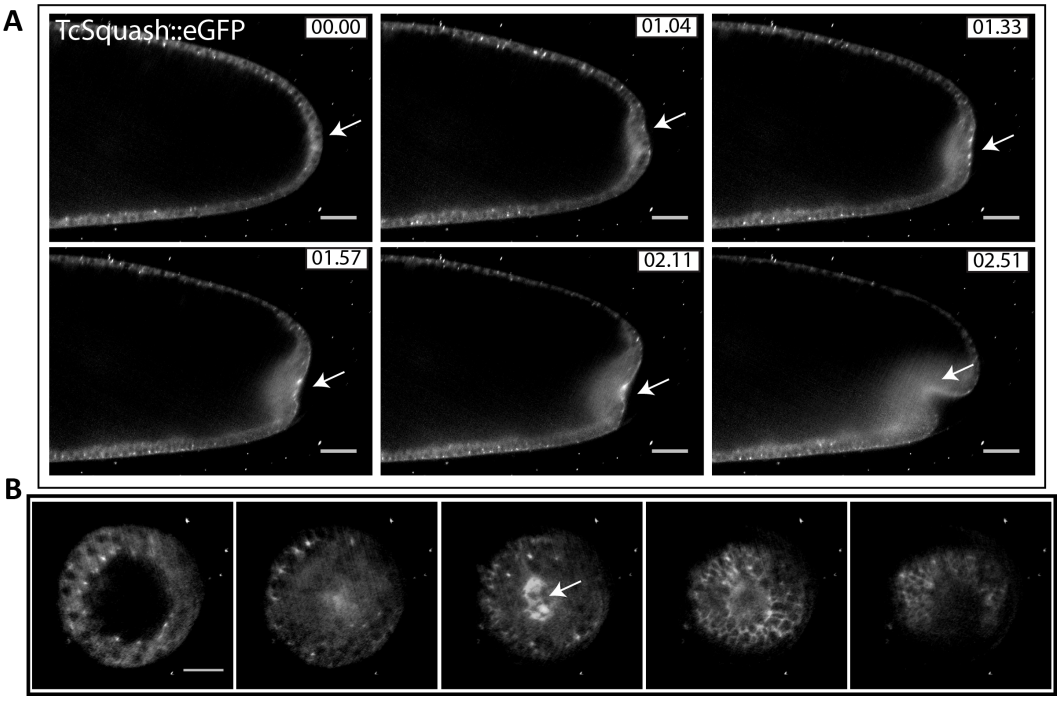

Figure 3.6: Tc-Squash accumulates at the posterior pole during primitive pit formation and amniotic fold formation. Images from a timelapse movie of embryos labelled with Tc-Squash::eGFP. The movie was acquired from 5 views at 5 minute time resolution and fused with multiview reconstruction plugin in Fiji. Selected images are shown using BigDataViewer. **A)** Lateral view shows Tc-Squash::eGFP accumulation in the apical region of cells. Arrow points to the posterior pole. **B)** Images show the posterior pole of embryos. Scale bar is 50 μm.

3.6). LifeAct::eGFP imaging indicated that cells at the posterior pole are the first to start columnarisation. This region then progressively becomes flatter and undergoes apical constrictions similar to the ventral furrow in *Drosophila* creating wedge shaped cells at the pole (Fig 3.5, A). Following the apical constrictions, a notch at the posterior pole is created and the amnion folds over the embryonic region, creating the amniotic fold. Interestingly, the pole projections showed that a group of cells in the center of the posterior pole undergo apical constrictions and invaginate (Fig 3.5, B).

Myosin has been extensively studied in cells which undergo constrictions. The ventral furrow in *Drosophila* shows apical constrictions by selective lo-

calisation of Myosin to the apical sides of the prospective mesodermal cells [Martin et al., 2009]. Myosin also localises apically in vertebrate neural tube cells that undergo apical constrictions [Rolo et al., 2009]. The multiview imaging of Tc-Squash in the embryos showed that Myosin starts accumulating in the posterior pole during differentiated blastoderm stage. As the primitive streak and the posterior amniotic fold formation progress, Myosin is seen enriched apically at the pole as seen in lateral sections(Fig 3.6, A). the polar projections also that that a group of cells in the middle of the posterior pole enrich a large amount of Tc-Squash::EGFP and this could correspond to the apically constricting cells as seen in embryos marked with LA::eGFP.

It was previously shown that the pole shows a narrow ring of *twist* positive cells [Handel et al., 2004] and that the transcripts for the *Tribolium* vasa gene, which is a widely conserved marker for germ cells, accumulate in the posterior pole [Schröder, 2006] My *vasa* and *tudor insitu* experiments also indicated that this is the region where the *Tribolium* germ cells could be forming (Appendix). Therefore, Myosin mediated apical constrictions might be important for the primitive pit and amniotic fold formation and internalisation of the putative *Tribolium*germ cells. Additionally, in *Drosophila*, fog, a secreted ligand is required for apical constrictions in the ventral furrow. It will be interesting to investigate if this role is conserved in *Tribolium* and the posterior pole accumulates Myosin apically via fog activity.

3.5 Myosin pulses during apical constriction of mesoderm cells

The ventral furrow is the region where the mesoderm invaginates during gastrulation. During condensation of the *Tribolium* embryonic primordium, the ventral furrow proceeds from posterior to anterior [Handel et al., 2004]. Like in the case of the posterior pole cells, Myosin becomes enriched in the apical domain (Fig 3.7, A, B, C) leading to the constriction and wedging of the

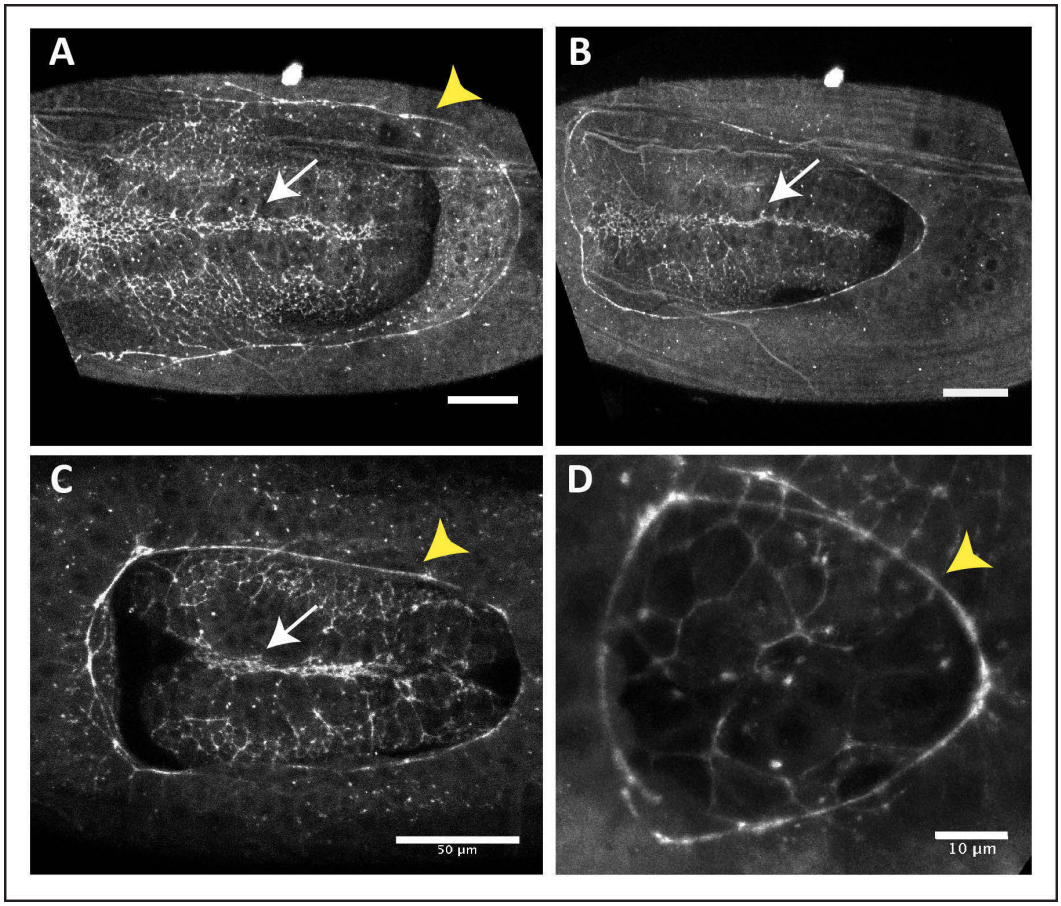

Figure 3.7: Tc-Squash localisation in ventral furrow and at serosa-amnion boundary. Images show Tc-Squash localisation on the ventral side of embryos at successive developmental stages, in a transgenic line with GFP tagged Tc-Squash expressed uniformly under the tubulin promoter. Arrows mark the Tc-Squash localisation in cells undergoing apical constrictions at the ventral furrow. Arrowheads mark a supracellular Myosin cable formed at the serosa window. Scale bar in **A-C** is 50 μm and **D)** is 10 μm.

internalising mesoderm cells.

It has been shown in *Drosophila* that apical constrictions in mesoderm cells are not continuous, but they take place in a stepwise manner through repeated cycles of constriction and stabilization of the apical surface resembling a mechanical ratchet [Martin et al., 2009] [Mason and Martin, 2011]. These constriction pulses are correlated with rounds of Myosin and Actin coalescence (and dissipation) from the perimeter to the center of the apical cell surface,

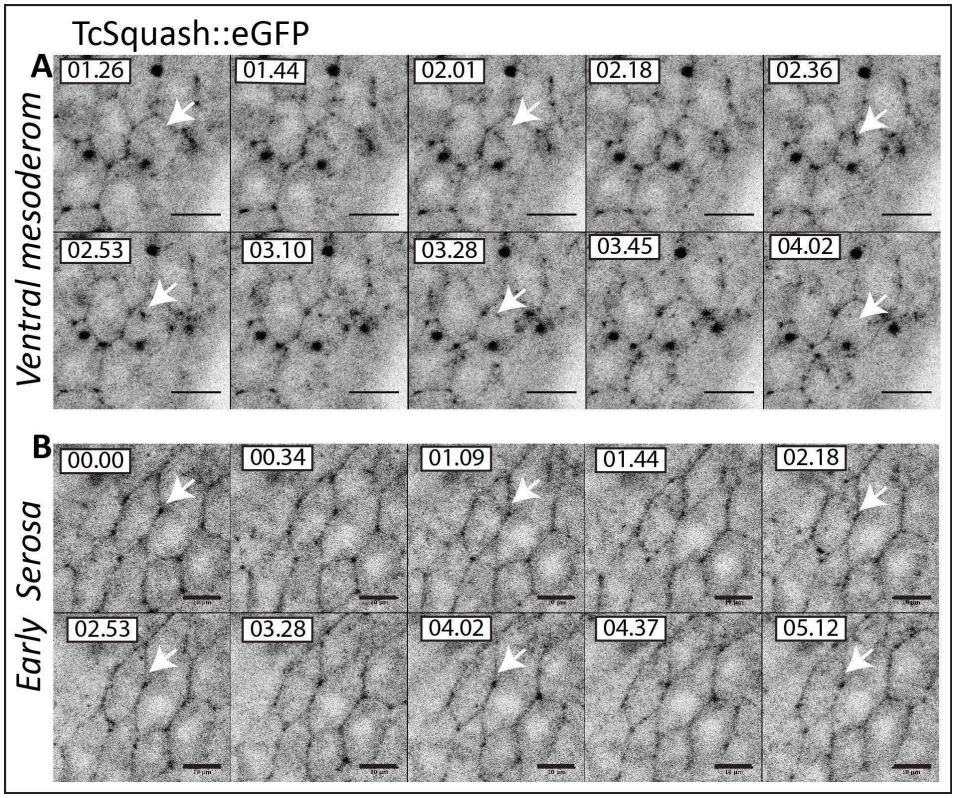

Figure 3.8: Tc-Squash localisation at the apical cortex of cells. Images from a time-lapse movie show Tc-Squash pulses on the apical side of cells in the ventral mesoderm region **A** and in serosa cells **B**. A transgenic line with GFP tagged Tc-Squash expressed uniformly under the tubulin promoter was used for imaging. Arrows mark the cortical pulses in the same cell.

representing the periodic contractions of the actomyosin network in the medial apical cortex [Martin et al., 2009; Roh-Johnson et al., 2012]. I also observed cortical pulsations of Myosin in the *Tribolium* mesoderm cells undergoing apical constrictions (Fig 3.8, A). In these cells, Myosin forms coalescing foci that appear and disappear periodically in the medial apical region, very similar to those described in *Drosophila*. Interestingly, similar Myosin pulses were also detected in the serosa cells close to the embryonic-extraembryonic boundary that may also contribute to the cell shape changes observed in this region (Fig 3.8, B).

3.6 Myosin accumulates at the extraembryonic-embryonic boundary to form a contractile supracellular cable.

The polarised localisation of Myosin in *Tribolium* embryos is detected transiently in single or few cell interfaces during intercalation of ectoderm cells (described above), but also in a stable enrichment across multiple cells at the interface between the extraembryonic and embryonic primordia. This higher order accumulation of Actin and myosin, generally known as an actomyosin cable, produces contractile forces in a variety of physiological and developmental processes [Röper, 2014]. I performed a systematic investigation of the formation, dynamics and mechanics of the *Tribolium* actomyosin cable during serosa epiboly and serosa window closure. These results are described in the next chapter (Chapter 4).

3.7 Summary

The imaging analysis of Myosin (Tc-Squash) during early embryogenesis of *Tribolium* identified its diverse roles in various developmental processes and morphogenesis events:

- Myosin forms contractile rings that close off the basal side of cells during cellularisation of the uniform blastoderm.
- Myosin becomes enriched apically in the putative germ cells causing the flattening and invagination of the primitive pit at the posterior pole.
- Pulsatile Myosin accumulations in the medial apical domains of mesoderm cells could contribute to apical constriction and invagination of mesoderm cells in the ventral furrow.

- The polarised enrichment of Myosin along the vertical cell junctions drives the dorsal-ventral intercalation and convergent extension movement of the ectoderm.
- Myosin forms a supracellular contractile cable at the extraembryonic-embryonic boundary that contributes to serosa epiboly. Most of the observed Myosin dynamics are conserved between *Drosophila* and *Tribolium*, while some are unique for *Tribolium* embryogenesis (see Discussion).

CHAPTER 4

A SUPRACELLULAR ACTOMYOSIN CABLE OPERATES DURING SEROSA EPIBOLY

Introduction

Supracellular actomyosin cables function in various processes such as wound healing, tissue compartmentalization and epithelial morphogenesis. They can be present as static structures separating cell populations at compartment boundaries, form circumferential contractile cables to seal gaps in epithelia or arise as short transient cables that facilitate cell intercalation during convergent extension movement of tissues [Röper, 2014]. In the case of *Tribolium*, it was previously postulated that an actomyosin cable might play an active role in serosa window closure in purse string-like manner [Benton et al., 2013; Handel et al., 2000]. During embryo gastrulating, the serosa extraembryonic epithelium expands dramatically in size to cover the entire egg surface, forming an outer layer underneath the vitelline membrane (Fig 1.3, schematic). This serosa epiboly is concomitant with the folding of the embry-

onic primordium and the involution of the prospective amnion first posteriorly, then laterally and finally anteriorly[Benton et al., 2013; Handel et al., 2000]. Once an oval amniotic fold has formed underneath the germband, the ensuing opening, known as serosa window, gradually closes until the outer serosa layer detaches from the inner amnion ((Fig 1.3, schematic). It has been suggested that the serosa epithelium is an evolutionary novelty of the insect eggs that protects them from desiccation and provides them with the full range of innate immune responses against pathogens [Jacobs et al., 2013, 2014; Jacobs and van der Zee, 2013].

In this chapter, I describe the emergence and spatiotemporal dynamics of an actomyosin cable at the extraembryonic-embryonic tissue boundary. I analyse the cable shape changes and the expansion and shrinkage dynamics during serosa epiboly and serosa window closure. Additionally, I explore the behaviours of serosa cells over time, both within the serosa tissue and at the edges contributing to cable formation. These descriptions are then supplemented with a mechanistic analysis of cable tension using laser ablations and genetic perturbation by RNAi knockdown. Throughout this chapter, I use the following staging system for Tribolium early embryogenesis:

- Formation of uniform blastoderm : Stage 0
- Initiation of blastoderm differentiation : Stage 1
- Initiation of the posterior amniotic fold : Stage 2
- Horseshoe amniotic fold : Stage 3
- Oval amniotic fold : Stage 4
- Serosa window closure : Stage 5

4.1 Actin and Myosin accumulate at the extraembryonic-embryonic boundary

The emergence of a supracellular actomyosin cable at the interface of the extraembryonic and embryonic primordia was previously identified as a membrane thickening in embryos labelled with the membrane GAP43-YFP reporter (REF Benton2013). In this work, I imaged the actual components of the presumptive cable using the LifeAct tag to label Actin and the *Tribolium* regulatory Myosin light chain (Tc-squash) to label the non-muscle Myosin II during serosa epiboly. The embryos were labelled either transiently with mRNA encoding the LifeAct::eGFP or Tc-squash::eGFP fusion proteins or stably with transgenic lines ubiquitously expressing these constructs (αTub-LifeAct::eGFP line kindly provided by Maurjin Van der Zee and αTub-Tc-Squash::eGFP line generated by our lab).

During the early stages, the actomyosin cable extended around the embryo circumference and only during the later stages coalesced at the ventral side. The availability of the SPIM multi-view acquisitions, the reconstruction of entire embryos over time, and the tissue cartography representations described in Chapter II enabled to trace the origin, dynamics and disappearance of the supracellular Actin and Myosin enrichment from early blastoderm stages until serosa window closure. Both Actin and Myosin start accumulating progressively at the extraembryonic-embryonic boundary when blastoderm differentiation becomes evident (Stage 1) (Fig 4.1, A,B) (Fig 3.7) (Fig 4.2). At this stage, the non-divdinging serosa cells change from cuboid to squamous and start expanding their apical areas, while the embryonic cells undergo the 13^{th} round of cell divisions and start becoming columnar. This creates a tissue boundary with cells of different fates and properties present on either side. The actomyosin accumulation becomes more pronounced as the extraembryonic-embryonic boundary passes around the posterior pole (Stage 2) and peaks during the last stages of serosa window formation and closure (Stage 3-5) (Fig 4.1, C,D).

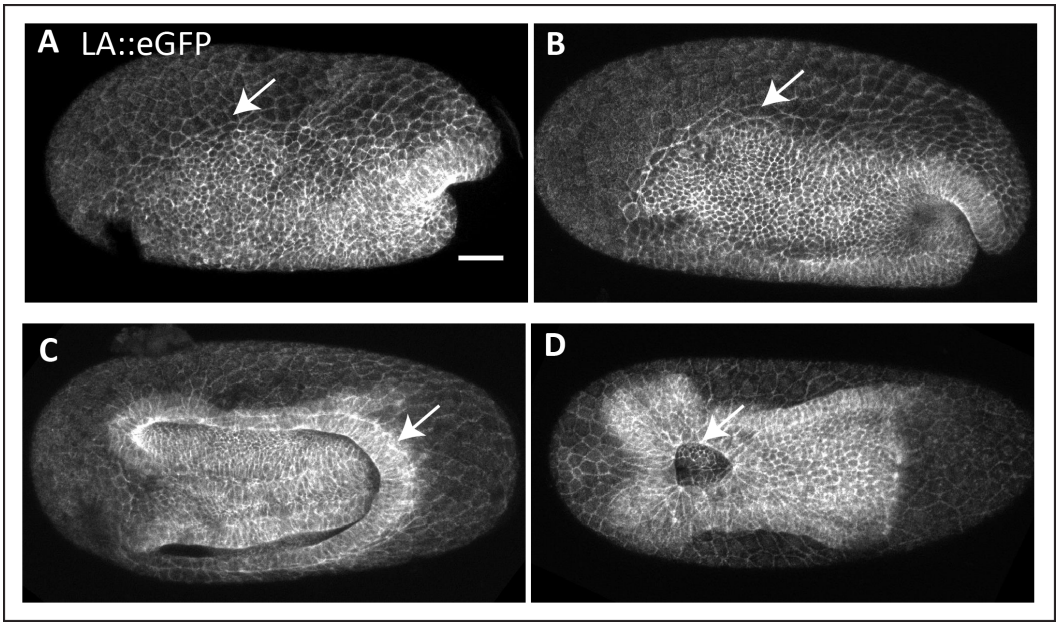

Figure 4.1: Actin accumulates in a supracellular cable like alignment. Maximum intensity projections of embryos labelled with LifeAct::eGFP to mark Actin are shown.The images were acquired using the Zeiss LSM 780 microscope. **A**,**B**) shows lateral projections of embryos at Stage 1 and 2 respectively. **C**,**D**) show ventral projections at Stage 3 and 4 respectively. Arrows mark the supracellular Actin assembly. Scale bar is 50 μm.

4.2 The actomyosin assembly migrates ventrally till it forms the rim of the serosa window

One particular problem that I needed to solve in my analyses is that the bright fluorescent edge of the involuting amnion and the auto-fluorescence from the underlying yolk obscure the actual cable in maximum intensity or average intensity projections. To address this issue, I performed tissue cartography by peeling the data into several layers to visualise the embryo at different specified z depths. I then combined the selected layers into a single image by color-coding differentially the surface layer (Fig 4.3, Cyan) and the deeper layer (Fig 4.3, magenta).This analysis first confirmed that during Stages 1-3 the actomyosin cable and the extraembryonic-embryonic boundary lag behind

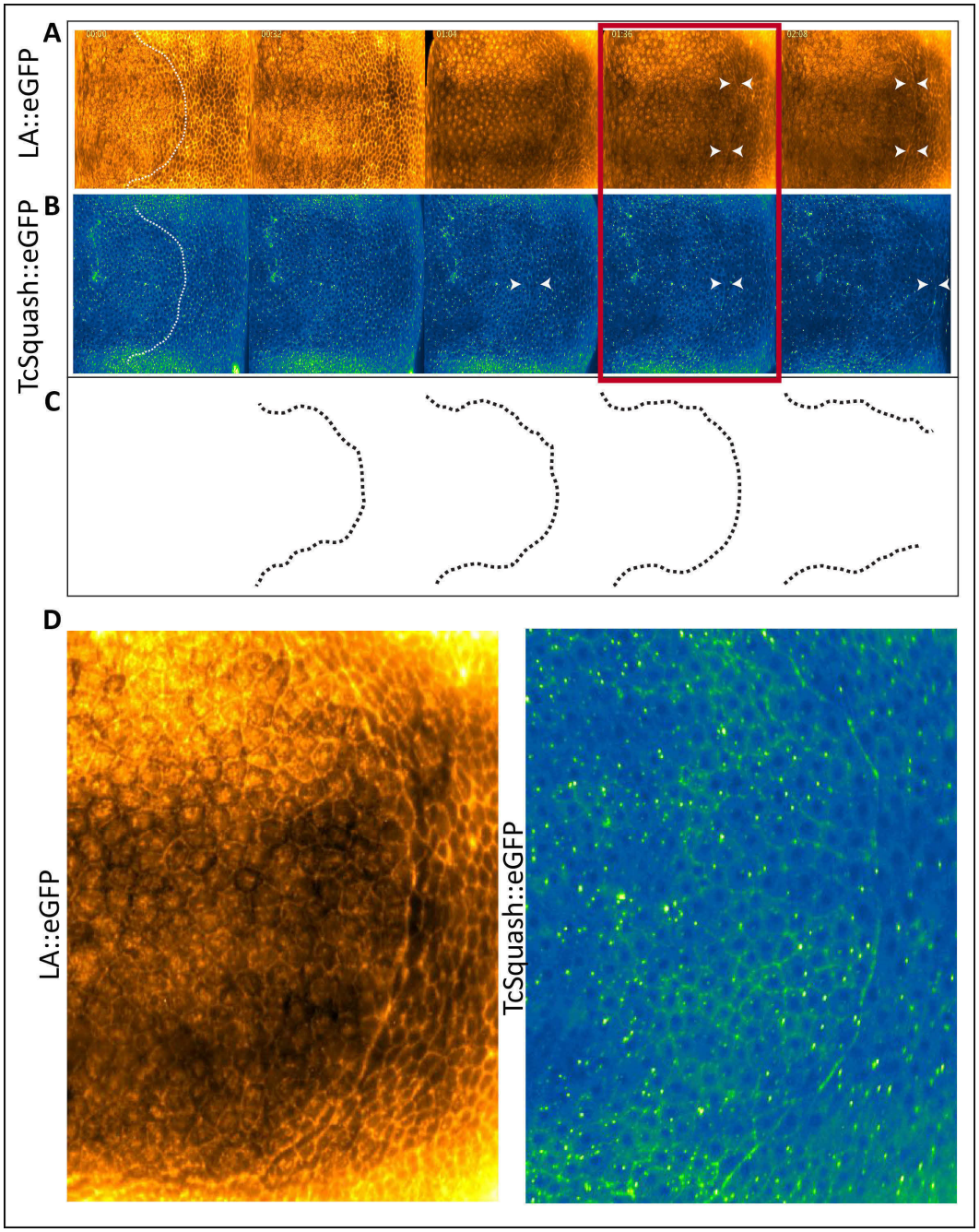

Figure 4.2: Actomyosin dynamics in the differentiated blastoderm.

Figure 4.2: Actomyosin dynamics in the differentiated blastoderm. Map projections show the dorsal side of the embryos in cartographic projections from a 4D timelapse movie of LifeAct::eGFP **A)** and Tc-squash::eGFP **B)** labelled embryos. Arrowheads point to the Actin and Myosin accumulation at the serosa-prospective amnion boundary. **C)** Illustration depicts the dynamic change in the shape of the actomyosin assembly on the dorsal side of embryos.

the involuting amnion on the posterior side of the embryo. Initially the tissue boundary is located at the surface of the embryo (Cyan) but it later becomes visible deeper in the embryo (magenta). Only once the amnion involution is completed and the serosa window is formed, the cable reaches the rim of the serosa window which is positioned a little deeper and not at at the surface of the embryo (Fig 4.3, 2:00 hr). These results suggest that the involuting amnion is pulling the serosa on all sides, eventually positioning the actomyosin cable and the tissue boundary at the rim of the serosa window. It seems plausible but still needs to be tested experimentally whether the condensation of the embryonic primordium is the primary force generator for this epithelial rearrangement.

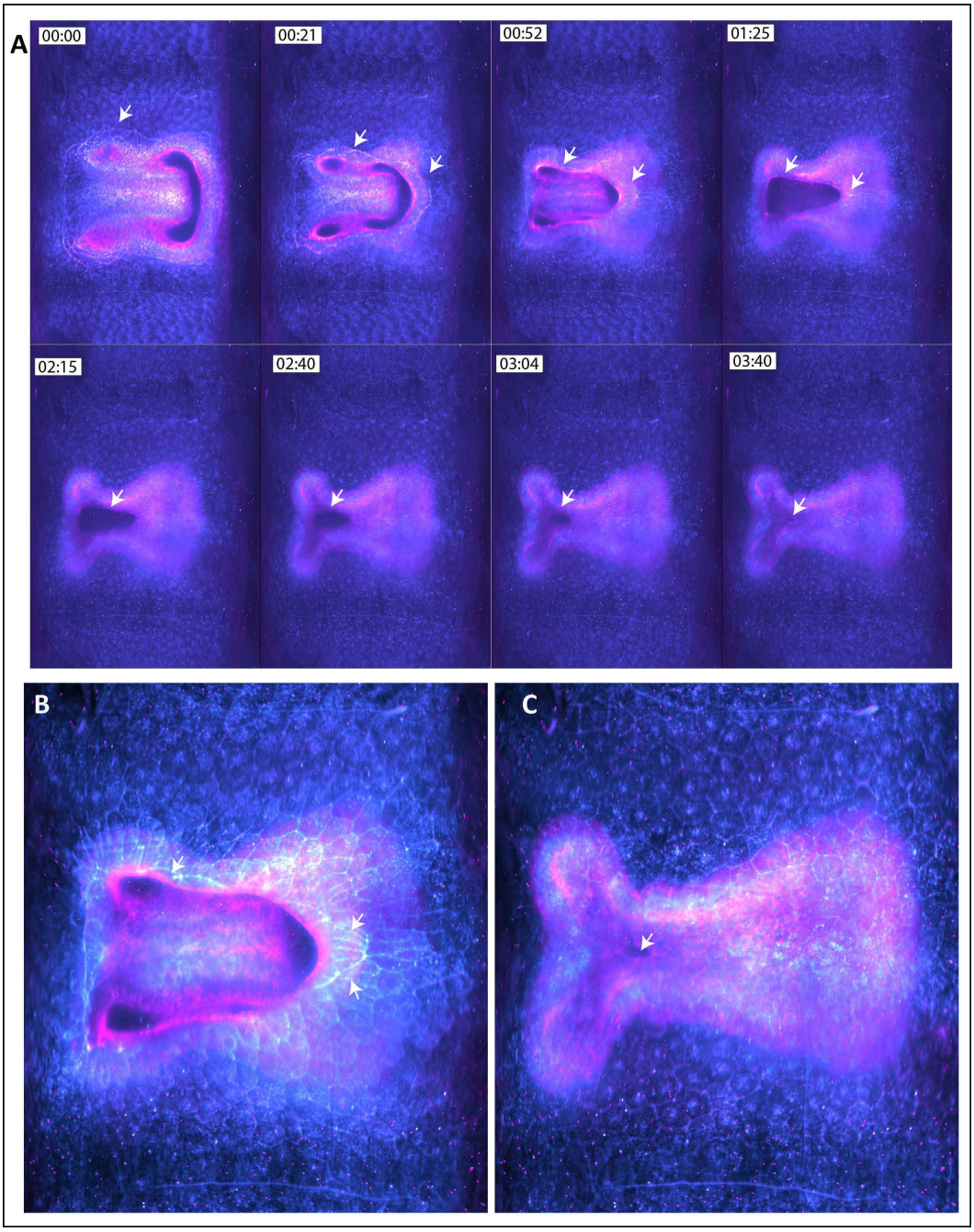

Figure 4.3: Actomyosin dynamics during serosa window closure.

Figure 4.3: Actomyosin dynamics during serosa window closure. Cartographic projection of a transgenic *Tribolium* embryo labelled with LifeAct::eGFP showing the ventral side. Images are depth coded with cyan representing the surface layer of the embryo and magenta showing the deeper underlying layers. The supracellular actomyosin assembly is indicated by arrows. The cable is initially visible in cyan and then later in magenta. Time is in hours.

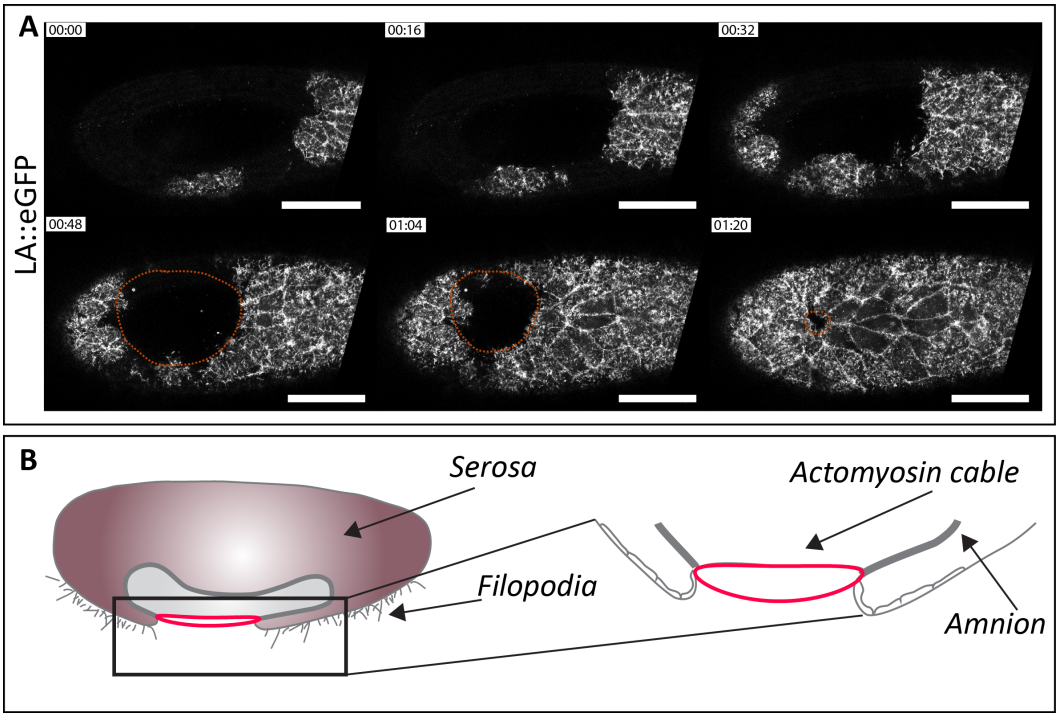

Figure 4.4: The cable changes in depth at the serosa window. A) Images from a time-lapse movie show LifeAct::eGFP on the apical surface of the embryo on the ventral region. Dynamic Actin filopodia are seen projecting to the vitelline membrane. Note the absence of the cable on the surface. **B)** Schematic shows the relative position of the actomyosin cable with respect to the serosa and amnion cells. The serosa cells become curved as they are pulled by the adjacent tissue. Time is in hours. Scale bar is 50 μm.

To visualize this change in depth at higher resolution, I imaged embryos labelled with LifeAct::eGFP under a confocal microscope. The confocal datasets confirmed that the cable follows the amnion involution from the surface of the embryo into the inner layer of the oval amniotic fold where it remains positioned at the rim of the serosa window (Fig 4.4, B). Interestingly, the supracellular Actin cable is not visible at the surface of the surface of the embryo

during the serosa window closure, although maximum intensity projections show its presence. This happens because the serosa cells at the boundary of the cable bend over the window (Fig 4.4, schematic). In addition, this experiment identified several active apical filopodia extending from the serosa cells to the vitelline membrane (Fig 4.4 A) as previously shown in electron microscopy images [Handel et al., 2000].

4.3 The actomyosin cable shows dynamic shape changes during serosa window closure

During serosa window closure, the cable shows very dynamic shape changes. In order to characterise these changes from early formation until complete closure of the window, I marked the cable outline at successive stages of a time-lapse SPIM movie projected as 2D map (Fig 4.5, A). This analysis revealed that the *Tribolium* actomyosin cable is very different from the previously reported cables, like the eye shaped cable involved in*Drosophila* dorsal closure or the more circular cables involved in wound healing [Brugués et al., 2014; Kiehart et al., 2000]. The *Tribolium* cable adopts several distinct shapes at different stages of serosa epiboly. It starts out as a loose zig-zag boundary between the amnion and the serosa (Fig 4.5, C). This boundary progressively becomes smoother and more refined as the closure proceeds. Once the extraembryonic-embryonic boundary moves to the ventral side of the embryo, the actomyosin cable appears stretched with an ordered alignment of the cell borders contributing to it. During serosa closure, the cable adopts several shapes starting as triangular, continuing as oval and ending up with a more isotropic circular shape (Fig 4.5, C).

The anterior part of the cable persists as a rigid, bar like linear boundary giving the cable a triangular shape. The triangular cable changes into a circular shape when the anterior bar becomes curved.

Finally, I used the distortion-corrected cartographic representations of SPIM imaged embryos (outlined in Chapter II) to measure the total length of the actomyosin cable from its formation to closure. This analysis revealed a biphasic actomyosin cable at the extraembryonic-embryonic boundary that initially increases in length followed by a progressive decrease in length (Fig 4.5, B) until it disappears completely after sealing the serosa epithelium.

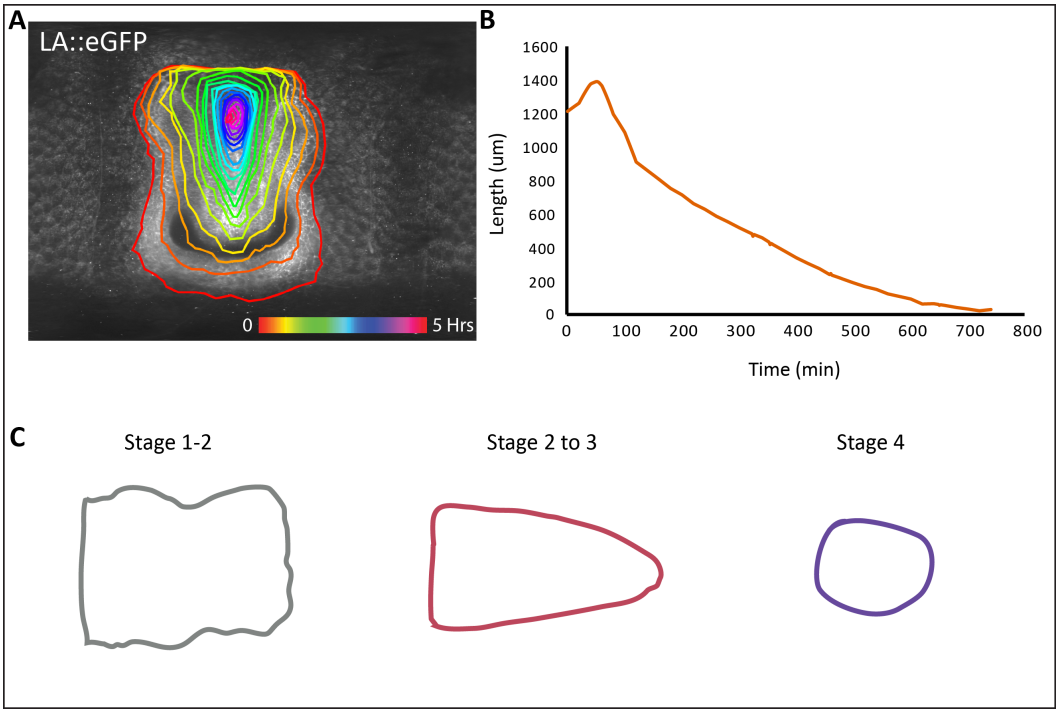

Figure 4.5: Time evolution of the actomyosin cable during serosa window closure. Cartographic projection of a transgenic *Tribolium* embryo labelled with LifeAct::eGFP. **A)** Dynamic change in the actomyosin cable shapes during serosa window closure with different timepoints indicated in different colours (stages 2-4). The colourbar indicates time from 0-5 hours. **B)** Change in the circumferential length of the cable measured on a 2D cartographic projection of a 4D SPIM dataset in which the embryo was labelled with LifeAct::eGFP. The cable shows biphasic length dynamics.**C)** The various shapes of the cable between Stage 1-4

4.4 Serosa cells increase in area till circular serosa window stage

It is well documented that the serosa cells expand their apical areas as they become squamous over time. In order to quantify this cell expansion, I measured the apical areas of serosa cells on the dorsal side of the embryos at about 50% embryo length. The apical cell areas increases and nearly triples from Stage 1 to Stage 3 (Mean area Stage 1-3 is 227 μm^2, 549 μm^2, 679 μm^2) till the serosa window becomes triangular (Stage 3) (Fig 4.6 A, B). Interestingly, the increase in apical cell area is not significant (p value between Stage 3 and 4 is 0.94) (Fig 4.6, B) between Stage 3 and Stage 4, when the serosa window is circular and decreases in size,. This indicates that the main phase of cell expansion - at least dorsally - ceases when the amnion involution is complete. It follows that the remainder of serosa epiboly until it fully covers the egg surface is effected by cell expansion in other parts of the serosa epithelium. Unfortunately, the very fast movement of the cells during serosa expansion prohibited tracking and quantification of expansion in single cells on a global scale, and will require SPIM datasets to be acquired with 30-60 sec temporal resolution. Despite this caveat, I identified several instances of serosa cell rearrangements during window closure. In particular, serosa cells close to the window underwent passive intercalation perpendicular to the cable pulling force (Fig A.1).

4.5 Tension in the serosa tissue increases during epibolic expansion

The observations that the serosa cells on the dorsal side of the embryos do not increase their area between Stage 3 and Stage 4 and that the cells become progressively squamous indicated that serosa tissue might change its mechanical properties over time.

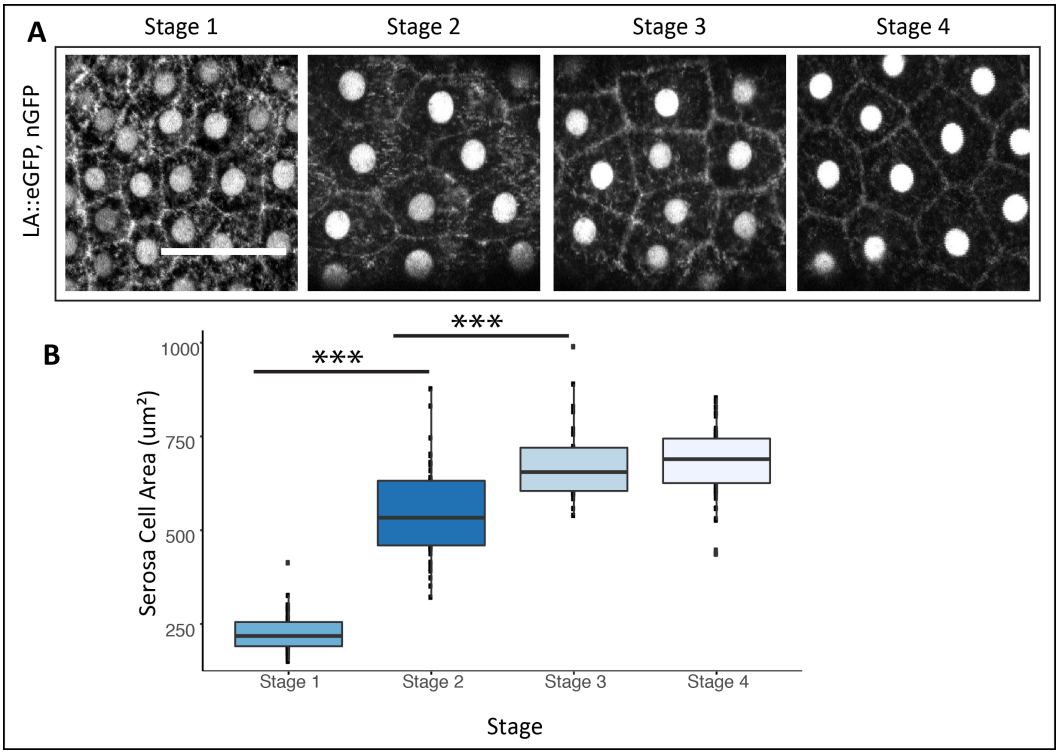

Figure 4.6: Quantifications of the increase in serosa cell area. The serosa cells increase their apical area as they become squamous. **A)** Images from double labelled embryos with LifeAct::eGFP and nGFP marking Actin and nuclei respectively. The dorsal area of the embryos was imaged. Scale bar is 10 μm. **B)** Boxplots show the total apical area of cells from Stage 1-4. Stage 3 and Stage 4 are not significantly different. The pair wise significance between appropriate pairs is tested using parametric Student's TTEST and p value between 0.05-0.01 is *, 0.009-0.001 is ** and highly significant < 0.001 is ***. The Stage 1 n = 72 and N= 4, Stage 2 n = 65 N = 6, Stage 3 n = 79 N = 4, Stage 4 n = 77 N = 8. n = no. of cells and N is number of embryos per stage.

The expansion and thinning of the serosa is one of the most salient features of early *Tribolium* embryogenesis. In order to get an insight into the mechanical basis of serosa epiboly, I measured the tension in the tissue by laser ablations at different developmental stages. Laser ablation is the most widely used method in vivo to study the role of mechanical stresses in morphogenesis by measuring the recoil velocity of the ablated edges [Farhadifar et al., 2007; Mayer et al., 2010; Rauzi and Lenne, 2011; Solon et al., 2009]. Laser cuts can be inflicted at the boundary of two cells or on a tissue wide scale by cutting

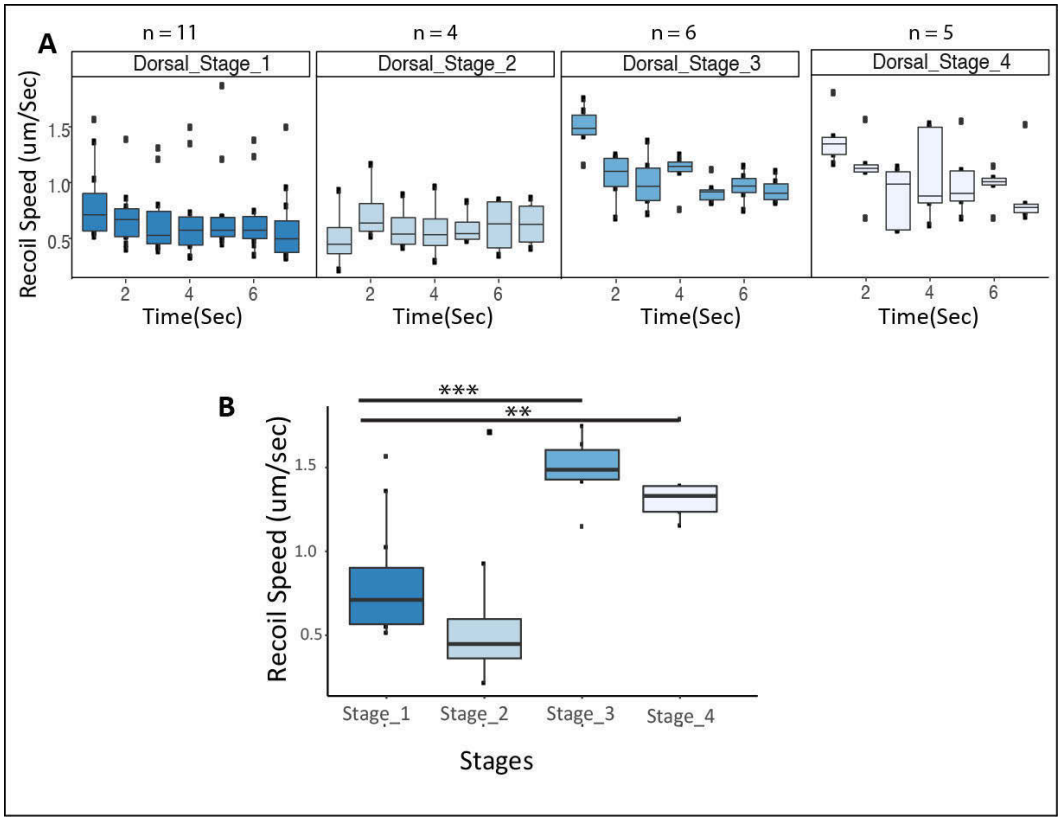

Figure 4.7: Analysis of tensions in the serosa tissue with laser ablations. A) Boxplots show the decay in the recoil velocity from laser ablations of the serosa performed at the same dorsal position of the embryo, from Stage 1-4. **B)** Initial recoil speeds are compared between Stage 1, Stage 3 and Stage 4. The pair wise significance between appropriate pairs is tested using parametric Student's TTEST and p value between 0.05-0.01 is *, 0.009-0.001 is ** and highly significant < 0.001 is ***.

several neighbouring cells in a single big cut [Aliee et al., 2012; Rauzi and Lenne, 2011]. I used the latter approach to estimate the tension in the serosa tissue by making a single big laser cut across 3-4 cells. The dorsal side of laser ablated embryos was targeted at the beginning of serosa expansion (Stage1), at the triangular cable shape (Stage 3) and at the circular cable stage (Stage 4). In all cases, the cell membranes snap apart and start retracting post ablation. The tension in the tissue is estimated by calculating the recoil velocity of the ablated edges with faster velocities indicating higher tension in the ablated

tissue [Smutny et al., 2014].

I observed that the initial recoil speed of the ablated serosa was lowest in stage 1, higher in stage 2 and highest in stage 3 indicating that the tension in serosa increases over time (Fig 4.7 B). Surprisingly, the decay in the recoil velocities of the ablated cells in stages 3 and 4 showed an oscillatory profile instead of the typical exponential decay seen post laser ablations (Fig 4.7 A). This finding suggests that the physical properties of the serosa epithelium may change over time as it becomes subjected to increased tension.

4.6 Serosa cells decrease their apical areas after laser ablation

Since the serosa tissue showed increased tension with time, laser cuts should release the tension and relax the tissue. To measure the effect of ablation on the rest of the serosa tissue, I measured the change in the apical areas of non-ablated cells adjacent to the laser ablated cells at Stages 3 and 4 (Fig 4.8). These neighbouring cells immediately start decreasing their apical areas post ablations. The 'first order' neighbours (cell making direct contacts with the ablated cells) decrease their apical areas to the smaller size observed at Stage 2 (Stage 3 cells decrease their area from 679 μm^2 to 494 μm^2 and Stage 4 cells 689 μm^2 to 474 μm^2) (Fig 4.8, After laser ablation). This result suggests that the cell flattening and epibolic expansion of the serosa is a passive process effected by the neighbouring tissues, in particular the pulling forces exerted by the condensing embryonic primordium. A similar relaxation of tension after laser ablations has also been reported in the amnioserosa tissue in *Drosophila* [Kiehart et al., 2000].

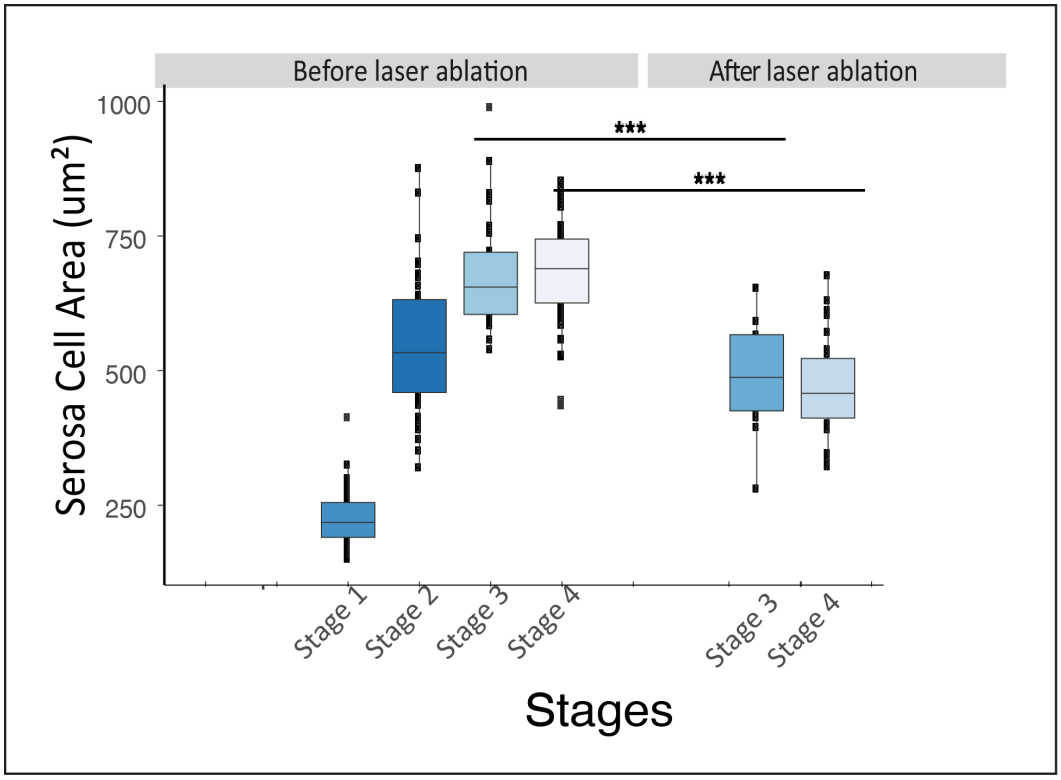

Figure 4.8: Neighbour cells decrease their apical areas post laser ablation. Comparison of the apical cell area of the serosa cells on the dorsal side of embryos before laser ablation (previously shown in Fig 4.6) and the area of the neighbouring cells after laser ablation (at Stage 3 and 4). Apical cell areas decreases significantly after ablations. The pair wise significance between appropriate pairs is tested using parametric Student's TTEST and p value between 0.05-0.01 is *, 0.009-0.001 is ** and highly significant < 0.001 is ***. After ablation Stage 3 n = 13 N = 5, Stage 4 n = 27 N = 7. n = no. of cells and N is number of embryos per stage.

4.7 Tension in the actomyosin cable increases during serosa epiboly

As described earlier, the actomyosin cable changes its length and shape during serosa epiboly (Fig 4.5). In addition, the tension in the serosa also increases indicating that it takes a larger force to pull the serosa over time. Together, these observations suggest that the tension in the actomyosin cable might also change during serosa expansion. I measured the change in cable tension by

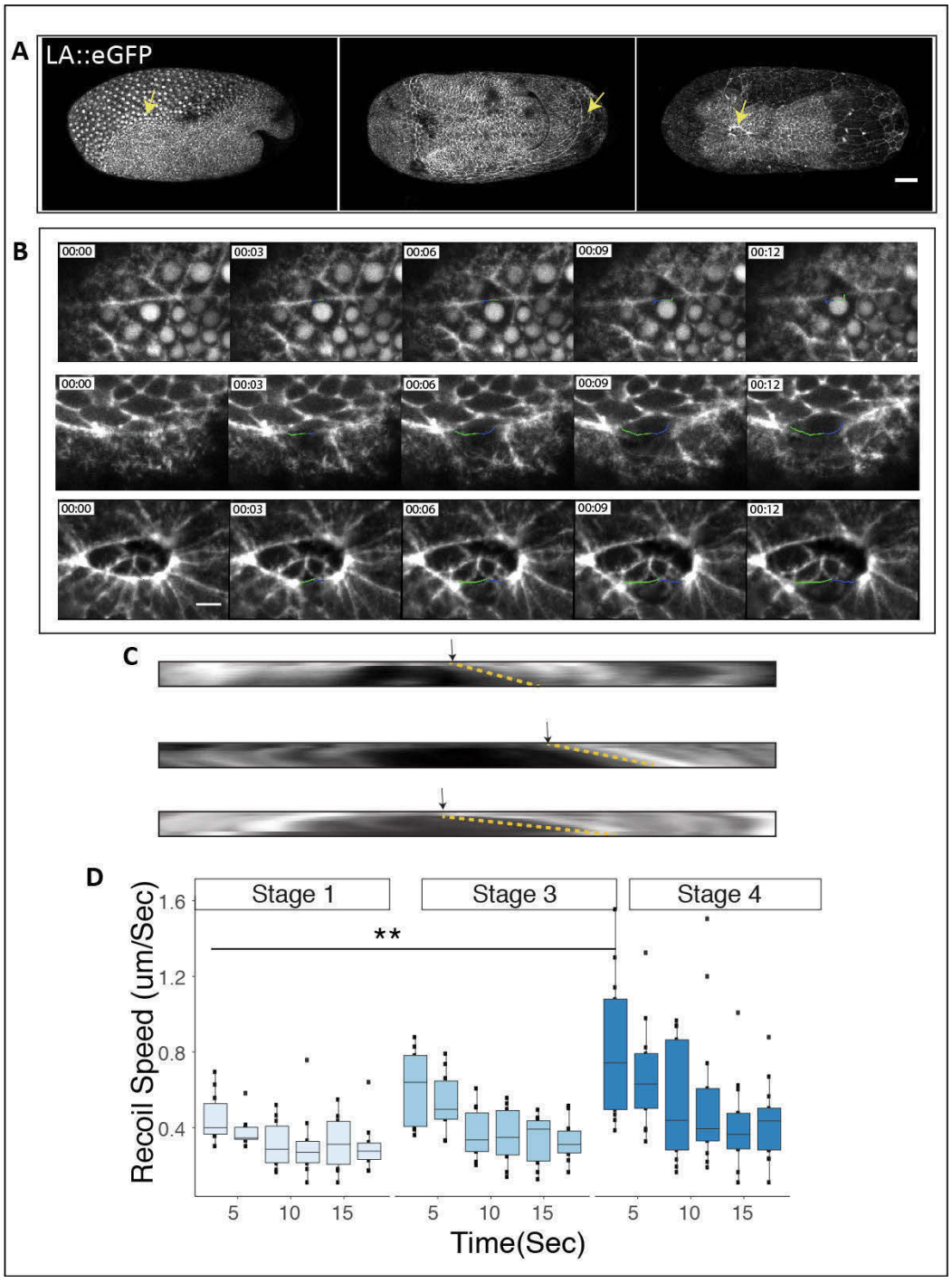

Figure 4.9: Analysis of cable tension with laser ablations.

Figure 4.9: Analysis of cable tension with laser ablations. A) Max projection of confocal z stacks from 3 different developmental stages (Stage1,2 and 4). Arrow points to the region of the cable that was ablated. Scale bar is 50 μm. **B)** Timelapse images to show the movement of the ablated edges post laser cut. Time is in seconds. Scale bar is 10 μm. **C)** Kymograph of the recoiling membrane edge at the 3 stages. Increased slope of the kymographs indicates the increase in the recoil velocity over time. **D)** The exponential decay in the recoil velocity of the ablated edges measured at the three stages. The initial recoil between Stage 1 and Stage 4 is significantly different.The pair wise significance between appropriate pairs is tested using parametric Student's TTEST and p value between 0.05-0.01 is *, 0.009-0.001 is ** and highly significant < 0.001 is ***. Stage 1 n $\geqslant$ 10 in each cases, n = number of embryos.

laser ablation and calculation of the recoil velocities between the two edges (Fig 4.9, C). As the cable spans across several cells and eventually forms the rim of the serosa window, I ablated individual boundaries between two cells perpendicular to the length of the cable. The cuts were performed near the anterior head lobe region at Stage 1 (Fig 4.9, A) and Stage 4. I also ablated the cable near the posterior pole at Stage 2 for an independent comparison at an intermediate stage. The distance between the two ablated edges of the boundary was calculated after ablation, to measure the recoil speeds (Fig 4.9, C).

As expected, the tension in the actomyosin cable increases over time. The initial recoil velocity becomes nearly double at the circular serosa window stage (Stage 4) as compared to the differentiated blastoderm stage (Stage 1) (Fig 4.9, D). The kymograph projections of the movement of the ablated edges also showed a faster recoil at Stage 4 (Fig 4.9, C). This increased cable tension presumably also results in the increased stretching and straightening of the cable over time. Previous studies on *Drosophila* wing disc have shown that the increase in the straightening of the actomyosin cable at the dorso-ventral compartment boundary correlates with an increased tension measured by laser ablations [Aliee et al., 2012]. Overall, these results are consistent with a scenario whereby an increasing amount of contractile cable force is required to successfully close and seal the serosa window, which could be due to the increasing resistance from the stretched serosa and/or the adjacent amnion epithelia.

4.8 Myosin dynamics at the cable changes between early and serosa window stage

Since Myosin is the force-generating molecular motor that pulls on Actin filaments, the increase in cable tension should be mediated by a change in Myosin contractility at the cable. It has been shown previously, that cell boundaries under higher tension exhibit increased levels of Myosin and lower rates of Myosin dissociation compared to cell boundaries under lower tension [Fernandez-Gonzalez et al., 2009; Fernandez-Gonzalez and Zallen, 2009]. I approached this question by measuring the change in Myosin intensity at the cable, as well as the rate of Myosin dissociation by **F**luorescence **R**ecovery **A**fter **P**hotobleaching assay (FRAP). I first imaged and compared the Myosin level in the cable in a Tc-squash::eGFP transgenic line from Stage 1 to Stage 4 (Fig 4.10). I observed an enrichment in Tc-squash::eGFP levels that exhibit a more homogeneous and dense labelling of the cable over time. Therefore, the increase in cable tension correlates with an increase in the amount of Myosin present on the cable. Unfortunately, despite several attempts, I could not obtain any specific staining in *Tribolium* embryos with the commercially available antibodies against the active phosphorylated form of myosin.

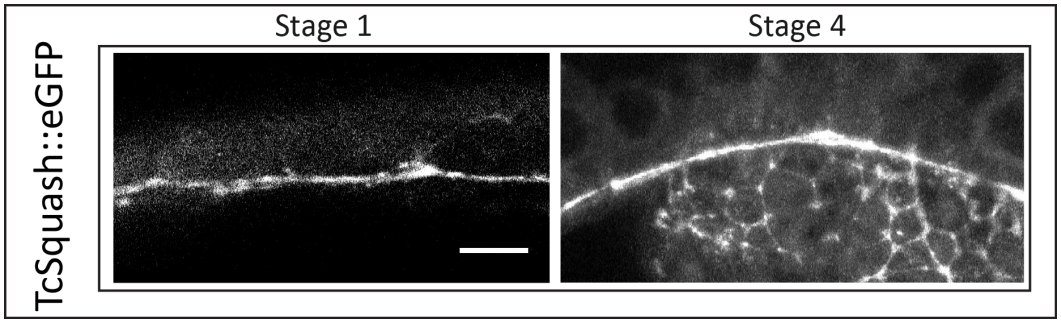

Figure 4.10: Myosin localisation and structure at the cable changes between early and serosa window stage. *Tc-squash*::GFP labelling of the cable at Stage 1 and Stage 4. Myosin localisation becomes denser at Stage 4. Scale bar is 10 μm.

In order to measure the increased stability of Myosin at the cable and the rate of dissociation, I performed the FRAP assay. FRAP assays are used

to monitor protein stability and dynamics by monitoring the fluorescence recovery in the region of interest after its bleaching with a high-intensity laser beam[White and Stelzer, 1999]. The total percentage of the recovered fraction is estimated by fitting an exponential curve to the fluorescence recovery profile after background correction and normalisation to the initial values. After quantification and fitting of the curve, the half time for the recovery ($\tau_{0.5}$) is measured, which indicates the time it takes to reach 50% of the final amount recovered. I bleached a small region of the cable and calculated the recovery of the Tc-squash::eGFP fluorescence signal. The analysis was performed at the early Stage (Stage 1) and the circular serosa window stage (Stage 4).

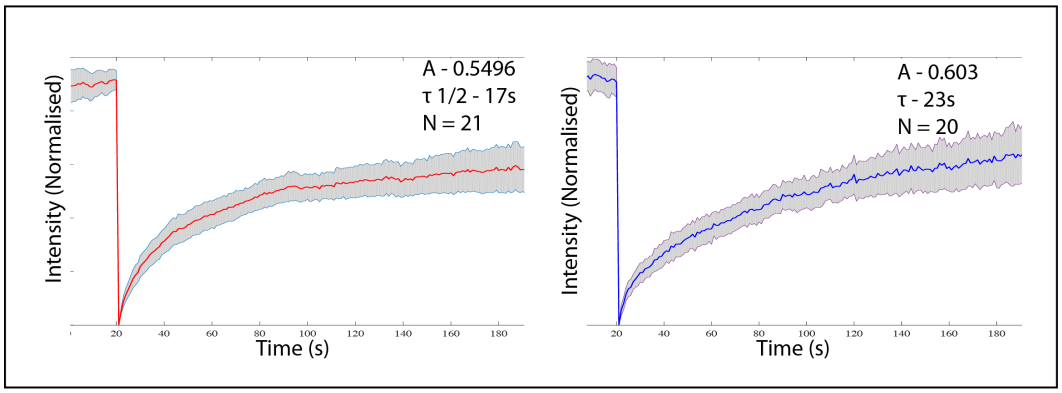

Figure 4.11: FRAP analysis of Myosin recovery. A) FRAP recovery profile of Tc-squash::eGFP from the Stage 1 (differentiated blastoderm, early cable) and **B)** from Stage 4 (Circular cable). 'A' denotes the mobile fraction and τ is the half time for recovery.

The preliminary analysis of FRAP experiments, showed significant differences in terms of mobile fraction and half time of recovery between early and late stages (Fig 4.11). In the late stage, the recovery is slower (based on τ _0.5) than early stage, however the overall mobile fraction seems to be increased. The slower recovery based on τ _0.5 can be due to lower dissociation of the mobile fraction, due to localized activity of the Myosin related to higher contraction of the cable or due to local recruitment of the protein. In both cases (Irrespective of due to recruitment or higher diffusivity), it indicates

stronger local dynamics of Myosin at the late-stage, which is consistent with the observation of higher local tension.

4.9 Individual cell membrane shrinkage and cell rearrangements decrease the cable circumference

The mechanism of cable contraction and sealing of the serosa window is still unclear. In other well-studied cases, actomyosin cables either show zippering to align the two sides of a tissue (e.g. neural tube closure) or circumferential purse string-like pulling of cells together to a central point (e.g. wound healing) [Röper, 2014]. To understand the mechanism of the serosa window closure and the dynamics of the supracellular cable in this process, I tracked the cells whose interfaces contribute to the constricting cable from the circular serosa window stage (Stage 4) onwards using the manual tracker plugin in Fiji (Fig 4.12).

Interestingly, I observed that serosa cells which form the cable, slowly decrease their cable forming edge and exclude from the cable (Fig 4.12, A). Although these cells progressively leave the cable, they intercalate between the neighbours thus remaining in the serosa epithelium (Fig 4.12, B). As a result, effectively the total number of cells that form the actomyosin cable decreases with time during the window closure. This results in shortening of the circumference of the serosa window. In conclusion, the *Tribolium* serosa window cable exhibits a modified purse string-like mechanism; its circumference shrinks centripetally reducing the number and size of participating cell edges similar to wound healing cables.

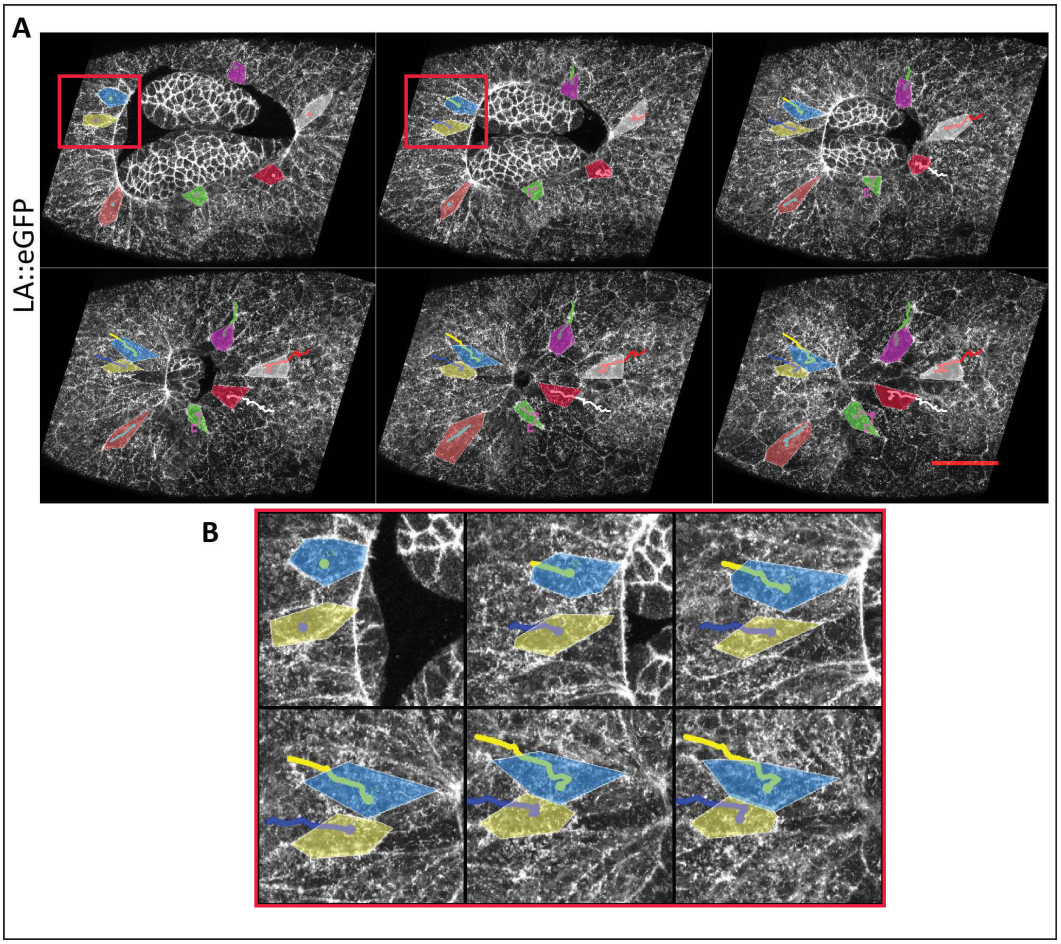

Figure 4.12: Cell behaviours at the edge of the actomyosin cable during its shrinkage. Selected cells contributing to the cable are indicated. Cells shrink their membranes and are slowly extruded from the cable leading to an overall decrease in cable circumference. **B)** An inset of the cell highlighted in blue and yellow from panel **A)**. Heterogeneity in *Tc-squash*::GFP (MyosinII) labelling along the cable circumference. Tc-squash is enriched in shrinking cell edges. **D)** Montage of a manually extracted and straightened cable over time from panel **C)**, Myosin enriched junctions shrink to a point. **E)** Cable tension is not relieved by consecutive cuts as indicated by the measured recoil speeds. Scale bar is 50 μm.

In order to describe the behaviour of the cable forming cells over time, I decided to compare the cable forming cells at an earlier stage when the amnion involution is still proceeding (Stage 2) and later stages. For this, I manually highlighted the cells that form the serosa window at Stage 2 and Stage 4 using Fiji plugins (Fig 4.13A and B respectively).

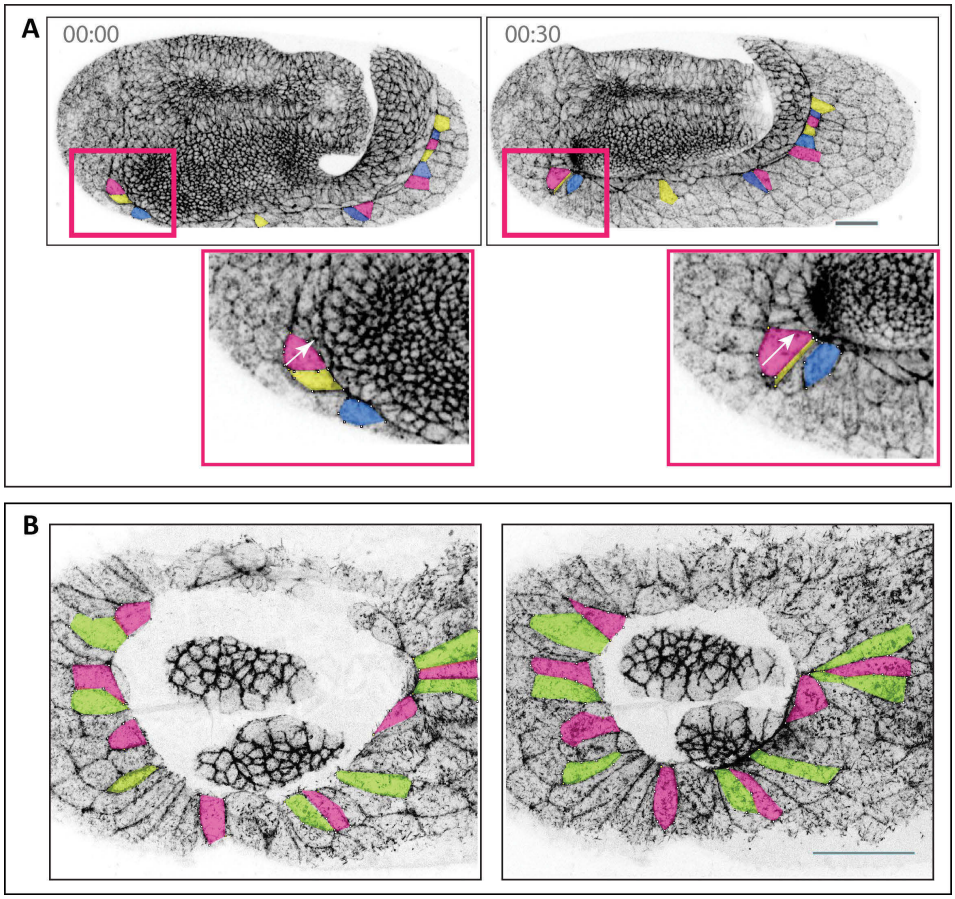

Figure 4.13: Cell shapes changes in the cable forming cells. Cell shape changes of the cable forming cells at Stage 2 **A)** and Stage 4 **B)**. **A)** Selected cells contributing to the cable are indicated. Cells elongate perpendicular to the cable. An inset of the highlighted cells which elongate in the direction of the arrow. **B)** Cell anisotropies show elongated cells at Stage 4. Cell shrink their cable forming edge. Time is in minutes. Scale bar is 50 μm.

I observed that not only the cells exclude from the cable, the cells forming the cable also slowly elongate, perpendicular to the serosa window. At both stages, the cells become increasingly anisotropic in their shape and appear to be pulled by the closing window. This indicated that the cells at the cable boundary are under high tension and probably as a passive response to the pulling forces exerted by the cable, the anisotropy in their shapes increases over time.

4.10 Myosin dynamics at the cable during serosa window closure

The analysis of the cable-forming serosa cells revealed that the circumference of the serosa window decreases due to cells shortening their cable forming edges. However, these cells contributed to the cable circumference with different lengths of their cable forming edges, suggesting that the degree of cell border shrinkage varies between cells in the cable. Additionally, the extruded cells intercalate between their neighbours in the serosa, a process that is mediated by planar polarised actomyosin enrichment during germband morphogenesis in *Drosophila* and *Tribolium*.

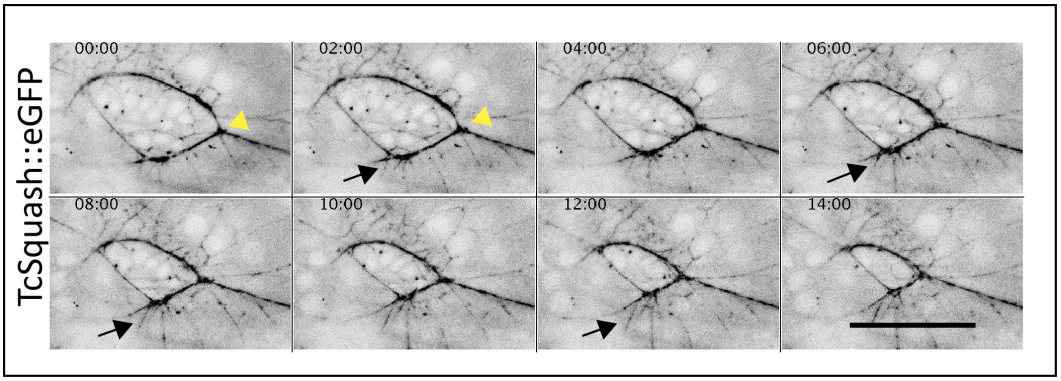

Figure 4.14: Myosin enrichment at cell junctions in the cable. Images are from a timelapse movie with Tc-squash::eGFP label. Heterogeneity in Tc-squash::eGFP labelling is seem along the cable circumference. Tc-squash is enriched in shrinking cell edges. Arrows mark a cell that leaves the cable and intercalates into serosa. Arrowheads point to increased Tc-squash intensity at a cell edge about to leave the cable. Time is in minutes. Scale bar is 50 μm.

For these reasons, I imaged Tc-squash::eGFP at very high temporal resolution together with a membrane marker during late serosa window closure stage (Fig 4.14) to understand the contribution of Myosin in the extrusion and intercalation of serosa cells. I observed that the *Tribolium* squash not only forms a supracellular circular alignment, it also shows enrichment at the cell-cell junctions on the cable and shows a patchy localisation. Addition-

ally, Myosin is enriched in cells that are shrinking their cable-forming edges, become highly anisotropic perpendicular to the cable and finally intercalate between their neighbours in the serosa.

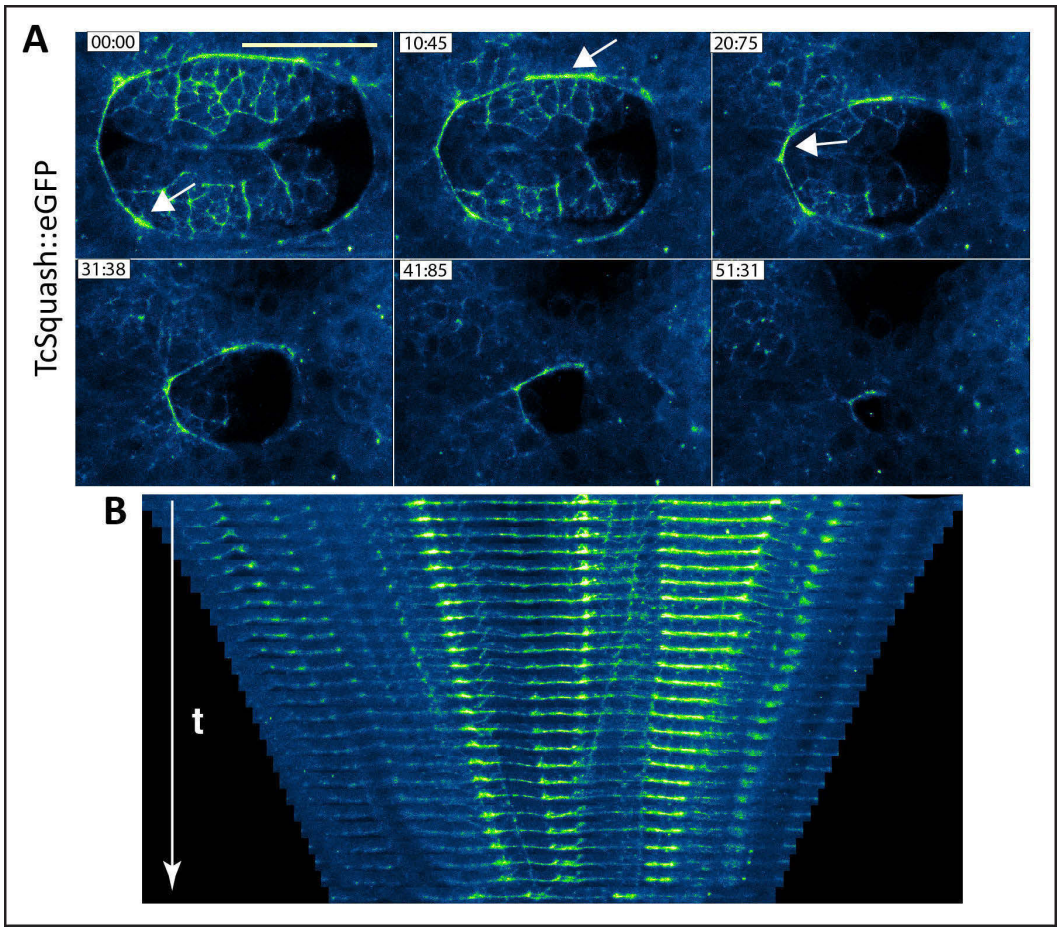

Figure 4.15: Myosin dynamics at the cable during serosa window closure. A) *Tc-squash*::eGFP shows patchy localisation along the cable circumference. Tc-squash is enriched in some cells (Arrows). **B)** Montage of a manually extracted and straightened cable over time from **A**. Images are displayed in the green fire blue LUT in Fiji and green corresponds to higher and blue to lower intensity levels. Time is in minutes. Scale bar is 50 μm.

I studied in more detail the variation in Myosin enrichment along the cable by imaging Tc-squash::eGFP labelled embryos during the circular serosa window stage (Stage 4) (Fig 4.15). I observed that although Tc-squash accumulation is continuous in the circular cable, its intensity is heterogeneous and

patchy (Fig 4.15, A) as the Myosin levels vary between the cable-forming edges of different cells. I used a Fiji based computational approach to segment the cable from time-lapse recordings and represent it as a straightened entity to study the Myosin dynamics in different regions of the cable . This analysis showed that the shrinking rates in different regions of the cable correlate with their Myosin levels (Fig 4.15, B). Cable segments with higher levels of Myosin appear to shrink faster suggesting that Myosin contractility varies between the cable-forming cells.

4.11 Tension in the cable is not relieved after multiple laser cuts

The different cells contributing to the cable showed variations in their cable-forming edges and associated Myosin levels, giving the cable a patchy appearance. These results raised the question whether the seemingly supracellular actomyosin cable is indeed a higher-order contractile structure or it is the sum of coordinated but still autonomous contractile cell units. I hypothesized that if the cells shrink their cable-forming edges in an autonomous manner, then their tension would not be affected by prior laser ablations at other position in the cable. For this reason, I performed sequential ablations in the cable at different regions (Fig 4.16, A) and observed that the tension in the cable is not decreased after the first cuts. Instead, the recoil speeds of the ablated cell edges remain comparable even after three successive cuts of the same cable (Fig 4.16, B, C). Although the tension in the abated cell is released after cutting, other cable-forming cells at a distance remain unaffected under high tension and continue shrinking autonomously. These results support the idea that cable-forming serosa cells host independent contractile actomyosin networks that somehow are coordinated and aligned in such a way to resemble a supracellular contractile apparatus.

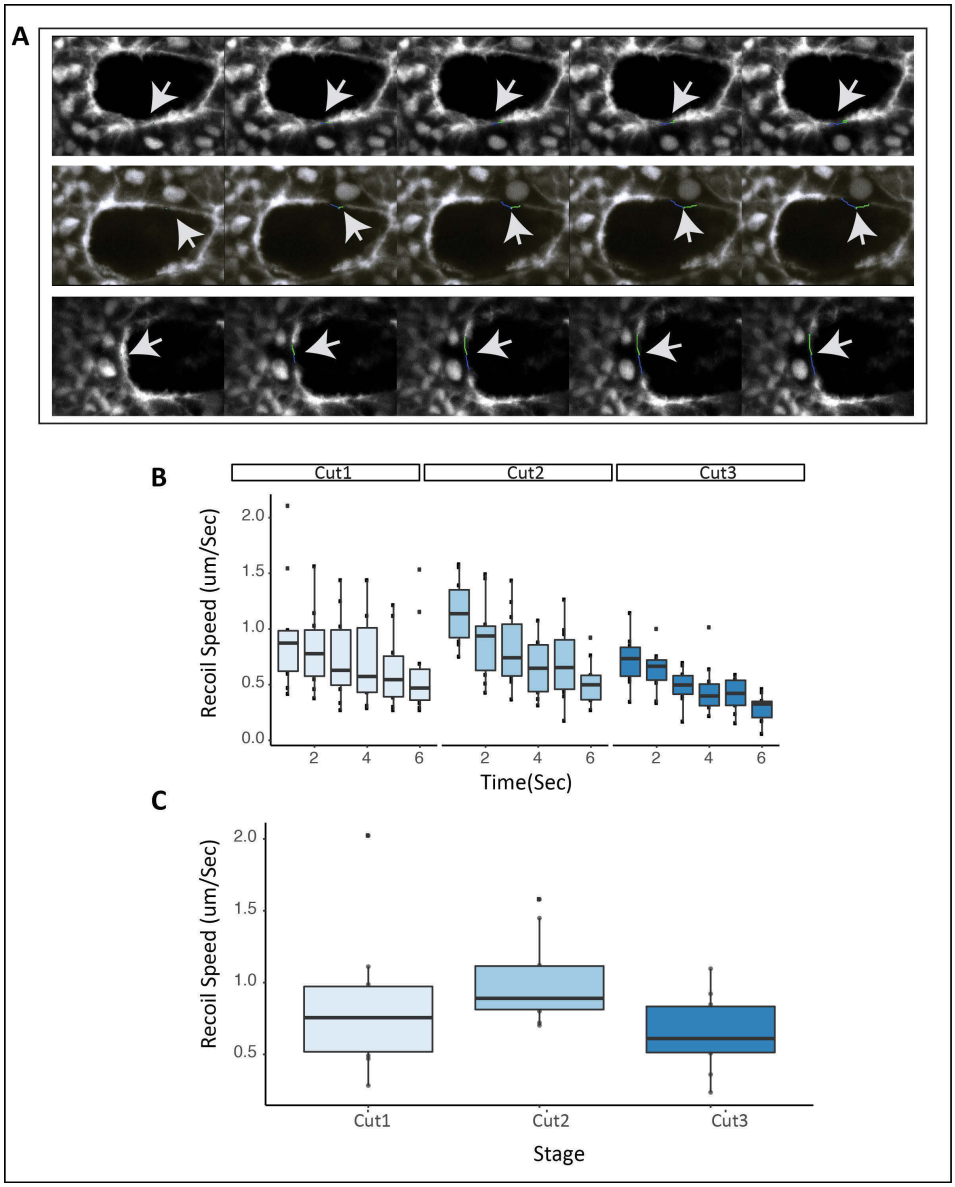

Figure 4.16: Successive laser cuts show comparable recoil velocities.

Figure 4.16: Successive laser cuts show comparable recoil velocities. Cable tension is not relieved by consecutive cuts as indicated by the measured recoil speeds. **A)** Maximum intensity projection of confocal z stacks from 3 successive and different laser cuts. Arrow points to the region of the cable that was ablated. Scale bar is 50 μm. **B)** The decay in the recoil velocity of the ablated edges measured for the three successive cuts. **C)** comparison of the initial recoil for the three cuts. The pair wise significance between appropriate pairs is tested using parametric Student's TTEST and p value between 0.05-0.01 is *, 0.009-0.001 is ** and highly significant < 0.001 is ***. n = 10 in all cases.

4.12 Analysis of the actomyosin cable in *Tc-zen 1* knockdown

The *Tribolium zerknült 1 (Tc-zen 1)* gene is a derived Hox3 homeodomain transcription factor that specifies the extraembryonic serosa primordium. It is expressed as an anterior dorsally tilted cap in the uniform blastoderm [van der Zee et al., 2005]. Parental and embryonic RNAi against *Tc-zen1* leads to a complete loss of serosa and an anterior shift in the embryo,Äôs fate map (Kristen Panfilio, personal communication) [van der Zee et al., 2005]. Embryos knocked down for *Tc-zen1* can develop normally and hatch but the serosa window formation and closure fail to complete. Since the actomyosin cable forms at the extraembryonic-embryonic interface, I hypothesized that no actomyosin cable would be detected after *Tc-zen1* knockdown.

For these experiments, eggs were co-injected with the dsRNA against *Tc-zen 1* and the mRNA encoding LA::eGFP. The injected embryos were incubated overnight at 25°C and imaged the following day. Surprisingly, I observed a partial knockdown phenotype with a reduced anterior serosa primordium and a corresponding increased and anteriorly shifted embryonic primordium (Fig 4.17). These embryos exhibit a delayed serosa window formation but eventually complete closure (Fig 4.18, A). Unlike in wildtype embryos, the amnion folding and involution are much slower, resulting in embryos that complete mesoderm invagination while they are still uncovered ventrally (4.17, B arrowhead). Such a hypomorphic phenotype has not been reported previously in *Tc-zen 1* RNAi experiments and may be associated with the co-injected LA::eGFP

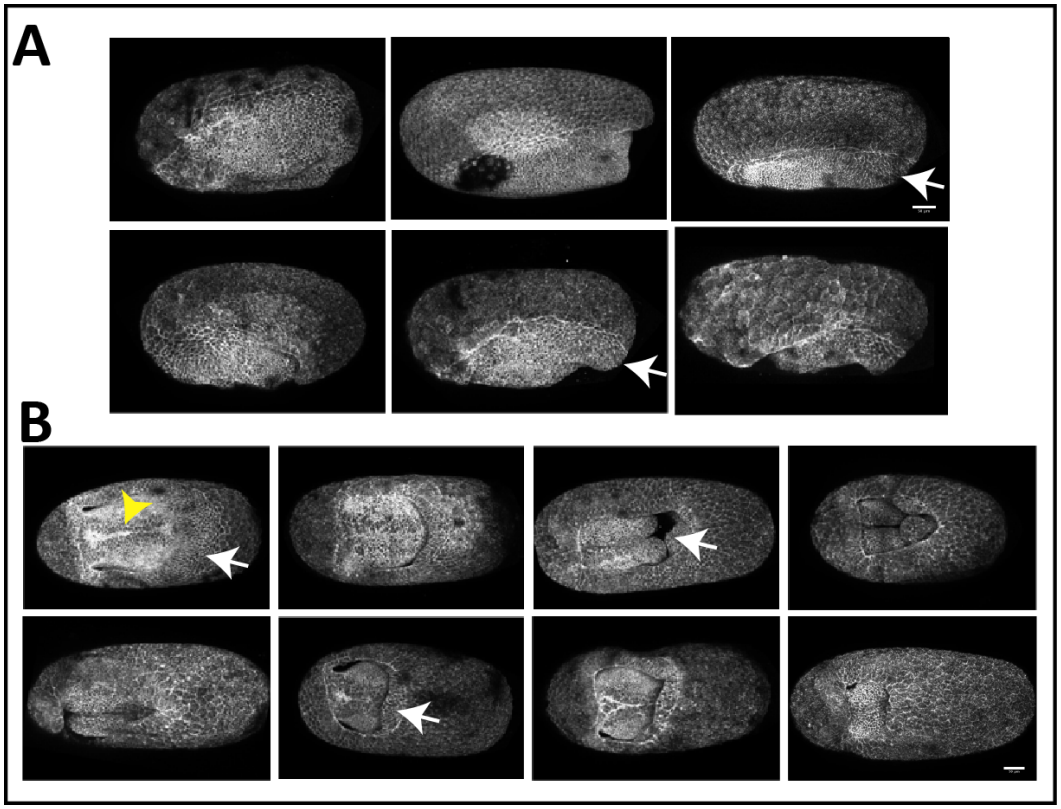

Figure 4.17: Embryonic knockdown of *Tc-zen*. Embryos were co injected with dsRNA for *Tc-zen* and LA::eGFP mRNA for labelling. Maximum intensity projection of confocal z stacks of different embryos to show the lateral **A)** and the ventral views **B)**. Arrow points to the amnion which is not completely involuted. Arrowhead points to the ventral furrow

Actin reporter and/or the overnight incubation of injected embryos at a lower temperature at 25°C. A detailed analysis of Tc-zen 1 RNAi phenotypes with other co-injected mRNA constructs and with different incubation temperatures is still needed to confirm the specificity of this partial phenotype.

Despite this caveat, this hypomorphic phenotype provided an ideal opportunity to investigate the actomyosin cable dynamics under perturbed conditions. As described earlier for wildtype embryos, I used SPIM imaging and laser ablations to analyse the cable shapes and tension in *Tc-zen 1* knockdown embryos (Fig 4.18, A) (Fig 4.3, 4.5). Unlike in the wildtype condition, the cable had a circular appearance after *Tc-zen 1* knockdown throughout the various

phases of serosa window formation and closure (Fig 4.18, B).

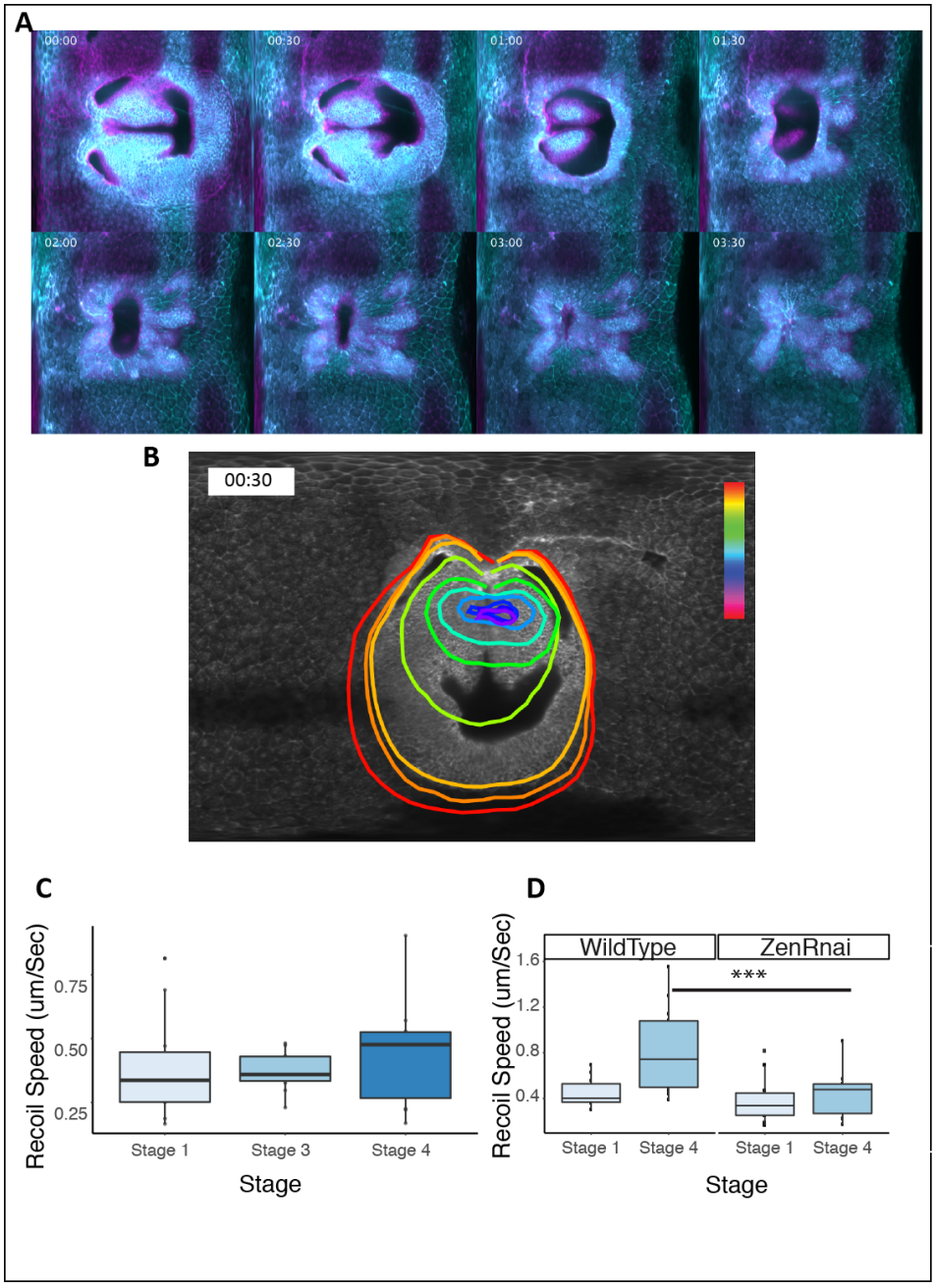

Figure 4.18: Cable dynamics during serosa window closure after *Tc-zen* knockdown by RNAi.

Figure 4.18: Cable dynamics during serosa window closure after *Tc-zen* knockdown by RNAi. *Tc-zen* homeodomain transcription factor specifies serosal cell fate. After *Tc-zen* knockdown the actomyosin cable exhibits an altered shape compared to wildtype.**A)** Panels show cartographic projections as in Fig4.3 **B)** Dynamic change in cable shapes during serosa window closure after *Tc-zen* knockdown with different timepoints indicated in different colors (stage 2-4) **C)** The Initial recoil velocity measured after laser ablations is not different between Stage 1, Stage 3, and Stage 4. **D)** Comparison of the initial recoil velocity post laser ablation between wildtype and knock down. The recoil velocity at Stage 4 is significantly different between the two. No increase in cable tension is seen in *Tc-zen* knockdown condition. The pair wise significance between appropriate pairs is tested using parametric Student's TTEST and p value between 0.05-0.01 is *, 0.009-0.001 is ** and highly significant < 0.001 is ***. . n $\geqslant$ 10 in each case.

The tension in cable increases over time (Fig 4.9). After *Tc-zen 1* knockdown, embryos have a prolonged amnion involution and a delayed formation and closure of the serosa window. I assessed the tensions in the cable with laser ablations at at comparable stages and positions described for wildtype embryos (Fig 4.18, C). The measurement of the initial recoil velocity post ablation at the three stages showed that the tension in the cable do not increase over time in the *Tc-zen 1* knockdown embryos. Interestingly, the initial recoil velocity in wildtype and *Tc-zen 1* knockdown remains comparable at Stage 1 and although it becomes nearly double in wildtype by Stage 4, it remains constant *Tc-zen 1* knockdown (Fig 4.18, D).

4.13 Summary

The results in this chapter show that an actomyosin cable forms at the embryo-extramembryonic boundary during serosa window closure in *Tribolium*. This cable starts appearing as an Actin and Myosin accumulation during the differentiated blastoderm stage (Stage 1) at the boundary between the serosa and future amnion. It spans across the dorso ventral diameter of the embryo and increases in size till it reaches the ventral side (Stage 2) after the posterior amniotic fold formation. Interestingly, the actomyosin cable is under high tension which increases as the serosa window closure proceeds. The cells in

serosa tissue on the dorsal side of the embryos increase in area to nearly triple, from Stage 1 -3. Concurrent with the expansion, the tension in the serosa epithelium also increases with time. This indicates that the serosa epithelium changes its mechanical properties and increased force is required to seal the epithelium during the serosa window closure. The actomyosin cable appears as a modified purse string as the cells which contribute to the cable sloly shrink their cable forming membrane and intercalate into the serosa, thereby decreasing the circumference of the cable. Additionally, the cell's seem to shrink in an autonomous manner as tension in different regions of the cable are not relieved after successive ablations. Lastly, the tension in the cable do not increase over time in *Tc-Zen1* knockdown embryos which have reduced serosa and expanded embryo. Together these results show that investigations into the dynamics of the actomyosin cable which plays a role in serosa window closure could provide interesting insights into the mechanics of actomyosin cable formation and function.

CHAPTER 5

DISCUSSION

5.1 Reconstruction of insect embryogenesis using lightsheet microscopy and tissue cartography

Early embryogenesis in *Tribolium* is not only a better representative of insects, but also is quite different from the well studied *Drosophila* embryogenesis. Unlike *Drosophila*, the extensive extraembryonic membranes show tissue expansion, tissue folds and involution. This provides an excellent opportunity to study how changing gene expression patterns and gene regulatory networks, between *Drosophila* and *Tribolium* have influenced cell behaviour and actomyosin dynamics between these systems. Therefore, the establishment of *Tribolium* as a model to study tissue morphogenesis, complemented with the existing studies on gene functions and expression patterns sets a platform for comparisons of cellular and molecular dynamics between different insect

species. Therefore, it has become imperative to provide an exhaustive and *in toto* description of the cell dynamics that mediate tissue morphogenesis, through shape changes, cell divisions, tissue folding, convergent extensions, etc. However, live imaging to study tissue dynamics in *Tribolium* is just beginning and protein dynamics during development haven't been described. This leaves a lot of scope and need for detailed characterisation of various developmental stages, to study morphogenesis in particular and development in general.

Recently, complete 4D dynamics of nuclei and cell behaviours are becoming available for embryogenesis in various model systems using lightsheet microscopy [Ahrens et al., 2013; Amat et al., 2015, 2014; Shah et al., 2017]. Therefore, I decided to not only use confocal based live imaging assays to investigate tissue morphogenesis in *Tribolium*, but rather combine SPIM imaging with confocal. The *in toto* information of 4D dynamics feeds into providing a global description of morphogenetic events, which can then be probed at higher resolutions using confocal. However, the rate limiting step in live SPIM imaging of non model species remains the lack of transgenics with proteins tagged to fluorescent labels. Generating transgenic lines in newly emerging systems can be a long and cumbersome protocol followed by screening the lines for good signal to noise ratio, viability and background affects. This often results in creation of lines which are not very useful due to dim signal, patchy expression etc. Alternatively, transient labelling with injection of dyes, proteins, DNA constructs or mRNA is becoming a method of choice in non model organisms. It is being widely used in systems like crustaceans, annelids etc. Its adaptation in *Tribolium* for both confocal imaging [Benton et al., 2013] and now SPIM allows for imaging nuclear, cellular and protein dynamics, circumventing the need for transgenics.

I have streamlined the steps of labelling, imaging and image analysis to study 4D cellular dynamics using the SPIM microscopes in *Tribolium* in a easy to adapt pipeline. This pipeline requires an initial step of cloning any protein of interest from the *Tribolium* genome into a plasmid containing a fluorescent tag and which is suitable for capped mRNA synthesis. The embryos are labelled

by mRNA injection, mounted and imaged with SPIM and then open access Fiji plugins are used for data processing. Following this, the 4D data can be manipulated such that slices can visualised using the BigDataViewer(BDV, Fiji)[Pietzsch et al., 2015] or IMARIS and cartographic maps can be made. Finally, it is also possible to make measurements on the 3D (2D + time) maps to provide a quantification of tissue behaviours. So far, I have used this workflow for gaining an overview of the Actin and Myosin dynamics in different regions of the embryo. The 3D maps were used to describe actomyosin behaviours right from the uniform blastoderm stage to serosa window closure. Next, this pipeline will be used for labelling, imaging and analysing nuclear and cell dynamics. I can track the serosa and embryo nuclei on the maps and this data will be used to identify tissue movements in the embryos. It is possible to calculate the cell shape change in any region of the embryo on the maps and I am using the BigDataViewer plugin in Fiji for analysing cross sections and sagittal sections of the embryo. This straightforward approach to visualise isotropic 3D data allows for observation on cellular and molecular dynamics in different regions of the embryo. As an example, I could observe the actomyosin dynamics at the posterior pole of the embryos and the cell shape changes such as apical constrictions using this approach.

The establishment of a SPIM image acquisition, processing and analysis pipeline for studying *Tribolium* embryogenesis now sets up a platform for analysing 4-Dimensional cell dynamics. Further, it is possible to investigate the conserved or novel role of proteins in tissue morphogenesis by labelling any protein of interest, co-labelling it with membrane and nuclei and studying its embryo wide dynamics in both wildtype and genetic knockdown conditions. However, the SPIM imaging remains limited in its applications, since it produces large datasets ranging up to a few terabytes. The injected embryos have lower viability compared to wildtype and transgenics and die more often while imaging. Therefore, the specific SPIM data observations need to be supplemented with higher replicates, collected for each stage using confocal. Together, these techniques combine to give pan embryo visualisations and dynamics

followed by high resolution analysis in specific regions and stages. In addition to providing *in toto* dynamics of *Tribolium* embryogenesis, this workflow provides a standardised approach for future investigations into non-model insect embryogenesis as well.

5.2 Conserved Myosin II behaviours and its implications on morphogenesis across insects

Contractile actomyosin networks are important force generatoring machinery in cells during morphogenesis. A summary of research in *Drosophila* indicates that Myosin II adopts various subcellular localisations depending on the constricting region, such as, Myosin II mediated contractility functions at the apical medial region of cells, in the junctional belt, in lateral membranes and at the basal side of cells in different events. This makes studying cellular Myosin II localisations very relevant from two perspectives- first, understanding signalling molecules that regulate Myosin II function at specific cellular regions in a tissue and second, the regulation of this activity between tissues and over the course of organism development.

Myosin II localisation and dynamics showed that it behaves in a very similar manner during *Tribolium* embryogenesis if compared to *Drosophila*. A summary of the comparable subcellular Myosin behaviours between *Tribolium* and *Drosophila* is shown in the Fig 5.1. During cellularisation, it forms contracting rings at the basal sides of both columnar and cuboid cells in *Drosophila* and *Tribolium* respectively indicating towards its conserved role in cellularisation across epithelia types [Xue and Sokac, 2016]. It localises apically and shows cortical pulsations in the apically constricting cells of the ventral furrow and the posterior pole of *Tribolium*. Both of these localisations are similar to the previously reported Myosin dynamics in *Drosophila* ventral furrow cells [Martin et al., 2009]. It shows planar polarity in the condensing

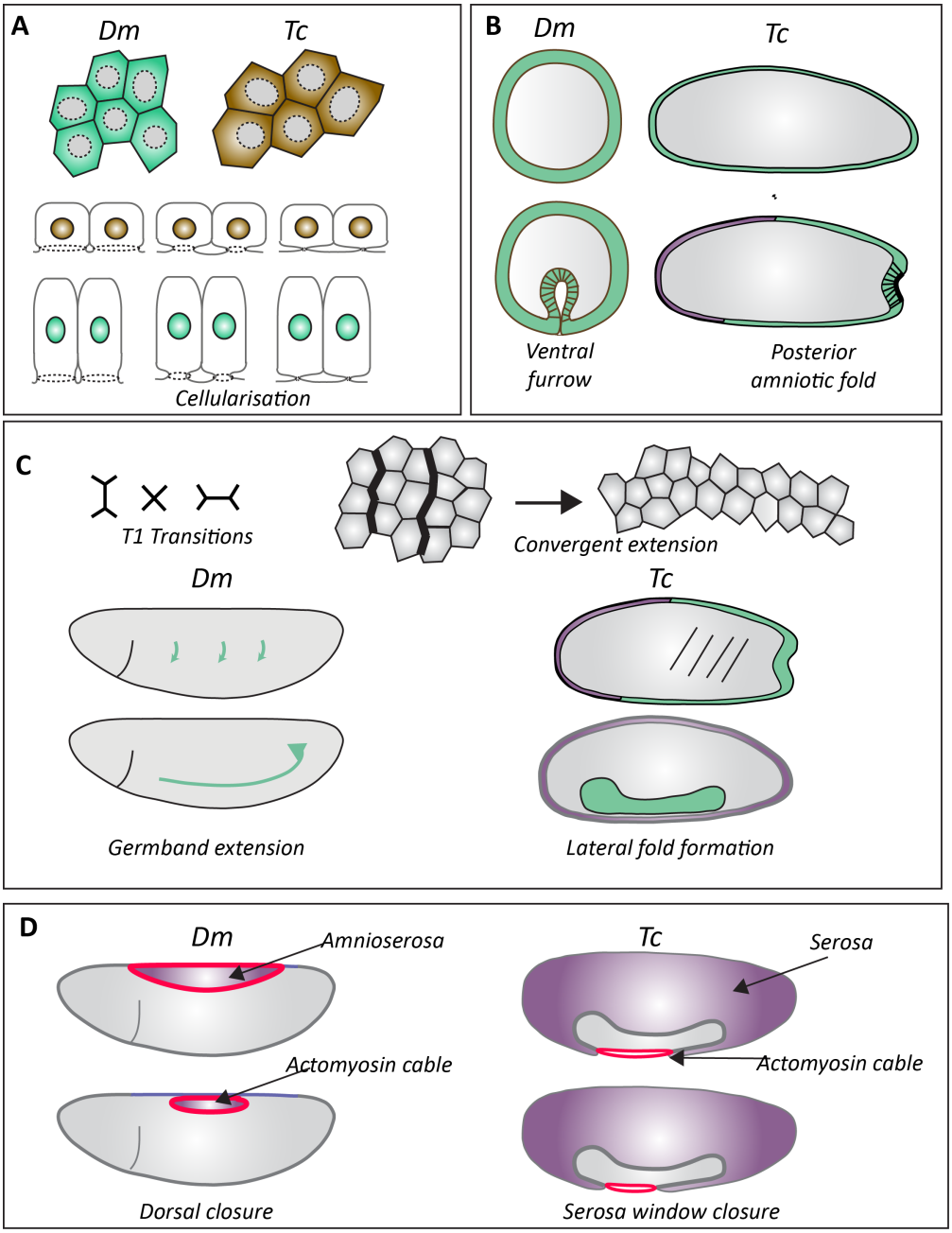

Figure 5.1: Comparison of Myosin functions during different stages of development between *Drosophila melanogaster* and *Tribolium castaneum*.

Figure 5.1: Comparison of Myosin functions during different stages of development between *Drosophila melanogaster* and *Tribolium castaneum*.
Dm = *Drosophila melanogaster* , Tc = *Tribolium castaneum*
A) Both *Drosophila* columnar cells and *Tribolium* cuboidal cells in the blastoderm show similar Myosin rings at the basal side of cells. **B)** Myosin is localised in the apical region of the mesoderm cells leading to apical constrictions in *Drosophila*. Myosin shows apical localisation in constricting cells in the *Tribolium* posterior pole and ventral furrow. **C)** T1 transitions by short contractile Myosin cables functions in germband extension in *Drosophila*. *Tribolium* ectoderm shows short Myosin cables and Myosin polarity. **D)** Myosin forms actomyosin cable during Dorsal closure in *Drosophila*. Myosin forms a contractile cable during serosa window closure in *Tribolium*.

lateral regions of the future ectoderm in *Tribolium*, similar to *Drosophila* [Zallen and Wieschaus, 2004] and lastly it forms a supracellular cable between the extraembryonic and embryonic tissue in both systems, albeit at different developmental stages [Franke et al., 2005]. These results indicate towards conserved functions of non-muscle Myosin II in several morphogenetic processes, in both short germ and long germ insects.

This opens up a field of questions regarding molecular mechanisms that regulate Myosin II activity in the short germ insects, in both holometabolous and hemimetabolus species, such as- How is the apico-basal and planar polarity systems established in the *Tribolium* embryo? How do they regulate Myosin activation in specific subcellular locations? Is the Rho-ROK mediated regulation of Myosin II activity a conserved mechanism across insects? Further, is the change in the expression pattern of early patterning genes and their regulations, the prime reason behind early morphogenetic diversity between *Drosophila* and *Tribolium* embryos? As an example, the developmental stages for which upstream gene expression functions have been previously studied and which could play a role in regulating celullar morphogenesis through actomyosin functions are discussed below.

- First, it is known that *twist* and *snail* in *Drosophila* regulate Myosin activity [Desprat et al., 2008; Leptin, 1991; Martin et al., 2009]. *Snail* initiates Myosin contractions at the apical sides of cells while *twist* is required for stabilisation of the constricted state of cell apices. In

the *Tribolium* embryos, *twist* and *snail* express in a ventral stripe and *Tc-twist* is expressed in a ring of cells in the posterior [Handel et al., 2004]. Additionally, *Tc-twist* is also required for mesoderm formation in the beetle. I observed that *Tribolium* squash localises apically in the ventral furrow cells which are undergoing constrictions and it also shows pulsations in the cortex. Whether *Tc-twist* and *Tc-snail* regulate Myosin activity in mediating apical constrictions in the beetle is not known. Therefore, by observing Myosin dynamics in the ventral furrow cells in knockdown, it would be interesting to see whether the *Tc-twist* and *Tc-snail* have conserved roles in regulating Myosin activity similar to *Drosophila* in the ventral furrow cells.

- Second, a combination of *toll* receptor genes express in stripes and regulate planar Myosin localisation during convergent extensions in *Drosophila* germband extension [Paré et al., 2014]. The *Tribolium toll* genes have been implicated in cell intercalations and also express in stripes [Benton et al., 2016]. This indicates that there might be a conserved role of *Tribolium* squash in axis elongation, which is under the control of *toll* genes. For this, the Myosin behaviour in *toll* knockdowns still need to be analysed.

- Third, one of the major challenges with conventional microscopy is that the anterior and posterior poles of embryo are very difficult to image since the depth of field is restricted and the embryos are curved. However, this limitation is circumvented with multiview SPIM imaging and reconstruction. I was able to observe the cell and actomyosin dynamics at the posterior pole of the embryos using 3D reconstructed embryos. The SPIM datasets showed that the cells at the posterior pole are among the first to begin columnarisation and then undergo apical constrictions. I also observed an apical accumulation of Myosin in the apically constricting cells at the posterior pole. These cells then create a posterior notch at which the posterior amniotic fold begins and the tissue involutes.

Interestingly, this region contains *mist* and *concertina* expressing cells and the primitive pit formation is blocked in the *Tc-fog* RNAi (Nadine Frey, Siegfried Roth, personal communication). In *Drosophila*, fog is a secreted ligand required for apical constrictions that binds to its receptor mist. This indicates that a mechanism very similar to the apically constricting ventral furrow cells in *Drosophila* could be functioning at the posterior pole of the beetle. Analysis of squash localisation in *fog*, *mist* and *concertina* knockdowns and its effect on apical constrictions might reveal that by changing the spatial region in which these genes function, similar morphogenetic process are seen.

- Lastly, the *Tribolium zen* gene expresses as a dorsally inclined anterior cap [van der Zee et al., 2005]. The *Drosophila* homologue expresses in a dorsal cap. A comparison of the serosa/amnion cell shapes and amnioserosa could reveal interesting parallels due to similar downstream mechanisms and actomyosin behaviour. I observed the formation of an actomyosin cable at the serosa-prospective amnion boundary in *Tribolium* which is a similar juncture as the amnioserosa and embryo boundary in *Drosophila*. However, the *Tribolium* serosa cable occurs at a much earlier developmental stage and has completely different dynamics and is discussed in the next section.

The conserved Myosin dynamics between *Drosophila* and *Tribolium* indicate that on a more local spatial scale, similar morphogenetic mechanisms occur at the cellular and molecular level in the embryos. Early embryogenesis however, is dramatically different between them with extensive tissue expansion and folds in case of *Tribolium*. This indicates that the patterning of specific Myosin mediated cellular morphogenesis events is largely regulated by the activity of the upstream regulatory genes. Therefore, developmental heterochrony leading to a change in expression pattern and timing of regulatory genes might play a key role in the resulting morphological differences between the embryos of these species. A possible testing of this hypothesis by altering

gene expression patterns and documenting the resulting cell shape and Myosin dynamics might reveal novel insights into developmental differences between embryos.

5.3 A contractile supracellular actomyosin cable functions serosa window closure in *Tribolium*

The expansion of the serosa tissue to envelop the entire embryo is a 3-dimensional and dynamic process. The serosa cells to do not divide but progressively flatten and become squamous while the embryonic cells become columnar and show tissue condensation. The increase in serosa area could be an active process by the serosa cells or could also result due to pulling forces generated by the condensing embryonic region. Following serosa expansion and the future amnion involution, a window is created in *Tribolium* embryos between the multiple layers of the anterior and posterior folded tissues. This window is sealed to generate a continuous serosa epithelium and joins the anterior and posterior amnion. It is not known how the serosa window seals and the tissue mechanics that could be involved were unclear as well.

I characterised the formation and evolution of a previously speculated contractile actomyosin cable at the serosa-prospective amnion boundary. A key step in *Tribolium* embryo patterning is the subdivision of the initially homogenous blastoderm into extraembryonic and embryonic regions. Differences in gene expression in these two domains divide them into different cell fates and functionally distinct regions. The cells of the serosa are not part of a lineage and rather are grouped into a domain by a higher order regulation through *zen* expression, forming a non-lineage boundary rather than a 'compartment' [Umetsu and Dahmann, 2015]. At this boundary, Actin and Myosin starts accumulating creating a higher tension interface. Actomyosin cables are often formed at tissue boundaries which have cells with different fates on either side.

The mechanism by which this boundary is sensed in *Tribolium* could depend on the *Tc-zen* expression. Previous studies have also shown that heterophilic interaction of adhesion molecules is required for sensing tissue boundaries and a similar mechanism might function at the embryo extraembryonic tissue boundary as well[Chang et al., 2011].

The *Tribolium* serosa cable appears as an irregular structure in the first phase due to cell arrangements. Cell divisions in the embryonic region and future amnion, and the change in shape of serosa cells make the cable boundary initially irregular. This irregular boundary transitions into a smooth and linear supracellular alignment as cell edges become more taut with time. Additional high resolution cell lineage analysis is required to ascertain whether cells at the boundary end up in the wrong domain by mixing, and if so whether they readjust their gene expression to become homogeneous with the tissue.

The serosa window actomyosin cable has completely unprecedented length and shape dynamics. It seems to have biphasic properties with an initial expansion phase and a second collapsing one. The boundary cable initially expands in length due to increased area of the serosa epithelium. Once the serosa moves over the posterior pole and the lateral embryonic folds are generated, the actomyosin boundary cable starts decreasing in size. This indicates that probably the initial expansion phase of serosa overcomes the contractility in the cable. However, once the serosa expansion and movement is stabilised and the serosa window is formed, the cable increases in tension due to increased actomyosin contractility.

The serosa window cable increases in tension concomitant with increased tension in the serosa. Additionally, the serosa cells on the dorsal region of the embryos expand till circular window stage. The increased tension in serosa indicates that the mechanical properties of the tissue change and it becomes harder to pull the tissue and seal the window. Therefore, the increased tension in the cable is required to overcome the resistance and continue with a continuous and constant closure rate. The increase in tension could be through increase in Myosin stability or an increase in Myosin activation by phosphory-

lation at the cable region. The serosa cells which are a part of the cable forming edge show high myosin, slowly constrict and intercalate into the serosa to leave the cable. This decrease in number of cable forming cells leads to an overall decrease in the circumference of the cable. This is also reflected in the increased anisotropy of cell shapes at the cable edge. The cable forming cells shrink their edge and leave the cable to intercalate in between their neighbours. This also indicates that the force generated by the cable could lead to rearrangements in the serosa that could be sufficient to seal the epithelium.

Interestingly, I also saw that the cable forming cells retain high tension even after successive ablations at different positions. This offers a new insight into our understanding of supracellular cables. It indicates that instead of a continuous supracellular cable, the *Tribolium* serosa window cable rather functions as a linked chain of individual contractile units. These units constrict irrespective of others in an autonomous manner. High Myosin intensity at the cell-cell junctions could be required to meditaed the force transmission across cells. The dynamic shape changes, biphasic closure profile and the increase in tension indicate that it could serve as an important system for gaining insight into actomyosin cable's formation and function. It was recently shown that the *Drosophila* dorsal closure cable is dispensable for the closure but rather functions in creating a seamless closure. The *Tribolium* serosa window cable also seems to function via individual and autonomous cell constrictions. This has important implications on our understanding of such supracellular assemblies. The cable could eventually be an alignment of cell edges due to force getting balanced as all cells constrict.

From a tissue mechanics perspective, the cable is formed at an interesting juncture. It is formed between the squamous serosa and the columnar embryonic cells. At this boundary, the cell adhesion and cell properties might be different and inhomogeneous. It seems that since the serosa cells increase in tension which is relieved by ablations, a tug of war might occur between the serosa and embryonic tissue, with the condensing embryo pulling the serosa which resists the pull and behaves as an elastic sheet. The release of tension

upon ablations indicates that the serosa cells also have some contractility and propensity towards decreasing their apical areas. It could play a role in increasing the tensions at the cable. Further, as it becomes harder to pull the serosa, the cells at or near the cable become more and more anisotropic. Is the constriction of cable forming edge resulting in cell area decreasing or is the cell area constant and just re-organising edges? The role of junction proteins in these processes is also unexplored. For e.g., in *Drosophila* echinoid mediated cell sorting is required but it would be relevant to see if it has a conserved role in *Tribolium*.

Contractile actomyosin cables seem to be highly conserved and function in various epithelium sealing events with dissimilar cell fates on either side of the cable. The *Tribolium* serosa window cable provides a first example of such a structure in short germ insects. It is a supracellular structure that is not formed in *Drosophila* since it lacks the extensive extraembryonic tissues during gastrulation. Since several insect embryos have varying degrees of serosa-amnion tissues, it will be interesting to see if they all form such cables. Also, whether the tension change in the cable is correlated with serosa amount and serosa properties can be asked by studying the serosa window cable in other insect embryos. Finally, it would be interesting to study whether the mechanism of cable closure is conserved, which is neither zipper but rather a modified purse string. This opens up the possibility to investigate whether dissimilar cell fates at the two sides of the cable lead to its formation and whether this plays a role in the directionality of serosa expansion and eventual position of serosa window. An experimental approach to understand these ideas would be best supplemented if modelling of morphogenesis in the beetle and other insect systems could be carried out computationally. Modelling and simulations of the mechanical properties of tissues and their impact on the tensions in an actomyosin cable could reveal important insights into the formation and functions of these structures.

CHAPTER 6

MATERIALS AND METHODS

6.1 *Tribolium* stock maintenance

All *Tribolium* stocks were cultured on bio whole wheat flour (Vollkorn) as previously described in the beetle book. Pre-sieved Vollkorn flour was used for egg lays. The flour was frozen at -20°C for 2 days and thawed at 65°C for 1 day before use. Yeast powder was added separately when changing flour for the beetles. The beetles were cultured in lock n' lock plastic boxes which have a 2-3 cm diameter wide hole in the lid covered with fine nylon mesh to allow air exchange. Stocks were also maintained in plastic bottles typically used for *Drosophila* cultures. All stocks were kept at 32°C and 70% humidity.

List of beetle stocks used:

-
- *Vermilion white*
- EFA::nGFP
- αTub:LifeAct::GFP

- EFA:Gap43::YFP,Hist::RFP (Averof lab, unpublished)
- αTub:Tc-Sqsh::eGFP

6.2 RNA extraction and cDNA synthesis

cDNA was synthesised from total RNA extracted from 24-48hr old egg lay. Total RNA was extracted using the TRIzol reagent (Invitrogen) according to the manufacturer's instructions. cDNA synthesis was carried out using the "Superscript III First-strand Synthesis System for RT-PCR" kit (Invitrogen), according to the manufacturer's instructions. The template was total RNA extracted from 0-48 hr old *Tribolium* embryos, and oligo(dT) primers were used.

6.3 Cloning of templates for mRNA synthesis and transgenesis

The following plasmids were generated for invitro mRNA synthesis or *Tribolium* transgenesis:

-pT7-TcSqsh::RFP^{Ruby}

-pCS2+-TcSqsh::eGFP

-pBAC-αTubTcSqsh::RFP^{Ruby}

-pBAC-αTubTcSqsh::eGFP

-pCS2+-Syn21TcSqsh::sfGFP

-pCS2+-Tczen1::eGFP

The predicted *Tribolium* Squash (non muscle myosin regulatory light chain) gene was cloned from cDNA into a pT7-H2B-RFP^{Ruby} plasmid, using primers (Tc-sqh-PciI-F 5'-ttaaacATGTCGTCCCGGAAAACCGTAAAC-3' Tc-sqh-XhoI-R 5'-acttctcgagTTGCTCATCCTTATCCTTGG-3').

The H2B sequence was replaced by the Tc-Sqsh fragment amplified from cDNA. The PciI and XhoI restrictions enzymes were used for linearizing the

plasmid. The gene shares 93% similarity with the *Drosophila* Squash gene and was identified using BLAST (NCBI). The following reagents were used in cloning from New England Biolabs : PciI (#R0655S), XhoI (#R0146S), EcoRI (#R3101S), NcoI (#R3193S), the Shrimp Alkaline Phosphatase (#M0371S), the T4 DNA ligase (#M0202S), the Phusion High-Fidelity DNA Polymerase (#M0530S) and dNTPs (#N0447S).

The Tc-Sqsh was subcloned into pCS2+ and pBac plasmids from the pT7-TcSqsh::RFP^{Ruby} construct.

The cloned Tc-Squash sequence-

ATGTCGTCCCGGAAAACCGTAAACCGCCGTGGCACCACGAAAAAACGAG

CCCAAAGGGCCACTTCCAACGTGTTTGCCATGTTCGACCAGGCCCAGATC

GCCGAATTCAAGGAGGCCTTCAACATGATTGACCAGAACCATGATGGGTT

TGTGGACAAGGAGGACCTGCACGACATGCTGGCCTCCTTGGGCAAGAAC

CCCACCGACGACTACCTCGATGGTATGATGAACGAGGCCCCGGGGCCCA

TCAACTTCACCATGTTCCTGACGCTGTTCGGGGAGAGGCTGCAAGGGACG

GACCCCGAGGACGTGATCAAGAACGCGTTTGGGTGCTTCGATGAGGACA

ACATGGGGGTTATCAACGAGGAGCGGCTGAGGGAGTTGCTGACTACGA

TGGGAGACAGGTTCACCGACGACGAGGTGGATGAGATGTACAGGGAGGCC

CCCATCAAGAACGGGTTGTTCGATTATGTGGAGTTCACTCGTATTTTGAA

ACATGGGGCCAAGGATAAGGATGAGCAA

I isolated two pBAC-αTubTcSqsh::RFP^{Ruby} transgenics in the lab using standard protocols. These lines were however, very dim and not very fertile. I then proceeded with generating transgenics using the pBAC-αTubTcSqsh::eGFP construct. I generated the plasmid and then shipped it to the company :TriGenES, IGFL, Johannes Schinko/Averof lab (29 rue Alexander Fleming 69007 Lyon France). Eight transgenic lines were isolated and shipped to us by the company. All eight lines show fluorescence and I proceeded with characterising and using the pBac-Tc-Sqsh::eGFP line #1 and/or #2 for all my experiments.

```
CLUSTAL 2.1 multiple sequence alignment


Tc-sqh1         MSSRKTVNRRGTTKKRAQRATSNVFAMFDQAQIAEFKEAFNMIDQNHDGFVDKEDLHDML 60
Tc-sqh2         MSSRKTVNRRGTTKKRAQRATSNVFAMFDQAQIAEFKEAFNMIDQNHDGFVDKEDLHDML 60
Dmel-sqh        MSSRKTAGRRATTKKRAQRATSNVFAMFDQAQIAEFKEAFNMIDQNRDGFVEKEDLHDML 60
                ******..**.************************************:*****:********

Tc-sqh1         ASLGKNPTDDYLDGMMNEAPGPINFTMFLTLFGERLQGTDPEDVIKNAFGCFDEDNMGVI 120
Tc-sqh2         ASLGKNPTDDYLDGMMNEAPGPINFTMFLTLFGERLQGTDPEDVIKNAFGCFDEDNMGVI 120
Dmel-sqh        ASLGKNPTDDYLDGMMNEAPGPINFTMFLTLFGERLQGTDPEDVIKNAFGCFDEENMGVL 120
                ************************************************:****:

Tc-sqh1         NEERLRELLTTMGDRFTDDEVDEMYREAPIKNGLFDYVEFTRILKHGAKDKDEQYIEEKN 180
Tc-sqh2         NEERLRELLTTMGDRFTDDEVDEMYREAPIKNGLFDYVEFTRILKHGAKDKDEQ------ 174
Dmel-sqh        PEDRLRELLTTMGDRFTDEDVDEMYREAPIKNGLFDYLEFTRILKHGAKDKDEQ------ 174
                 *:***************::*****************:****************

Tc-sqh1         GFSMTSLNDNDDNSTGTQECEYFEDCQ 207
Tc-sqh2         ---------------------------
Dmel-sqh        ---------------------------
```

Figure 6.1: Alignment of Squash isoforms from *Drosophila melanogaster* and *Tribolium castaneum*.

6.4 dsRNA synthesis for RNAi experiments

The *Tc-zen* was knocked down in embryos using dsRNA synthesised from CDNA using the primers Zen1: FW- ggccgcggTTTGAAAACCAAGCCGTTCT and REV- cccggggcCGTTGGGGTTGAGTTTCTTG

The dsRNa against *Tc-zen* and *Tc-caudal* were also ordered from the company Eupheria Biotech (Eupheria Biotech GmbH, Tatzberg 47-51, 01307 Dresden, Germany. phone: +49(0)351-463-40285. web: www.eupheria.com). This company sysnthesised the dsRNA for the iBeetle screen [Schmitt-Engel et al., 2015] and the numbers for *Tc-zen* and *Tc-caudal* are iB-01304 and iB-04348 respectively.

6.5 Capped, single stranded RNA synthesis

Plasmids were linearised using NotI or EcoRI. Linearized DNA was purified then precipitated and resuspended in nuclease-free water to give a concentration of approximately 500 ng/μl. Capped mRNA was prepared from linearized plasmid DNA using either the T7 (for pT7) or SP6 (for pCS2+) mMESSAGE

mMACHINE (Ambion #AM1344 and #AM1340) kit, according to the manufacturer's instructions. After digestion with TURBO-DNase, RNA was purified by LiCl precipitation overnight at -20C. RNA was precipitated by centrifugation, and resuspended in 5 μl nuclease-free water to achieve about 3 μg/μl final concentartion and quantified on a Nanodrop spectrophotometer.

6.6 Fluorescence image acquisition

Dechorionation

Tribolium eggs were dechorionated prior to micro injections and live imaging with very mild bleach treatment. The eggs were collected in embryonic sieves. Two wells, in a six well plate, were filled with about 16% commercial Klorix in PBS. The remaining four wells were filled with PBS. The eggs were lightly washed with PBS and then moved to the bleach containing wells for 30secs each. The eggs were repeatedly stirred by continuously pouring bleach into the sieve with Pasteur pipettes. After 1 minute of bleaching, the eggs were washed with PBS in the remaining four wells for 30 seconds each along with continuous agitation as before.

Microinjection

The eggs were either injected under oil for confocal imaging or under air for SPIM. For confocal imaging, the eggs were picked up with a very soft brush and lined on the center of a square cover slip that is stuck to a glass slide using a water drop. Once the eggs dry and stick to the cover slip they were covered with Halocarbon oil (Sigma 700). Microinjections were done with silver Sigma needles and using an Eppendorf injector. The needle was inserted from the anterior pole of the egg up to one third of the egg length and the eggs were injected till a little yolk droplet is seen. The coverslip was then stuck to a glass bottom petridish from which the coverslip was previously removed. The eggs were then incubated at 32°C or 25°C till imaging.

The microinjection protocol was specially modified for imaging with SPIM. In SPIM the eggs are imaged under water and therefore they cannot be covered with oil during microinjections. The halocarbon oil prevents eggs from drying and also allows gaseous exchange. For transgenesis, the eggs are typically injected under air and then incubated in humid chambers. Further the injected eggs need to be picked up with a brush and mounted in agar using capillaries as per standard SPIM protocols. The combined effect of drying out during air injections and them mechanical stress during removal form slide and mounting ensured that we had very little to zero survival of embryos during imaging. In order to ensure maximum humidity and minimum mechanical stress, we started injecting eggs that were lined on agar beds. About 750 μl of 1% agar in PBS was poured onto a glass slide lengthwise. Eggs were lined in a little water on the agar bed with their anterior pole facing outwards. The eggs upon drying a little stick to the agar. The slide was then placed in a humid chamber till the time of injection. The eggs were quickly injected in air and again incubated in the humid chamber till mounting in the capillaries. The eggs are removed from the agar bed by pouring a little water as they start floating. The injection mixture consisted of capped mRNA for single or double labelling and mixed with dsRNA for knockdowns. The concentrations of each component was adjusted such the H2B::RFP was 1-2 ug/ul final concentration, LifeAct::GFP 0.5-1 μg/μl , Sqsh::GFP 2.5-3 μg/μl and GAP43::YFP was 1.5-2 μg/μl across experiments. The dsRNA for *Tc-zen, Tc-caudal* and *Tc-doc* knockdowns was 1μg/μl final concentration in the injection mix.

Confocal

Confocal time lapses were taken on Zeiss 780 microscope or Zeiss 880 microscope using 25X and 40X multi immersion objective. The eggs were either imaged under halocarbon oil (SIGMA, CAS Number 9002-83-9) or under water in glass bottom petridishes.

SPIM

The Zeiss LZ1 was used for SPIM imaging of *Tribolium* embryogenesis. Transgenic or mRNA injected eggs were mounted in capillaries in 1% agar and fluorescent bead solution. The protocol was adapted from standard *Drosophila* SPIM imaging [Schmied and Tomancak, 2016]. Detailed SPIM imaging protocol that modified for injected *Tribolium* embryos is described in Chapter-2.

FRAP Analysis

Timelapse images were collected for different developmental stages of embryos from the TcSquash::GFP transgenic line at 1 sec frame rate. The images were stabilized for drift and cable movement using the template matching Fiji plugin. The cable was then straightened using the volume manager plugin developed by the scientific imaging facility at MPI-CBG. Finally the images were analysed for FRAP using a Matlab code written by Mr. Arghyadip Mukherjee (Grill, lab).

Laser ablations

Tensions in the actin cable were estimated by cutting the cable using laser ablations. The Zeiss 780 inverted microscope and 800 nm pulsed infrared laser were used for making the cuts.

The sample was imaged in water by a 40X dipping water objective and the zoom was fixed at 1X, 2X or 2.5X to focus the cable in distinct experiments. The acquisition frame was set at 800x550 pixel and ablation was done in an

ellipse of about 75X10 pixel in serosa cuts. The pixel size was around 0.20 μm and 0.08μm respectively. The ablation was performed in the 4th frame after 3 pre-bleach frames were acquired using 80% of infrared laser and 6x speed. The quantifications were done from the 5th frame onwards by tracking the edges of the ablated tissue using manual tracking by trackmate plugin in Fiji. The speeds of membrane retraction post ablation were then plotted using R.

APPENDIX A

APPENDIX

Serosa cells undergo passive intercalations and exchange their neighbours

The serosa shows dramatic expansion and ends up covering the entire embryo. I had observed that cells in the dorsal region of the embryo increase their apical areas from Stage 1-3 but not at Stage 4. This indicated that probably the cells in the later stages show rearrangements via intercalations. The neighbour exchange of cells occurs through T1 transitions. Therefore, I tracked a few serosa cells at the dorsal region of the embryo and near the posterior pole from Stage 2 till serosa window closure. The individual cells were tracked over time using manual tracking plugin in Fiji (Fig A.1, highlighted cells). I observed that several serosa cells exchange their neighbours during the course of serosa window closure in both the dorsal and the ventral region. The cells in the posterior and ventral region arranged more linearly with time and seem to elongate the serosa in the anterior - posterior direction (Fig

A.1, region marked by a red ellipse). However, these intercalations appear to be passive since I did not observe any Myosin enrichment to mediate the intercalations through short and transient myosin cable formations which can aid in T1 transitions.

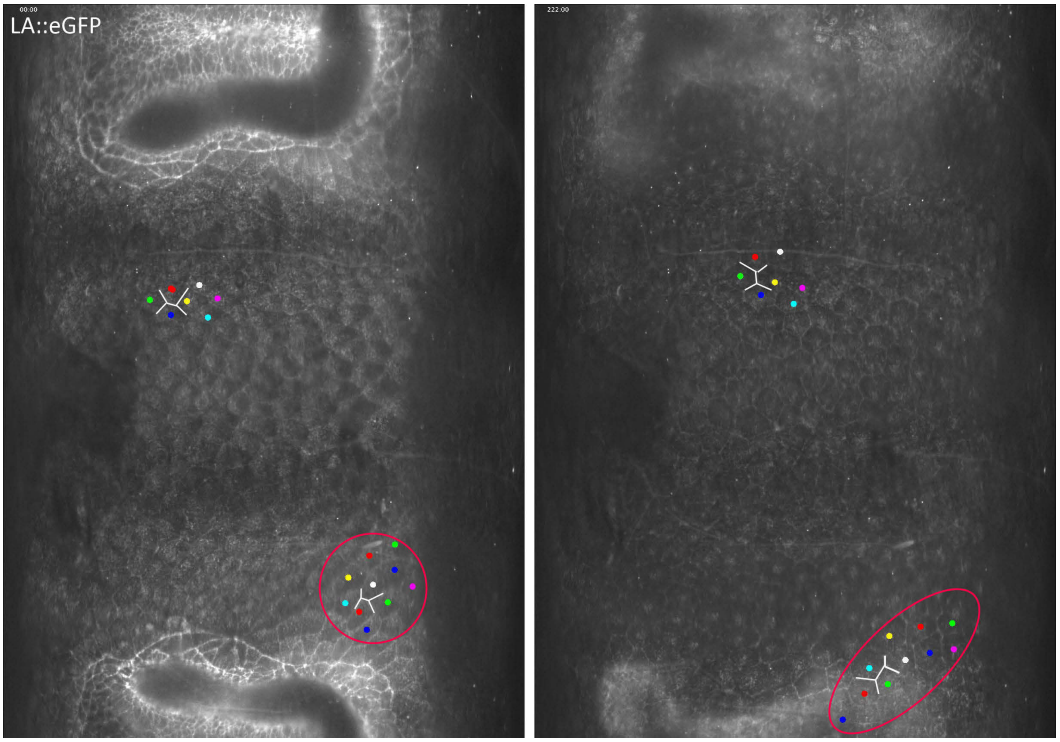

Figure A.1: Serosa cells show passive intercalations. The figure shows 2D projections from a 4D SPIM movie of embryos labelled with LifeAct::eGFP. The colored dots correspond to individual cells which were manually tracked over time. The red ellipse points to elongation of the tissue region formed by the marked cells.

High resolution images of 2D map projections

The 4D imaging movies acquired with the Zeiss LZ1 are extremely high resolution and size heavy datasets. To visualise the data in 2D and for easy downstream analysis, I have projected the 3D datasets into 2D cartographic projections, as explained in Chapter II. In this section, I have added full page

images of a few datasets as an example of the spatial quality. The first six images are from a time-series of 2D map projections from a fused SPIM movie of a transgenic *Tribolium* embryo that uniformly expresses H2A::GFP (Kindly provided to us by Peter Kitzmann, Bucher lab). The movie covers about 13 hrs of development at 22°C (also shown in Fig 2.10).

The next two images are from a 2D projection of a transgenic *Tribolium* embryo labelled with LifeAct::eGFP. Images are depth coded with cyan representing the surface layer of the embryo and magenta showing the deeper underlying layers.

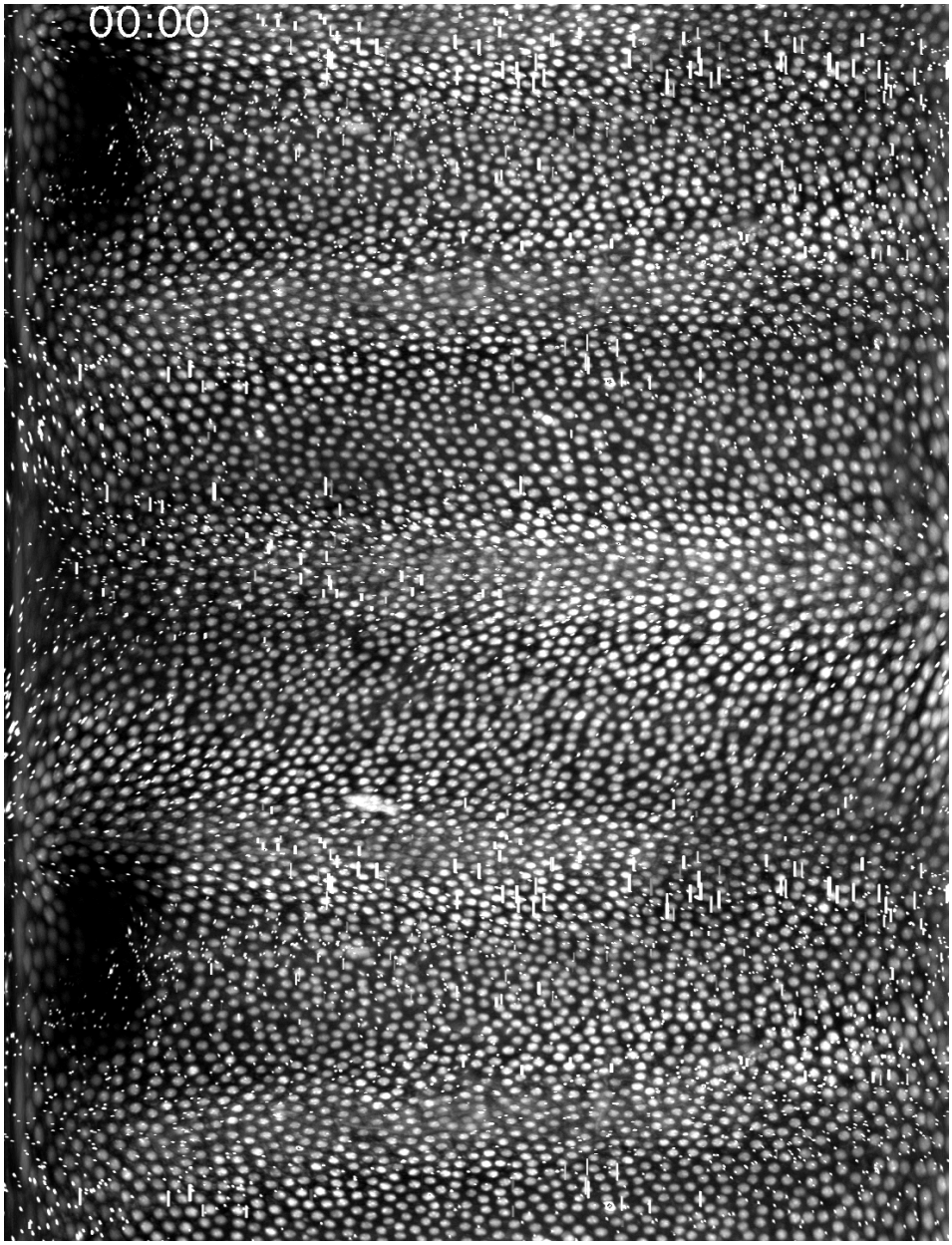

Figure A.2:
2D projection of a 3D reconstructed embryo labelled with Hist2A::GFP athe uniform blastoderm stage

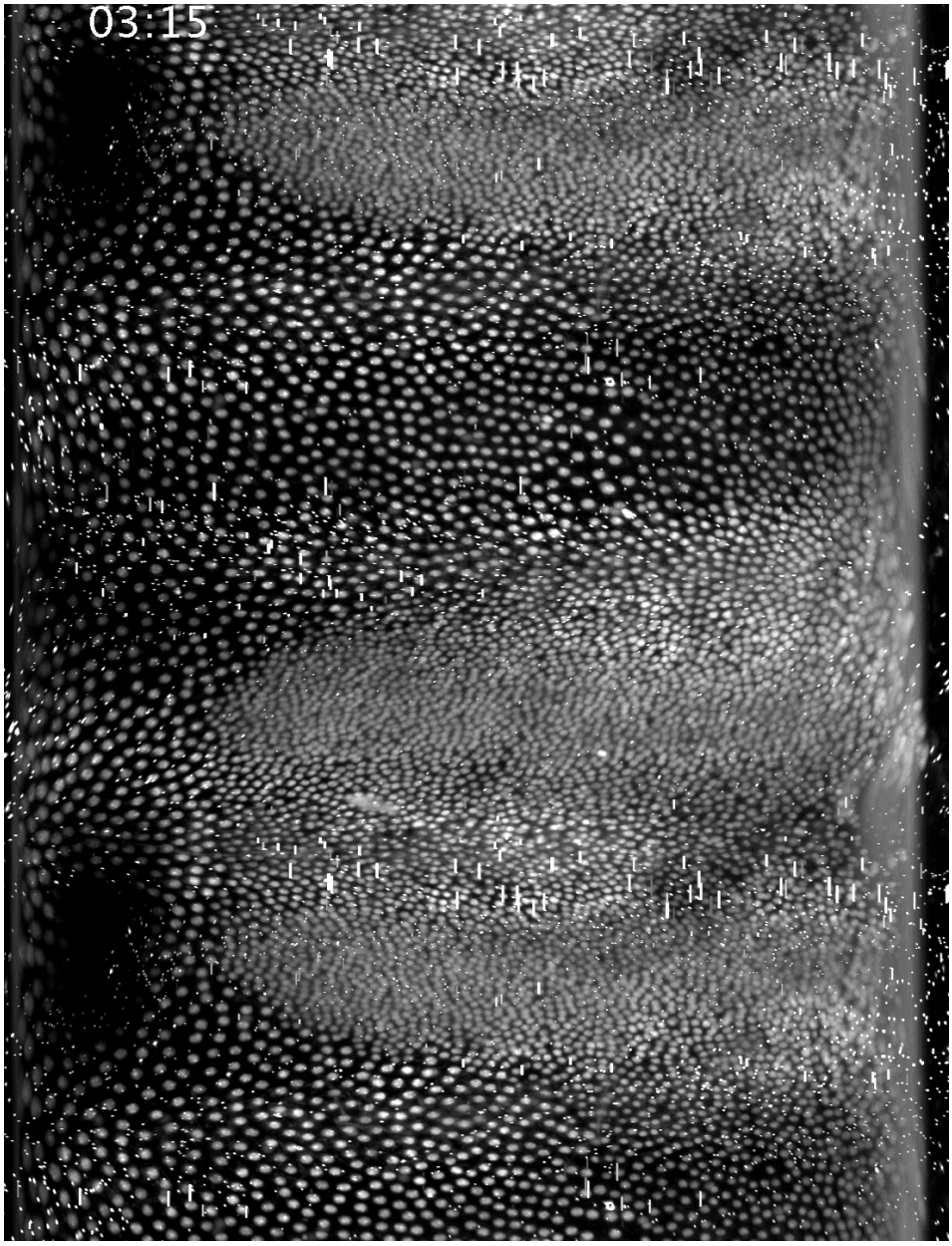

2D projection of a 3D reconstructed embryo labelled with Hist2A::GFP at differentiated blastoderm stage

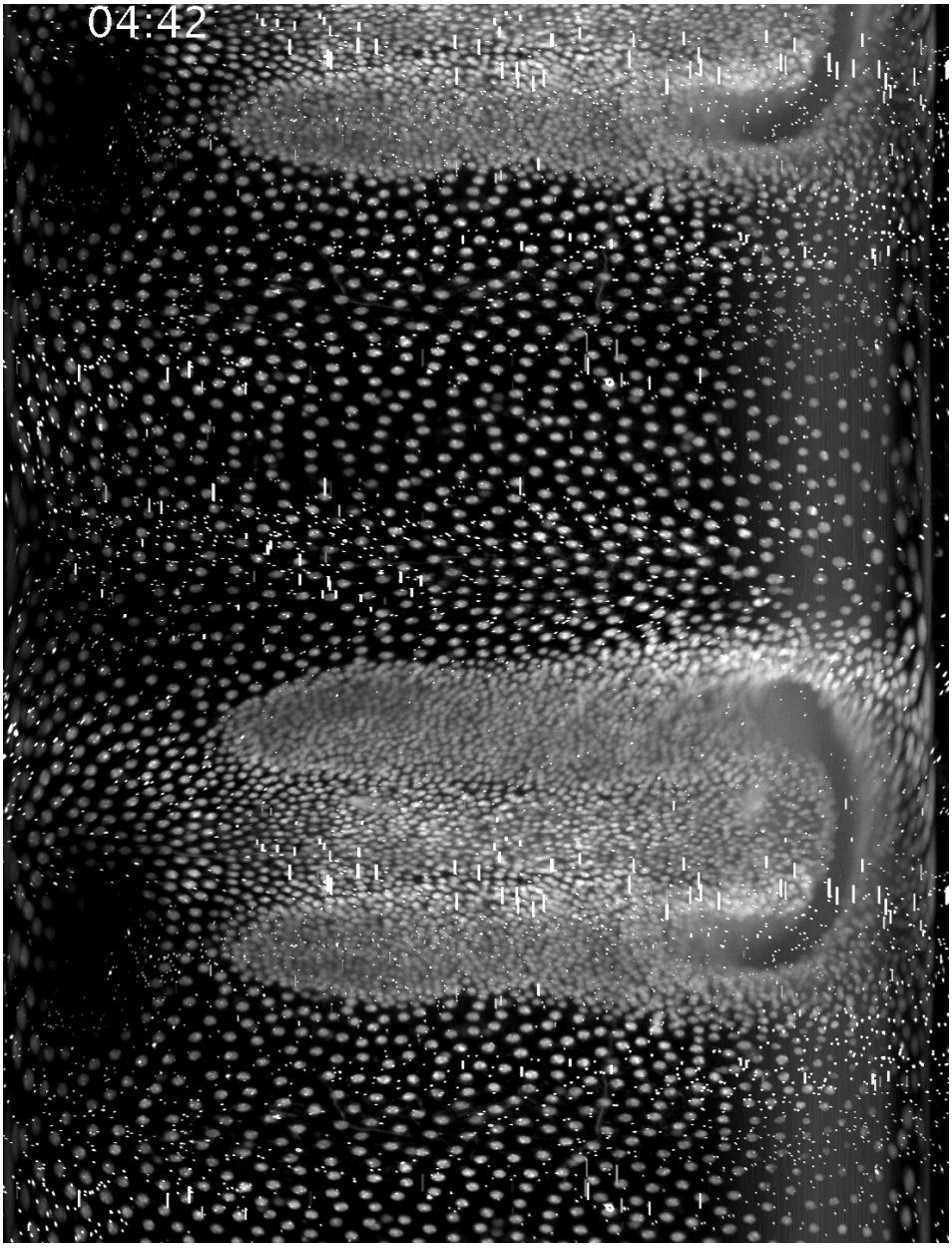

2D projection of a 3D reconstructed embryo labelled with Hist2A::GFP at the posterior amniotic fold formation stage

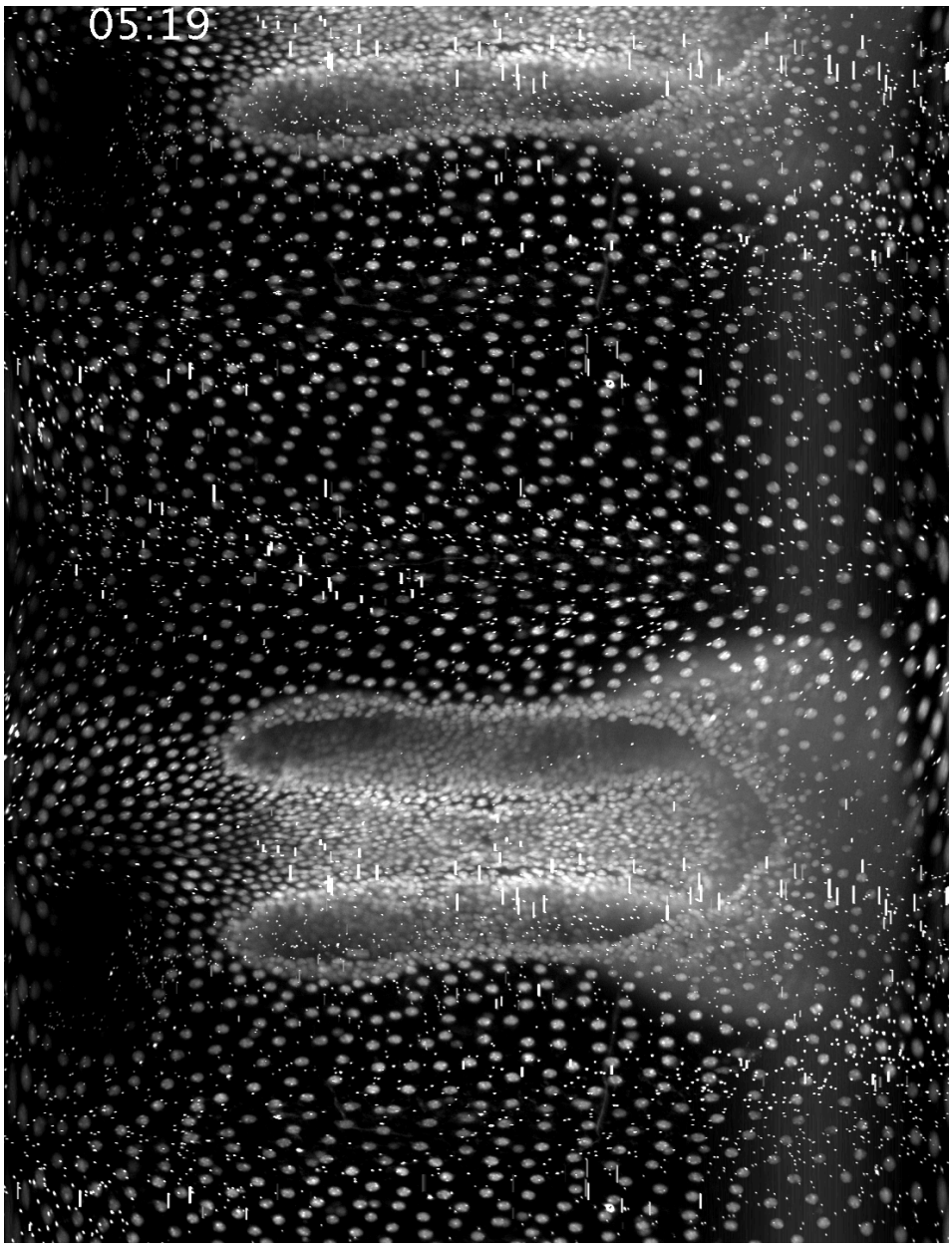

2D projection of a 3D reconstructed embryo labelled with Hist2A::GFP at horseshoe amniotic fold stage

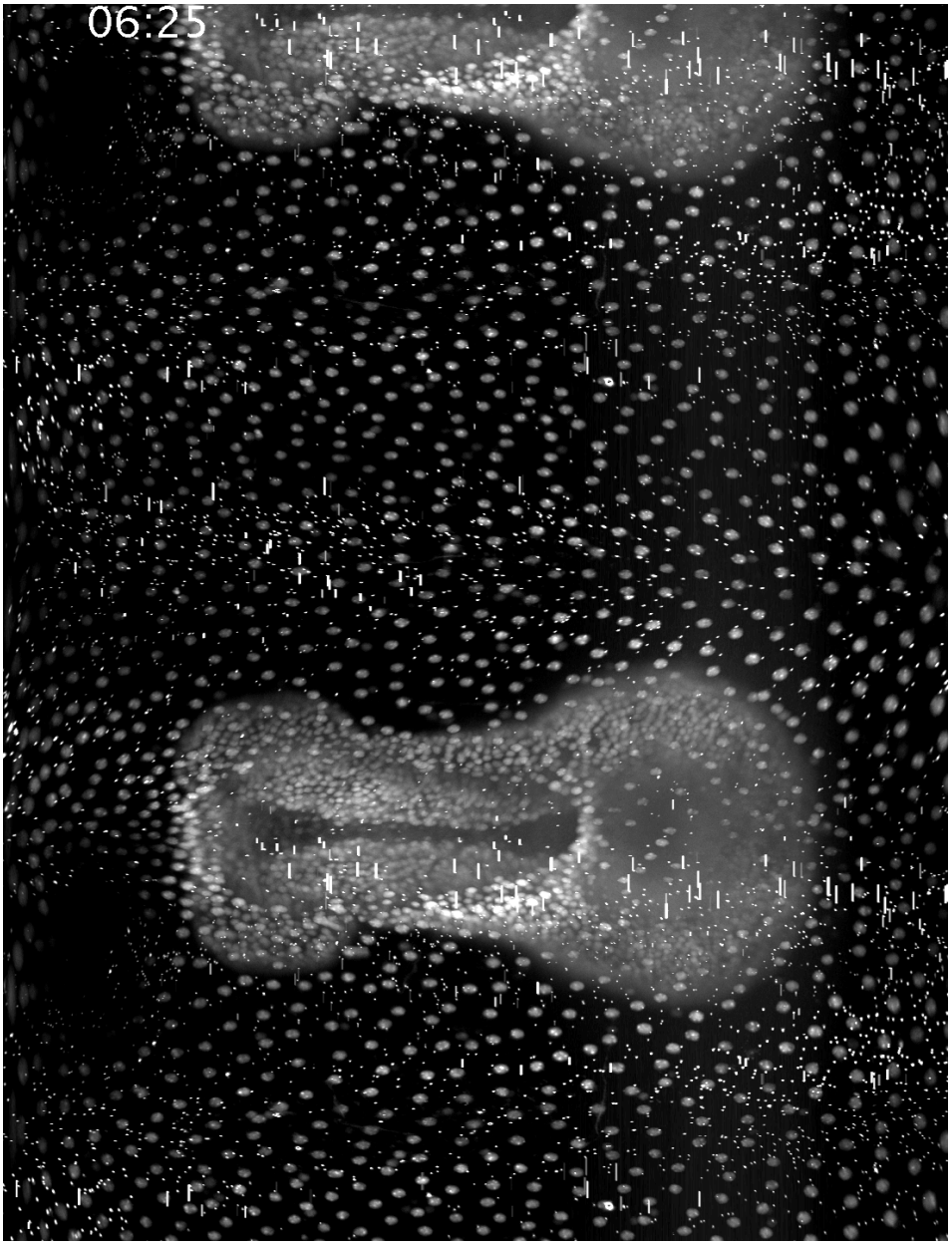

2D projection of a 3D reconstructed embryo labelled with Hist2A::GFP at oval serosa window stage

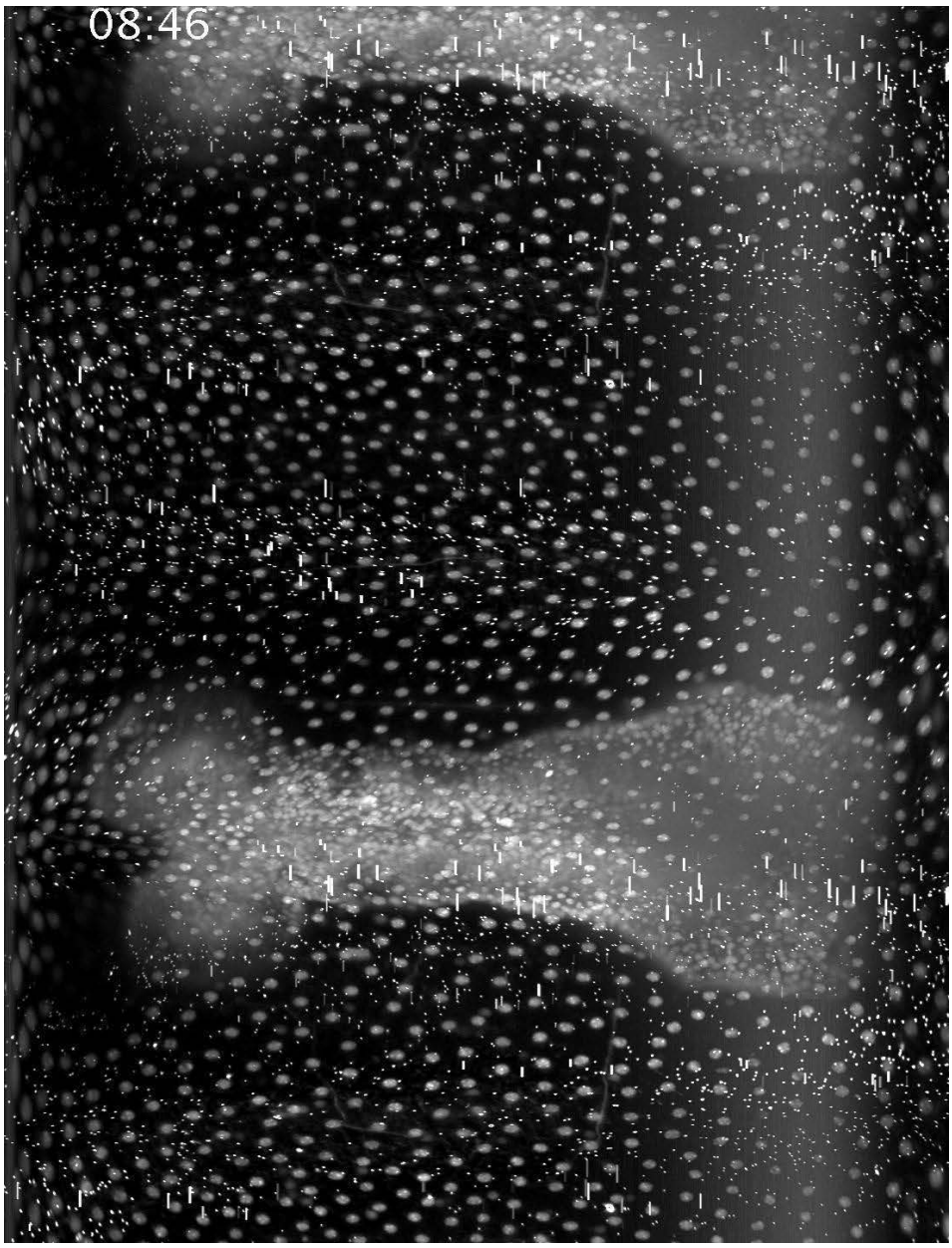

2D projection of a 3D reconstructed embryo labelled with Hist2A::GFP germband extension stage

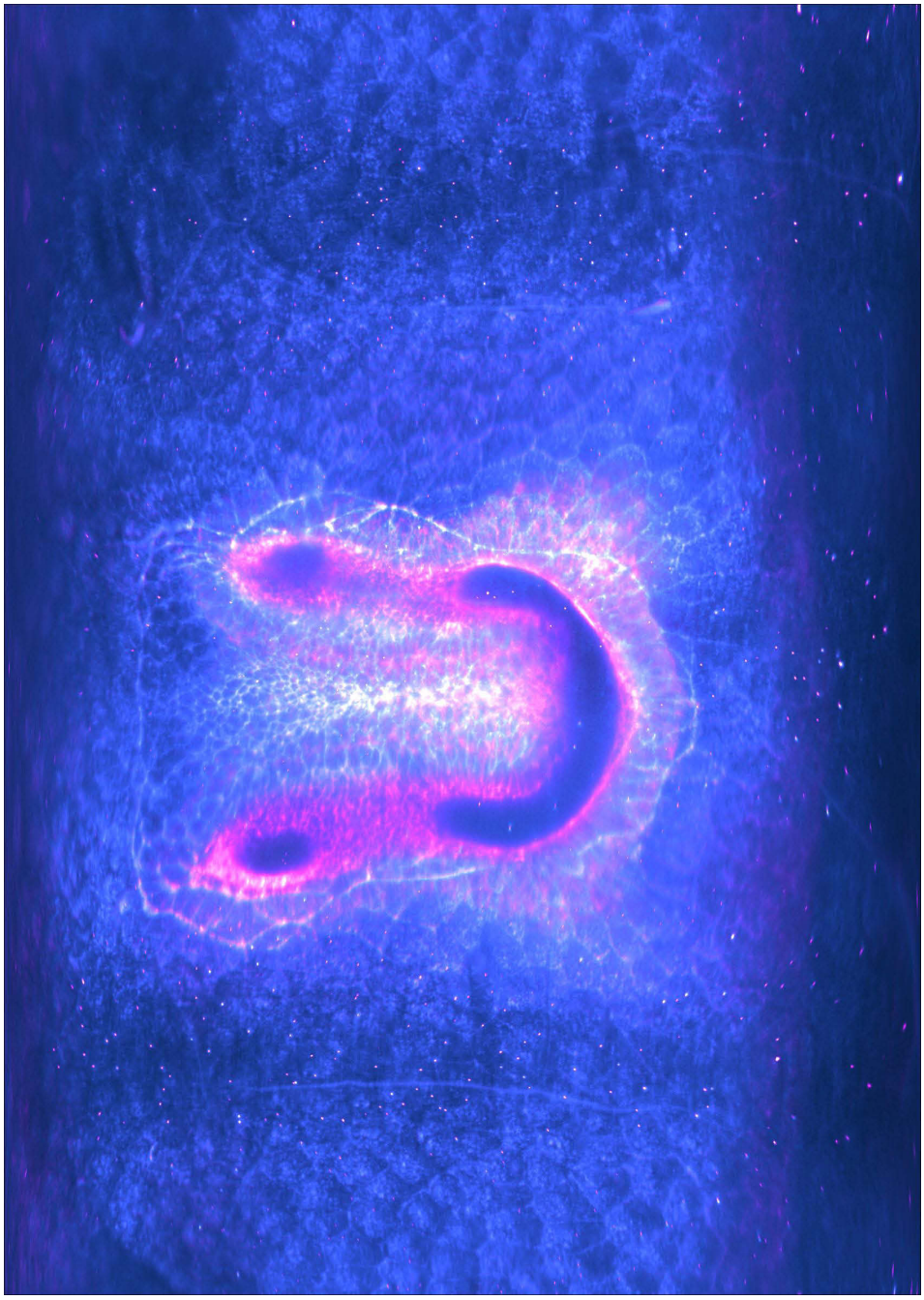

Figure A.3:
2D projection of a 3D reconstructed embryo labelled with LifeAct::GFP to shows that the cable lags behind the involuting amnion

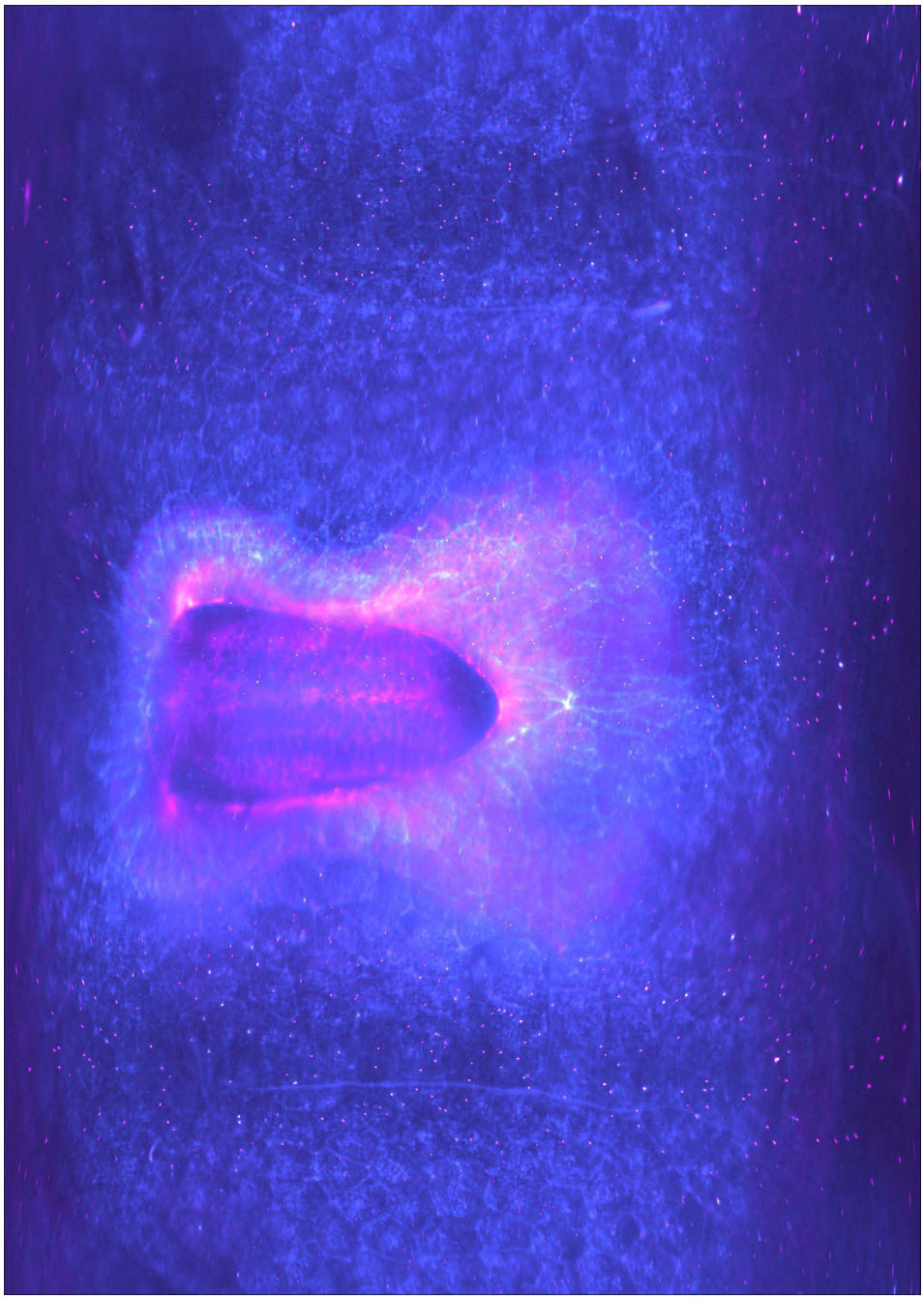

2D projection of a 3D reconstructed embryo labelled with LifeAct::GFP to shows that the cable lags behind the involuting amnion

BIBLIOGRAPHY

Abreu-Blanco, M. T., Verboon, J. M., Liu, R., Watts, J. J., and Parkhurst, S. M. (2013). Drosophila embryos close epithelial wounds using a combination of cellular protrusions and an actomyosin purse string. *Journal of cell science*, 125(24):5984–5997.

Ahrens, M. B., Orger, M. B., Robson, D. N., Li, J. M., and Keller, P. J. (2013). Whole-brain functional imaging at cellular resolution using light-sheet microscopy. *Nature Methods*, 10(5):413–420.

Akam, M. (2000). Arthropods: Developmental diversity within a (super) phylum. *Proceedings of the National Academy of Sciences*, 97(9):4438–4441.

Aliee, M., ROper, J.-C., Landsberg, K. P., Pentzold, C., Widmann, T. J., Jülicher, F., and Dahmann, C. (2012). Physical Mechanisms Shaping the Drosophila Dorsoventral Compartment Boundary. *Current biology : CB*, 22(11):967–976.

Amat, F., Höckendorf, B., Wan, Y., Lemon, W. C., McDole, K., and Keller, P. J. (2015). Efficient processing and analysis of large-scale light-sheet microscopy data. *Nature protocols*, 10(11):1679–1696.

Amat, F., Lemon, W., Mossing, D. P., McDole, K., Wan, Y., Branson, K., Myers, E. W., and Keller, P. J. (2014). Fast, accurate reconstruction of cell lineages from large-scale fluorescence microscopy data. *Nature Methods*, 11(9):951–958.

Anderson, D. T. (1972). development of holometabolous insects. *Counce, S. J., ed. Developmental Systems: Insects*, v. 1972, 1.

Arthur, W. (2002). The emerging conceptual framework of evolutionary developmental biology. *Nature*, 415(6873):757–764.

Beeman, R. W., Stuart, J. J., Haas, M. S., and Denell, R. E. (1989). Genetic analysis of the homeotic gene complex (HOM-C) in the beetle Tribolium castaneum. *Developmental Biology*, 133(1):196–209.

Bement, W. M., Forscher, P., and Mooseker, M. S. (1993). A novel cytoskeletal structure involved in purse string wound closure and cell polarity maintenance. *The Journal of cell biology*, 121(3):565–578.

Bengough, A. G., Hans, J., Bransby, M. F., and Valentine, T. A. (2009). PIV as a method for quantifying root cell growth and particle displacement in confocal images. *Microscopy Research and Technique*, 23:NA–NA.

Benton, M. A., Akam, M., and Pavlopoulos, A. (2013). Cell and tissue dynamics during Tribolium embryogenesis revealed by versatile fluorescence labeling approaches. *Development*, 140(15):3210–3220.

Benton, M. A., Pechmann, M., Frey, N., Stappert, D., Conrads, K. H., Chen, Y.-T., Stamataki, E., Pavlopoulos, A., and Roth, S. (2016). Toll Genes Have an Ancestral Role in Axis Elongation. *Current biology : CB*, pages 1–21.

Bertet, C., Sulak, L., and Lecuit, T. (2004). Myosin-dependent junction remodelling controls planar cell intercalation and axis elongation. *Nature*, 429(6992):667–671.

Bieling, P., Li, T.-D., Weichsel, J., McGorty, R., Jreij, P., Huang, B., Fletcher, D. A., and Mullins, R. D. (2016). Force Feedback Controls Motor Activity and Mechanical Properties of Self-Assembling Branched Actin Networks. *Cell*, 164(1-2):115–127.

Bilder, D. and Irvine, K. D. (2017). Taking Stock of the DrosophilaResearch Ecosystem. *Genetics*, 206(3):1227–1236.

Blankenship, J. T., Backovic, S. T., Sanny, J. S. P., Weitz, O., and Zallen, J. A. (2006). Multicellular Rosette Formation Links Planar Cell Polarity to Tissue Morphogenesis. *Developmental Cell*, 11(4):459–470.

Bolinger, C., Zasadil, L., Rizaldy, R., and Hildebrand, J. D. (2010). Specific isoforms of drosophila shroom define spatial requirements for the induction of apical constriction. *Developmental Dynamics*, 239(7):2078–2093.

Brown, S. J. and Denell, R. E. (1996). Segmentation and dorsoventral patterning in Tribolium. *Seminars in Cell & Developmental Biology*, 7(4):553–560.

Brown, S. J., Parrish, J. K., Denell, R. E., and Beeman, R. W. (1993). Genetic control of early embryogenesis in the red flour beetle, Tribolium castaneum. *American Zoologist*, 34(3):343–352.

Brugués, A., Anon, E., Conte, V., Veldhuis, J. H., Gupta, M., Colombelli, J., Muñoz, J. J., Brodland, G. W., Ladoux, B., and Trepat, X. (2014). Forces driving epithelial wound healing. *Nature Physics*, 10(9):683–690.

Carroll, S. B. (2008). Evo-Devo and an Expanding Evolutionary Synthesis: A Genetic Theory of Morphological Evolution. *Cell*, 134(1):25–36.

Chang, L. H., Chen, P., Lien, M. T., Ho, Y. H., Lin, C. M., Pan, Y. T., Wei, S. Y., and Hsu, J. C. (2011). Differential adhesion and actomyosin cable collaborate to drive Echinoid-mediated cell sorting. *Development*, 138(17):3803–3812.

Chhetri, R. K., Amat, F., Wan, Y., Höckendorf, B., Lemon, W. C., and Keller, P. J. (2015). Whole-animal functional and developmental imaging with isotropic spatial resolution. *Nature Methods*, 12(12):1171–1178.

Combs, C. A. (2010). Fluorescence Microscopy: A Concise Guide to Current Imaging Methods. In *Current Protocols in Neuroscience*. John Wiley & Sons, Inc.

Conchello, J.-A. and Lichtman, J. W. (2005). Optical sectioning microscopy. *Nature Methods*, 2(12):920–931.

Copp, A. J. and Greene, N. D. (2009). Genetics and development of neural tube defects. *The Journal of Pathology*, 135:n/a–n/a.

Counce, S. J. (1961). Analysis of Insect Embryogenesis. *Annual review of entomology*, 6:295–+.

Dahmann, C., Oates, A. C., and Brand, M. (2011). Boundary formation and maintenance in tissue development. *Nature Reviews Genetics*, 12(1):43–55.

Davis, G. K. and Patel, N. H. (2002). Short, long, and beyond: Molecular and embryological approaches to insect segmentation. *Annual review of entomology*, 47(1):669–699.

Dawes-Hoang, R. E., Parmar, K. M., Christiansen, A. E., Phelps, C. B., Brand, A. H., and Wieschaus, E. F. (2005). folded gastrulation, cell shape change and the control of myosin localization. *Development*, 134(24):4507–4507.

Desprat, N., Supatto, W., Pouille, P.-A., Beaurepaire, E., and Farge, E. (2008). Tissue Deformation Modulates Twist Expression to Determine Anterior Midgut Differentiation in Drosophila Embryos. *Developmental Cell*, 15(3):470–477.

Ettinger, A. and Wittmann, T. (2014). Fluorescence live cell imaging. In *Quantitative Imaging in Cell Biology*, pages 77–94. Elsevier.

Farhadifar, R., ROper, J.-C., Aigouy, B., Eaton, S., and Jülicher, F. (2007). The Influence of Cell Mechanics, Cell-Cell Interactions, and Proliferation on Epithelial Packing. *Current Biology*, 17(24):2095–2104.

Fernandez-Gonzalez, R., de Matos Simoes, S., ROper, J.-C., Eaton, S., and Zallen, J. A. (2009). Myosin II Dynamics Are Regulated by Tension in Intercalating Cells. *DEVCEL*, 17(5):736–743.

Fernandez-Gonzalez, R. and Zallen, J. A. (2009). Cell Mechanics and Feedback Regulation of Actomyosin Networks. *Science Signaling*, 2(101):pe78–pe78.

Flores-Benitez, D. and Knust, E. (2016). ScienceDirect Dynamics of epithelial cell polarity in Drosophila: how to regulate the regulators? *Current Opinion in Cell Biology*, 42:13–21.

Franke, J. D., Montague, R. A., and Kiehart, D. P. (2005). Nonmuscle Myosin II Generates Forces that Transmit Tension and Drive Contraction in Multiple Tissues during Dorsal Closure. *Current Biology*, 15(24):2208–2221.

Fristrom, D. (1988). The cellular basis of epithelial morphogenesis. A review. *Tissue & cell*, 20(5):645–690.

Gilles, A. F. and Averof, M. (2014). Functional genetics for all: engineered nucleases, CRISPR and the gene editing revolution. *EvoDevo*, 5(1):43–13.

Gilles, A. F., Schinko, J. B., and Averof, M. (2015). Efficient CRISPR-mediated gene targeting and transgene replacement in the beetle Tribolium castaneum. *Development*, 142(16):2832–2839.

Gray, R. S., Roszko, I., and Solnica-Krezel, L. (2011). Planar Cell Polarity: Coordinating Morphogenetic Cell Behaviors with Embryonic Polarity. *DEVCEL*, 21(1):120–133.

Gregor (2009). The Beetle Book. pages 1–34.

Guillot, C. and Lecuit, T. (2013). Mechanics of epithelial tissue homeostasis and morphogenesis. *Science*, 340(6137):1185–1189.

Guirao, B., Rigaud, S. U., Bosveld, F., Bailles, A., López-Gay, J., Ishihara, S., Sugimura, K., Graner, F., and Bellaïche, Y. (2015). Unified quantitative characterization of epithelial tissue development. *Elife*, 4:773.

Hale, R. and Strutt, D. (2015). Conservation of Planar Polarity Pathway Function Across the Animal Kingdom. *Annual Review of Genetics*, 49(1):529–551.

Handel, K., Basal, A., Fan, X., and Roth, S. (2004). Tribolium castaneum twist: gastrulation and mesoderm formation in a short-germ beetle. *Development Genes and Evolution*, 215(1):13–31.

Handel, K., Grünfelder, C. G., Roth, S., and Sander, K. (2000). Tribolium embryogenesis: a SEM study of cell shapes and movements from blastoderm to serosal closure. *Development Genes and Evolution*, 210(4):167–179.

Harris, T. J. C. (2017). Sculpting epithelia with planar polarized actomyosin networks: Principles from Drosophila. *Seminars in Cell & Developmental Biology*, pages 1–8.

Hartman, M. A. and Spudich, J. A. (2012). The myosin superfamily at a glance. *Journal of cell science*, 125(Pt 7):1627–1632.

He, B., Doubrovinski, K., Polyakov, O., and Wieschaus, E. (2014). Apical constriction drives tissue-scale hydrodynamic flow to mediate cell elongation. *Nature*, pages 1–17.

Heemskerk, I. and Streichan, S. J. (2015). Tissue cartography: compressing bio-image data by dimensional reduction. *Nature Methods*, pages 1–5.

Helmchen, F. and Denk, W. (2005). Deep tissue two-photon microscopy. *Nature Methods*, 2(12):932–940.

Hilbrant, M., Horn, T., Koelzer, S., and Panfilio, K. A. (2016). The beetle amnion and serosa functionally interact as apposed epithelia. *Elife*, 5:14217.

Hildebrand, J. D. and Soriano, P. (1999). Shroom, a PDZ domain-containing actin-binding protein, is required for neural tube morphogenesis in mice. *Cell*, 99(5):485–497.

HOWE, R. W. (1967). Temperature Effects on Embryonic Development in Insects. *Annual review of entomology*, 12(1):15–&.

Huisken, J. and Stainier, D. Y. R. (2009). Selective plane illumination microscopy techniques in developmental biology. *Development*, 136(12):1963–1975.

Huisken, J., Swoger, J., Del Bene, F., Wittbrodt, J., and Stelzer, E. H. K. (2004). Optical sectioning deep inside live embryos by selective plane illumination microscopy. *Science*, 305(5686):1007–1009.

Icha, J., Weber, M., Waters, J. C., and Norden, C. (2017). Phototoxicity in live fluorescence microscopy, and how to avoid it. *BioEssays*, 39(8):1700003–15.

Irvine, K. D. and Wieschaus, E. (1994). Cell intercalation during Drosophila germband extension and its regulation by pair-rule segmentation genes. *Development*, 120(4):827–841.

Jacobs, C. G. C., Rezende, G. L., Lamers, G. E. M., and van der Zee, M. (2013). The extraembryonic serosa protects the insect egg against desiccation. *Proceedings of the Royal Society B: Biological Sciences*, 280(1764):20131082–20131082.

Jacobs, C. G. C., Spaink, H. P., and van der Zee, M. (2014). The extraembryonic serosa is a frontier epithelium providing the insect egg with a full-range innate immune response. *Elife*, 3:e52004–21.

Jacobs, C. G. C. and van der Zee, M. (2013). Immune competence in insect eggs depends on the extraembryonic serosa. *Developmental and Comparative Immunology*, 41(2):263–269.

Johnston, D. S. and Sanson, B. (2011). Epithelial polarity and morphogenesis. *Current Opinion in Cell Biology*, 23(5):540–546.

Kaltschmidt, J. A., Lawrence, N., Morel, V., Balayo, T., Fernandez, B. G., Pelissier, A., Jacinto, A., and Martinez Arias, A. (2002). Planar polarity and actin dynamics in the epidermis of Drosophila. *Nature Cell Biology*, 4(12):937–944.

Kanesaki, T., Hirose, S., Grosshans, J., and Fuse, N. (2013). Heterotrimeric G protein signaling governs the cortical stability during apical constriction in Drosophila gastrulation. *Mechanisms of Development*, 130(2-3):132–142.

Kasza, K. E., Farrell, D. L., and Zallen, J. A. (2014). Spatiotemporal control of epithelial remodeling by regulated myosin phosphorylation. *Proceedings of the National Academy of Sciences*, 111(32):11732–11737.

Keller, P. J., Schmidt, A. D., Wittbrodt, J., and Stelzer, E. H. K. (2008). Reconstruction of Zebrafish Early Embryonic Development by Scanned Light Sheet Microscopy. *Science*, 322(5904):1065–1069.

Keller, P. J. and Stelzer, E. H. (2008). Quantitative in vivo imaging of entire embryos with Digital Scanned Laser Light Sheet Fluorescence Microscopy. *Current Opinion in Neurobiology*, 18(6):624–632.

Keller, R. (2002). Shaping the Vertebrate Body Plan by Polarized Embryonic Cell Movements. *Science*, 298(5600):1950–1954.

Keller, R., Davidson, L., Edlund, A., Elul, T., Ezin, M., Shook, D., and Skoglund, P. (2000). Mechanisms of convergence and extension by cell intercalation. *Philosophical Transactions of the Royal Society B: Biological Sciences*, 355(1399):897–922.

Khairy, K. and Keller, P. J. (2011). Reconstructing embryonic development. *genesis*, 49(7):488–513.

Kiehart, D. P., Galbraith, C. G., Edwards, K. A., Rickoll, W. L., and Montague, R. A. (2000). Multiple forces contribute to cell sheet morphogenesis for dorsal closure in Drosophila. *The Journal of cell biology*, 149(2):471–490.

Koelzer, S., Hilbrant, M., Horn, T., and Panfilio, K. A. (2015). The beetle amnion and serosa functionally interact as apposed epithelia. Technical report.

Laissue, P. P., Alghamdi, R. A., Tomancak, P., Reynaud, E. G., and Shroff, H. (2017). Assessing phototoxicity in live fluorescence imaging. *Nature Publishing Group*, 14(7):657–661.

Lecuit, T. and Le Goff, L. (2007). Orchestrating size and shape during morphogenesis. *Nature*, 450(7167):189–192.

Lecuit, T. and Lenne, P.-F. (2007). Cell surface mechanics and the control of cell shape, tissue patterns and morphogenesis. *Nature Publishing Group*, 8(8):633–644.

Leptin, M. (1991). twist and snail as positive and negative regulators during Drosophila mesoderm development. *Genes & Development*, 5(9):1568–1576.

Lorenzen, M. D., Berghammer, A. J., Brown, S. J., Denell, R. E., Klingler, M., and Beeman, R. W. (2003). piggyBac-mediated germline transformation in the beetle Tribolium castaneum. *Insect Molecular Biology*, 12(5):433–440.

Lynch, J. A., El-Sherif, E., and Brown, S. J. (2011). Comparisons of the embryonic development of Drosophila, Nasonia, and Tribolium. *Wiley Interdisciplinary Reviews: Developmental Biology*, 1(1):16–39.

Major, R. J. and Irvine, K. D. (2006). Localization and requirement for Myosin II at the dorsal-ventral compartment boundary of theDrosophila wing. *Developmental Dynamics*, 235(11):3051–3058.

Martin, A. C. (2010). Pulsation and stabilization: Contractile forces that underlie morphogenesis. *Developmental Biology*, 341(1):114–125.

Martin, A. C. and Goldstein, B. (2014). Apical constriction: themes and variations on a cellular mechanism driving morphogenesis. *Development*, 141(10):1987–1998.

Martin, A. C., Kaschube, M., and Wieschaus, E. F. (2009). Pulsed contractions of an actin-myosin network drive apical constriction. *Nature*, 457(7228):495–501.

Mason, F. M. and Martin, A. C. (2011). Tuning cell shape change with contractile ratchets. *Current Opinion in Genetics & Development*, 21(5):671–679.

Mason, F. M., Tworoger, M., and Martin, A. C. (2013). Apical domain polarization localizes actin–myosin activity to drive ratchet-like apical constriction. *Nature Cell Biology*, 15(8):926–936.

Matsumura, F. (2005). Regulation of myosin II during cytokinesis in higher eukaryotes. *Trends in Cell Biology*, 15(7):371–377.

Mayer, M., Depken, M., Bois, J. S., Jülicher, F., and Grill, S. W. (2010). Anisotropies in cortical tension reveal the physical basis of polarizing cortical flows. *Nature*, 467(7315):617–621.

McGreevy, E. M., Vijayraghavan, D., Davidson, L. A., and Hildebrand, J. D. (2015). Shroom3 functions downstream of planar cell polarity to regulate myosin II distribution and cellular organization during neural tube closure. *Biology open*, 4(2):186–196.

Medina, M. Á. and Schwille, P. (2002). Fluorescence correlation spectroscopy for the detection and study of single molecules in biology. *BioEssays*, 24(8):758–764.

Misof, B., Liu, S., Meusemann, K., Peters, R. S., Donath, A., Mayer, C., Frandsen, P. B., Ware, J., Flouri, T., Beutel, R. G., Niehuis, O., Petersen, M., Izquierdo-Carrasco, F., Wappler, T., Rust, J., Aberer, A. J., Aspöck, U., Aspöck, H., Bartel, D., Blanke, A., Berger, S., Böhm, A., Buckley, T. R., Calcott, B., Chen, J., Friedrich, F., Fukui, M., Fujita, M., Greve, C., Grobe, P., Gu, S., Huang, Y., Jermiin, L. S., Kawahara, A. Y., Krogmann, L., Kubiak, M., Lanfear, R., Letsch, H., Li, Y., Li, Z., Li, J., Lu, H., Machida, R., Mashimo, Y., Kapli, P., McKenna, D. D., Meng, G., Nakagaki, Y., Navarrete-Heredia, J. L., Ott, M., Ou, Y., Pass, G., Podsiadlowski, L., Pohl, H., von Reumont, B. M., Schütte, K., Sekiya, K., Shimizu, S., Slipinski, A., Stamatakis, A., Song, W., Su, X., Szucsich, N. U., Tan, M., Tan, X., Tang, M., Tang, J., Timelthaler, G.,

Tomizuka, S., Trautwein, M., Tong, X., Uchifune, T., Walzl, M. G., Wiegmann, B. M., Wilbrandt, J., Wipfler, B., Wong, T. K. F., Wu, Q., Wu, G., Xie, Y., Yang, S., Yang, Q., Yeates, D. K., Yoshizawa, K., Zhang, Q., Zhang, R., Zhang, W., Zhang, Y., Zhao, J., Zhou, C., Zhou, L., Ziesmann, T., Zou, S., Li, Y., Xu, X., Zhang, Y., Yang, H., Wang, J., Wang, J., Kjer, K. M., and Zhou, X. (2014). Phylogenomics resolves the timing and pattern of insect evolution. *Science*, 346(6210):763–767.

Mohan, S., Rizaldy, R., Das, D., Bauer, R. J., Heroux, A., Trakselis, M. A., Hildebrand, J. D., and VanDemark, A. P. (2012). Structure of Shroom domain 2 reveals a three-segmented coiled-coil required for dimerization, Rock binding, and apical constriction. *Molecular biology of the cell*, 23(11):2131–2142.

Monier, B., Pélissier-Monier, A., Brand, A. H., and Sanson, B. (2009). An actomyosin-based barrier inhibits cell mixing at compartmental boundaries in Drosophila embryos. *Nature Cell Biology*, 12(1):60–65.

Monier, B., Pélissier-Monier, A., and Sanson, B. (2011). Establishment and maintenance of compartmental boundaries: role of contractile actomyosin barriers. *Cellular and Molecular Life Sciences*, 68(11):1897–1910.

Munjal, A. and Lecuit, T. (2014). Actomyosin networks and tissue morphogenesis. *Development*, 141(9):1789–1793.

Naganathan, S. R., Fürthauer, S., Nishikawa, M., Jülicher, F., and Grill, S. W. (2014). Active torque generation by the actomyosin cell cortex drives left–right symmetry breaking. *Elife*, 3:5820–16.

Ossipova, O., Chu, C.-W., Fillatre, J., Brott, B. K., Itoh, K., and Sokol, S. Y. (2015). The involvement of PCP proteins in radial cell intercalations during Xenopus embryonic development. *Developmental Biology*, 408(2):316–327.

Ossipova, O., Kim, K., Lake, B. B., Itoh, K., Ioannou, A., and Sokol, S. Y. (2014). Role of Rab11 in planar cell polarity and apical constriction during vertebrate neural tube closure. *Nature Communications*, 5:3734.

Pantazis, P. and Supatto, W. (2014). Advances in whole-embryo imaging: a quantitative transition is underway. *Nature Publishing Group*, 15(5):327–339.

Paré, A. C., Vichas, A., Fincher, C. T., Mirman, Z., Farrell, D. L., Mainieri, A., and Zallen, J. A. (2014). A positional Toll receptor code directs convergent extension in Drosophila. *Nature*, 515(7528):523–527.

Pavlopoulos, A. (2004). Efficient Transformation of the Beetle Tribolium castaneum Using the Minos Transposable Element: Quantitative and Qualitative Analysis of Genomic Integration Events. *Genetics*, 167(2):737–746.

Pietzsch, T., Saalfeld, S., Preibisch, S., and Tomancak, P. (2015). BigDataViewer: visualization and processing for large image data sets. *Nature Methods*, 12(6):481–483.

Pilot, F. and Lecuit, T. (2005). Compartmentalized morphogenesis in epithelia: From cell to tissue shape. *Developmental Dynamics*, 232(3):685–694.

Pitrone, P. G., Schindelin, J., Stuyvenberg, L., Preibisch, S., Weber, M., Eliceiri, K. W., Huisken, J., and Tomancak, P. (2013). OpenSPIM: an open-access light-sheet microscopy platform. *Nature Publishing Group*, 10(7):598–599.

Posnien, N., Schinko, J., Grossmann, D., Shippy, T. D., Konopova, B., and Bucher, G. (2009). RNAi in the Red Flour Beetle (Tribolium). *Cold Spring Harbor Protocols*, 2009(8):pdb.prot5256–pdb.prot5256.

Preibisch, S., Amat, F., Stamataki, E., Sarov, M., Singer, R. H., Myers, E., and Tomancak, P. (2014). Efficient Bayesian-based multiview deconvolution. *Nature Methods*, 11(6):645–648.

Preibisch, S., Saalfeld, S., Schindelin, J., and Tomancak, P. (2010). Software for bead-based registration of selective plane illumination microscopy data. *Nature Publishing Group*, 7(6):418–419.

Rauzi, M. and Lenne, P.-F. (2011). *Cortical Forces in Cell Shape Changes and Tissue Morphogenesis*, volume 95. Elsevier Inc., 1 edition.

Rauzi, M., Verant, P., Lecuit, T., and Lenne, P.-F. (2008). Nature and anisotropy of cortical forces orienting Drosophila tissue morphogenesis. *Nature Cell Biology*, 10(12):1401–1410.

Richards, S., Denell, R., Beeman, R. W., Gibbs, R., Beeman, R. W., Bucher, G., Schröder, R., Zdobnov, E. M., Muzny, D., Weinstock, G. M., Attaway, T., Bell, S., Buhay, C. J., Chandrabose, M. N., Chavez, D., Clerk-Blankenburg, K. P., Cree, A., Dao, M., Davis, C., Chacko, J., Dinh, H., Dugan-Rocha, S., Fowler, G., Garner, T. T., Garnes, J., Gnirke, A., Hawes, A., Hernandez, J., Hines, S., Holder, M., Hume, J., Jhangiani, S. N., Joshi, V., Khan, Z. M., Jackson, L., Kovar, C., Kowis, A., Lee, S., Lewis, L. R., Margolis, J., Morgan, M., Nazareth, L. V., Nguyen, N., Okwuonu, G., Parker, D., Ruiz, S.-J., Santibanez, J., Scherer, S. E., Schneider, B., Sodergren, E., Vattahil, S., Villasana, D., White, C. S., Wright, R., Park, Y., Lord, J., Brown, S., Wang, L., Savard, J., Tautz, D., Weinstock, G., Gibbs, R. A., Liu, Y., Worley, K., Weinstock, G., Elsik, C. G., Reese, J. T., Elhaik, E., Landan, G., Graur, D., Arensburger, P., Atkinson, P., Beidler, J., Demuth, J. P., Drury, D. W., Du, Y.-Z., Fujiwara, H., Maselli, V., Osanai, M., Park, Y., Robertson, H. M., Tu, Z., Wang, J.-j., Wang, S., Song, H., Zhang, L., Werner, D., Stanke, M., Morgenstern, B., Solovyev, V., Kosarev, P., Brown, G., Chen, H.-C., Ermolaeva, O., Hlavina, W., Kapustin, Y., Kiryutin, B., Kitts, P., Maglott, D., Pruitt, K., Sapojnikov, V., Souvorov, A., Mackey, A. J., Waterhouse, R. M., Wyder, S., Wyder, S., Kriventseva, E. V., Kadowaki, T., Aranda, M., Bao, R., Beermann, A., Berns, N., Bolognesi, R., Bonneton, F., Bopp, D., Brown, S. J., Butts, T., Chaumot, A., Denell, R. E., Ferrier, D. E. K., Friedrich, M., Gordon, C. M., Jindra, M., Klingler, M., Lan, Q., Lattorff, H. M. G., Laudet, V., von Levetsow, C., Liu,

Z., Lutz, R., Lynch, J. A., da Fonseca, R. N., Posnien, N., Reuter, R., Roth, S., Savard, J., Schinko, J. B., Schmitt, C., Schoppmeier, M., Shippy, T. D., Simonnet, F., Marques-Souza, H., Tomoyasu, Y., Trauner, J., van der Zee, M., Vervoort, M., Wittkopp, N., Wimmer, E. A., Yang, X., Jones, A. K., Sattelle, D. B., Ebert, P. R., Nelson, D., Scott, J. G., Muthukrishnan, S., Kramer, K. J., Arakane, Y., Zhu, Q., Hogenkamp, D., Dixit, R., Oppert, B., Jiang, H., Zou, Z., Marshall, J., Elpidina, E., Vinokurov, K., Oppert, C., Zou, Z., Evans, J., Lu, Z., Zhao, P., Sumathipala, N., Altincicek, B., Vilcinskas, A., Williams, M., Hultmark, D., Hetru, C., Jiang, H., Grimmelikhuijzen, C. J. P., Hauser, F., Cazzamali, G., Williamson, M., Li, B., Tanaka, Y., Predel, R., Neupert, S., Schachtner, J., Verleyen, P., Raible, F., Bork, P., Walden, K. K. O., Angeli, S., Forêt, S., Schuetz, S., Maleszka, R., Wimmer, E. A., Lorenzen, M., Tomoyasu, Y., Miller, S. C., and Grossmann, D. (2008). The genome of the model beetle and pest Tribolium castaneum. *Nature*, 452(7190):949–955.

Roh-Johnson, M., Shemer, G., Higgins, C. D., McClellan, J. H., Werts, A. D., Tulu, U. S., Gao, L., Betzig, E., Kiehart, D. P., and Goldstein, B. (2012). Triggering a Cell Shape Change by Exploiting Preexisting Actomyosin Contractions. *Science*, 335(6073):1232–1235.

Rolo, A., Skoglund, P., and Keller, R. (2009). Morphogenetic movements driving neural tube closure in Xenopus require myosin IIB. *Developmental Biology*, 327(2):327–338.

Röper, K. (2012). Anisotropy of Crumbs and aPKC Drives Myosin Cable Assembly during Tube Formation. *DEVCEL*, 23(5):939–953.

Röper, K. (2014). Supracellular actomyosin assemblies during development. *BioArchitecture*, 3(2):45–49.

Royou, A., Field, C., Sisson, J. C., Sullivan, W., and Karess, R. (2004). Reassessing the role and dynamics of nonmuscle myosin II during furrow formation in early Drosophila embryos. *Molecular biology of the cell*, 15(2):838–850.

Rozbicki, E., Chuai, M., Karjalainen, A. I., Song, F., Sang, H. M., Martin, R., Knölker, H.-J., MacDonald, M. P., and Weijer, C. J. (2015). Myosin-II-mediated cell shape changes and cell intercalation contribute to primitive streak formation. *Nature Cell Biology*, 17(4):397–408.

Sai, X., Yonemura, S., and Ladher, R. K. (2014). Junctionally restricted RhoA activity is necessary for apical constriction during phase 2 inner ear placode invagination. *Developmental Biology*, 394(2):206–216.

Sarrazin, A. F., Peel, A. D., and Averof, M. (2012). A Segmentation Clock with Two-Segment Periodicity in Insects. *Science*, 336(6079):338–341.

Sawyer, J. M., Harrell, J. R., Shemer, G., Sullivan-Brown, J., Roh-Johnson, M., and Goldstein, B. (2010). Apical constriction: A cell shape change that can drive morphogenesis. *Developmental Biology*, 341(1):5–19.

Schermelleh, L., Heintzmann, R., and Leonhardt, H. (2010). A guide to super-resolution fluorescence microscopy. *The Journal of cell biology*, 190(2):165–175.

Schindelin, J., Arganda-Carreras, I., Frise, E., Kaynig, V., Longair, M., Pietzsch, T., Preibisch, S., Rueden, C., Saalfeld, S., Schmid, B., Tinevez, J.-Y., White, D. J., Hartenstein, V., Eliceiri, K., Tomancak, P., and Cardona, A. (2012). Fiji: an open-source platform for biological-image analysis. *Nature Methods*, 9(7):676–682.

Schinko, J., Posnien, N., Kittelmann, S., Koniszewski, N., and Bucher, G. (2009). Single and Double Whole-Mount In Situ Hybridization in Red Flour Beetle (Tribolium) Embryos. *Cold Spring Harbor Protocols*, 2009(8):pdb.prot5258–pdb.prot5258.

Schinko, J. B., Hillebrand, K., and Bucher, G. (2012). Heat shock-mediated misexpression of genes in the beetle Tribolium castaneum. *Development Genes and Evolution*, 222(5):287–298.

Schinko, J. B., Weber, M., Viktorinova, I., Kiupakis, A., Averof, M., Klingler, M., Wimmer, E. A., and Bucher, G. (2010). Functionality of the GAL4/UAS system in Tribolium requires the use of endogenous core promoters. *BMC developmental biology*, 10(1):53.

Schmid, B., Shah, G., Scherf, N., Weber, M., Thierbach, K., Campos, C. P. e. r., Roeder, I., Aanstad, P., and Huisken, J. (2013). High-speed panoramic light-sheet microscopy reveals global endodermal cell dynamics. *Nature Communications*, 4:1–10.

Schmidt-Ott, U. and Kwan, C. W. (2016a). Morphogenetic functions of extraembryonic membranes in insects. *Current opinion in insect science*, 13:86–92.

Schmidt-Ott, U. and Kwan, C. W. (2016b). ScienceDirect Morphogenetic functions of extraembryonic membranes in insects. *Current opinion in insect science*, 13:86–92.

Schmied, C., Stamataki, E., and Tomancak, P. (2014). *Open-source solutions for SPIMage processing*, volume 123. Elsevier Inc., 1 edition.

Schmied, C., Steinbach, P., Pietzsch, T., Preibisch, S., and Tomancak, P. (2016). An automated workflow for parallel processing of large multiview SPIM recordings. *Bioinformatics (Oxford, England)*, 32(7):1112–1114.

Schmied, C. and Tomancak, P. (2016). Sample Preparation and Mounting of Drosophila Embryos for Multiview Light Sheet Microscopy. *Methods in molecular biology (Clifton, N.J.)*, 1478(Chapter 10):189–202.

Schmitt-Engel, C., Schultheis, D., Schwirz, J., hlein, N. S. o., Troelenberg, N., Majumdar, U., Dao, V. A., Grossmann, D., Richter, T., Tech, M., nitz, J. u. r. D. o., Gerischer, L., Theis, M., Schild, I., Trauner, J., Koniszewski, N. D. B., ster, E. K. u., Kittelmann, S., Hu, Y., Lehmann, S., Siemanowski, J., Ulrich, J., Panfilio, K. A., der, R. S. o., Morgenstern, B., Stanke, M., Buchhholz, F., Frasch, M., Roth, S., Wimmer, E. A., Schoppmeier, M., Klingler, M., and Bucher, G. (2015). The iBeetle large-scale RNAi screen reveals gene

functions for insect development and physiology. *Nature Communications*, 6:1–10.

Schröder, R. (2006). vasa mRNA accumulates at the posterior pole during blastoderm formation in the flour beetle Tribolium castaneum. *Development Genes and Evolution*, 216(5):277.

Sellers, J. R. (2000). Myosins: a diverse superfamily. *Biochimica et biophysica acta*, 1496(1):3–22.

Shah, G., Thierbach, K., Schmid, B., Reade, A., Roeder, I., Scherf, N., and Huisken, J. (2017). Pan-embryo cell dynamics of germlayer formation in zebrafish. pages 1–16.

Shindo, A. and Wallingford, J. B. (2014). PCP and septins compartmentalize cortical actomyosin to direct collective cell movement. *Science*, 343(6171):649–652.

Simoes, S. and Tepass, U. (2016). Muscle versus Snail: Muscle wins. *The Journal of cell biology*.

Smutny, M., Behrndt, M., Campinho, P., Ruprecht, V., and Heisenberg, C.-P. (2014). UV Laser Ablation to Measure Cell and Tissue-Generated Forces in the Zebrafish Embryo In Vivo and Ex Vivo. In *Quantitative Image Analysis of Cell Behavior and Molecular Dynamics During Tissue Morphogenesis*, pages 219–235. Springer New York, New York, NY.

Sokol, S. Y. (2015). Spatial and temporal aspects of Wnt signaling and planar cell polarity during vertebrate embryonic development. *Seminars in Cell & Developmental Biology*, 42:78–85.

Sokoloff, A. A. (1966). *The genetics of Tribolium and related species*. Advances in genetics. Supplement ; 1. Academic Press, New York.

Solon, J., Kaya-Copur, A., Colombelli, J., and Brunner, D. (2009). Pulsed Forces Timed by a Ratchet-like Mechanism Drive Directed Tissue Movement during Dorsal Closure. *Cell*, 137(7):1331–1342.

Sommer, C., Straehle, C., and Koethe, U. (2011). Ilastik: Interactive learning and segmentation toolkit. ... *Imaging: From Nano* ..., pages 230–233.

Stegmaier, J., Amat, F., Lemon, W. C., McDole, K., Wan, Y., Teodoro, G., Mikut, R., and Keller, P. J. (2016). Real-Time Three-Dimensional Cell Segmentation in Large-Scale Microscopy Data of Developing Embryos. *DEVCEL*, 36(2):225–240.

Stelzer, E. H., Wacker, I., and De Mey, J. R. (1991). Confocal fluorescence microscopy in modern cell biology. *Seminars in cell biology*, 2(3):145–152.

Stern, C. (2004). *Gastrulation: from cells to embryo*. Cold Spring Harbor Press.

Strobl, F. and Stelzer, E. H. K. (2014). Non-invasive long-term fluorescence live imaging of Tribolium castaneum embryos. *Development*, 141(11):2331–2338.

Sulston, I. A. and Anderson, K. V. (1996). Embryonic patterning mutants of Tribolium castaneum. *Development*, 122(3):805–814.

Sweeton, D., Parks, S., Costa, M., and Wieschaus, E. (1991). Gastrulation in Drosophila: the formation of the ventral furrow and posterior midgut invaginations. *Development*, 112(3):775–789.

Tepass, U. (2012). The Apical Polarity Protein Network in DrosophilaEpithelial Cells: Regulation of Polarity, Junctions, Morphogenesis, Cell Growth, and Survival. *Annual review of cell and developmental biology*, 28(1):655–685.

Thielicke, W. (2010). Example: Analyzing a series of images. pages 1–4.

Thielicke, W. and Stamhuis, E. J. (2014). PIVlab – Towards User-friendly, Affordable and Accurate Digital Particle Image Velocimetry in MATLAB. *Journal of Open Research Software*, 2:1202–10.

Thorn, K. (2016). A quick guide to light microscopy in cell biology. *Molecular biology of the cell*, 27(2):219–222.

Tomer, R., Khairy, K., and Keller, P. J. (2011). Shedding light on the system: studying embryonic development with light sheet microscopy. *Current Opinion in Genetics & Development*, 21(5):558–565.

Trauner, J., Schinko, J., Lorenzen, M. D., Shippy, T. D., Wimmer, E. A., Beeman, R. W., Klingler, M., Bucher, G., and Brown, S. J. (2008). Large-scale insertional mutagenesis of a coleopteran stored grain pest, the red flour beetle Tribolium castaneum, identifies embryonic lethal mutations and enhancer traps. *BMC Biology*, 7(1):73–73.

Umetsu, D. and Dahmann, C. (2015). Signals and mechanics shaping compartment boundaries in Drosophila. *Wiley Interdisciplinary Reviews: Developmental Biology*, 4(4):407–417.

Umetsu, D. and Kuranaga, E. (2017). ScienceDirect Planar polarized contractile actomyosin networks in dynamic tissue morphogenesis. *Current Opinion in Genetics & Development*, 45:90–96.

van der Zee, M., Benton, M. A., Vazquez-Faci, T., Lamers, G. E. M., Jacobs, C. G. C., and Rabouille, C. (2015). Innexin7a forms junctions that stabilize the basal membrane during cellularization of the blastoderm in Tribolium castaneum. *Development*, 142(12):2173–2183.

van der Zee, M., Berns, N., and Roth, S. (2005). Distinct Functions of the Tribolium zerknu¨llt Genes in Serosa Specification and Dorsal Closure. *Current Biology*, 15(7):624–636.

van Drongelen, R. and Vazquez-Faci, T. (2017). Mechanics of epithelial tissue formation. *arXiv.org*.

Walck-Shannon, E. and Hardin, J. (2014). Cell intercalation from top to bottom. *Nature Publishing Group*, 15(1):34–48.

Wallingford, J. B. (2012). Planar Cell Polarity and the Developmental Control of Cell Behavior in Vertebrate Embryos. *Annual review of cell and developmental biology*, 28(1):627–653.

Wang, Y. and Nathans, J. (2007). Tissue/planar cell polarity in vertebrates: new insights and new questions. *Development*, 134(4):647–658.

Westerweel, J. (1999). Fundamentals of digital particle image velocimetry. *Measurement Science and Technology*, 8(12):1379–1392.

White, J. and Stelzer, E. (1999). Photobleaching GFP reveals protein dynamics inside live cells. *Trends in Cell Biology*, 9(2):61–65.

Wolff, C., Tinevez, J.-Y., Pietzsch, T., Stamataki, E., Harich, B., Preibisch, S., Shorte, S., Keller, P. J., Tomancak, P., and Pavlopoulos, A. (2017). Reconstruction of cell lineages and behaviors underlying arthropod limb outgrowth with multi-view light-sheet imaging and tracking. *bioRxiv*, pages 1–54.

Xue, Z. and Sokac, A. M. (2016). Back-to-back mechanisms drive actomyosin ring closure during Drosophilaembryo cleavage. *The Journal of cell biology*, 215(3):335–344.

Zallen, J. A. (2007). Planar Polarity and Tissue Morphogenesis. *Cell*, 129(6):1051–1063.

Zallen, J. A. and Wieschaus, E. (2004). Patterned gene expression directs bipolar planar polarity in Drosophila. *Developmental Cell*, 6(3):343–355.

Zallen, J. A. and Zallen, R. (2004). Cell-pattern disordering during convergent extension in Drosophila. *Journal of Physics: Condensed Matter*, 16(44):S5073–S5080.